

## ABSTRACT

Title of Dissertation:               SYNTHETIC ION CHANNELS FROM  
  LIPOPHILIC GUANOSINE DERIVATIVES

Ling Ma, Doctor of Philosophy, 2009

Dissertation directed by:       Professor Jeffery T. Davis  
  Department of Chemistry and Biochemistry

Synthetic ion channels and pores not only represent models of natural transmembrane ion channels, but also demonstrate their potential applications in the areas of drug delivery, biosensors, antimicrobial agents and other molecular devices. In this thesis, lipophilic guanosine derivatives that combine both “molecular recognition” and “membrane soluble” features are utilized for the development of the self-assembled synthetic ion channels.

The potential of lipophilic G-quadruplexes to function as synthetic ion channels has been investigated by tracing the cation exchange process between free cations and G-quadruplex bound cations. Cation exchange between bulk cations ( $K^+$ ,  $NH_4^+$ ) in solution

and the bound cations in G-quadruplexes  $(G \mathbf{1})_{16} \cdot 4Na^+ \cdot 4DNP^-$  was investigated by electrospray ionization mass spectrometry and by  $^1H$ ,  $^{15}N$  NMR spectroscopy. The ESI-MS and  $^1H$  NMR data showed that G-quadruplexes containing “mixed cations” formed through a sequential ion exchange process. The use of NMR-“visible”  $^{15}NH_4^+$  cations in the NMR titration experiments allowed the determination of two “mixed-cation” intermediates by  $^{15}N$ -filtered  $^1H$  NMR and selective NOE spectroscopy. A “central insertion” pathway was proposed for the cation exchange process from  $(G \mathbf{1})_{16} \cdot 4Na^+ \cdot 4DNP^-$  to  $(G \mathbf{1})_{16} \cdot 4NH_4^+ \cdot 4DNP^-$ . In the lipophilic G-quadruplex, the “central”  $Na^+$ , bound between the 2 symmetry related  $G_8-Na^+$  octamers, is bound less strongly than are the 2 “outer”  $Na^+$  ions sandwiched within the  $G_8$ -octamers. These results demonstrated the dynamic nature of lipophilic G-quadruplex in solution and directed the design of a ditopic guanosine-sterol conjugate as an approach toward making synthetic ion channels.

Guanosine-sterol conjugate **3-1** was prepared by coupling 2', 3'-bis-TBDMS, 5'-amino guanosine with a bis-lithocholic acid derivative. Voltage clamp experiments demonstrated a series of stable, single ion channel conductances when compound **3-1** was incorporated into a planar phospholipid membrane. These channels are large; with nanoSiemens conductance values and they last for seconds of “open” time. This feature distinguishes them from most synthetic channels, which typically conduct in the picosiemens range with millisecond lifetimes. The structural studies using the bis-lithocholamide linker demonstrated that the guanosine moiety plays an essential role in the self-assembly of the transmembrane ion channels. The sizes of the most prevalent single channels calculated by Hille's equation are much larger than the diameter of a G-quartet, which suggested that the ion transport proceeded through larger pore(s) that form

upon self-assembly of lipophilic guanosine-lithocholate **3-1** within the phospholipid membrane. The large transmembrane pore(s) could be envisioned as a supramolecular structure with hydrophobic walls of bis-lithocholate linker and a central pillar of a cation-filled G-quadruplex.

The use of a bis-urea functionality in the bis-lithocholic acid linker generated guanosine-sterol conjugate **4-1**. The ion channel activity of **4-1** was demonstrated by voltage clamp experiment. Large ion channels formed from **4-1** had longer life-times than those formed from compound **3-1**. The extra stabilization of self-assembled ion channels attributed to the bisurea hydrogen bonding is consistent with the structural hypothesis of ion channels. The stable large transmembrane ion channels self-assembled by lipophilic guanosine derivatives have potential for delivery of drugs or biomolecules.

# **Synthetic Ion Channels From Lipophilic Guanosine Derivatives**

By

Ling Ma

Dissertation submitted to the Faculty of the Graduate School of the  
University of Maryland, College Park in partial fulfillment  
of the requirements for the degree of  
Doctor of Philosophy  
2009

## Advisory Committee:

Professor Jeffery T. Davis, Chair

Professor Dorothy Beckett

Professor Marco Colombini

Professor Lyle Isaacs

Professor Steven E. Rokita

© Copyright by

Ling Ma

2009

## Dedication

To my parents, my mother-in-law, my husband, my brother, and my daughter for all your  
love and support.

## Acknowledgements

First, I would like to express my heartfelt gratitude to my research advisor and mentor Professor Jeffery T. Davis. Thank you for giving me the freedom, guidance, and encouragement throughout my whole graduate career. Special thanks go to Professor Marco Colombini for providing access to his voltage clamp facilities. I am truly grateful for his generosity and his helpful advice. I am also thankful for our discussions on membranes and on life in general. I would also like to thank Prof. Lyle Isaacs for his helpful suggestions in chemistry and career advice. I would also like to thank professors Steven Rokita, Dorothy Beckett, Michael Doyle, and Daniel Falvey for their valuable discussions and suggestions.

I am very grateful to Dr. Yiu-Fai Lam and Dr. Yinde Wang for their training and help in NMR spectroscopy. Particularly, I would like to thank Yiu-Fai for his help with my research project. He taught me so many new techniques and helped me set up numerous special experiments. Yiu-Fai, Thank you!

I am thankful for the electrospray ionization mass spectrometry training provided by Noel Whittaker and Dr. Yue Li. I would also like to acknowledge Dr. Fred Khachik for the use of his HPLC instrument and Dr. Peter Zavalij for the crystal structures.

I would like to express my gratitude to the Davis research group. You have made my graduate life much more enjoyable! I would especially like to thank Dr. Mark Kaucher for helping me start my Ph.D. program, teaching me how to use CD spectrophotometer, and providing helpful advice. I would also like to thank Jennifer Seganish, Sofya Berezin, William Harrell, Oluyomi Okunola, Doriann Dejesus, and

Monique Pichon for their discussion and friendship. I would also like to thank Dr. Paul Santacroce for teaching me new techniques and helpful discussions. Particularly, I would like to thank Dr. Monica Melegari from University of Parma, Italy. She was always there to discuss chemistry and made my “membrane-making” experience fun. Thanks also go to the undergraduates I had the pleasure to work with: Emily Ryan and Jonathan Jinhoon Park. Thank you for the excellent synthesis work.

I extend my appreciation to my fellow classmates and friends who supported each other and in shared the graduate school experience: Drs. Becky Vieira, Regan Nally, Soumyadip Ghosh, Wei-hao Huang, Sofya Berezin, JuHee Park. In particular, I would like to thank Dr. Becky Vieira and Regan Nally for their friendship. Dr. Becky, thank you for your generous help and patience in correcting my writing.

Lastly, I would like to send my deepest thanks to my family. I have the most wonderful family in this world. I would like to thank my parents and brother for always being there to love and support me. I thank my mother-in law for her help and encouragement. I thank my daughter for being an excellent kid and making me a proud Mom. I would like to especially thank my husband for his understanding, patience, support and love. I love you all very dearly.



# Table of Contents

LIST OF TABLES .....	x
LIST OF FIGURES .....	xi
LIST OF SCHEMES.....	xvii
<b>Chapter 1. Introduction.....</b>	<b>1</b>
1.1 Introduction.....	1
1.2 Thesis Organization .....	1
1.3 Nucleobases and Lipids as Building Motifs for Supramolecular Structures .....	2
1.3.1 Nucleobases: Molecular Recognition Motif .....	2
1.3.2 Lipid Bilayer: Structure Unit of Functional Biological Membrane.....	5
1.4 Lipophilic Nucleobases, Nucleosides and Oligonucleotides: The Nucleolipids .....	6
1.4.1 Natural Nucleolipids .....	6
1.4.2 Molecular Recognition of Synthetic Nucleolipids.....	9
1.4.3 Membrane Association Properties of Nucleolipids .....	13
1.5 Functional Nanostructures from Amphiphilic Nucleobases .....	14
1.5.1 Molecular Recognition in Aqueous Solution: Amphiphilic Nucleobase- Derived Supramolecular Receptors .....	15
1.5.2 Lipophilic Nucleobases Approach Toward Functional Biological Surfaces...	17
1.6 Synthetic Nucleolipid for Transport of Biomolecules .....	21
1.6.1 Lipophilic Nucleobase as Carrier for Nucleotide Monophosphate Transport	21
1.6.2 Nucleolipids for DNA Transfection.....	23

1.7 Lipophilic Guanosine: Building Block of Transmembrane Ion Channels .....	25
1.7.1 Ion Channel Model From DNA G-quadruplex .....	25
1.7.2 Lipophilic Guanosine Derivatives .....	27
1.8 Summary .....	29
<b>Chapter 2. Cation Exchange in Lipophilic G-Quadruplexes: Not All Ion Binding Sites</b>	
<b>Are Equal .....</b>	<b>30</b>
2.1 Introduction.....	30
2.1.1 Cation-Dependent Self-Assembly of DNA G-Quadruplex Structures .....	31
2.1.2 DNA G-quadruplex as an Ion Channel Model .....	32
2.1.3 Lipophilic G-Quadruplexes.....	35
2.2 Mass Spectrometry Shows Mixed-Cation G-Quadruplexes Formed by Sequential Ion Exchange. ....	37
2.3 Proton NMR Indicates that the Central Na <sup>+</sup> Is the First Cation Exchanged for K <sup>+</sup> in Formation of Mixed Na <sup>+</sup> , K <sup>+</sup> G-Quadruplexes. ....	40
2.4 Use of <sup>15</sup> NH <sub>4</sub> <sup>+</sup> Cation to Probe the Cation Exchange Process Within a Lipophilic G-quadruplex .....	43
2.4.1 NMR Studies with <sup>15</sup> NH <sub>4</sub> <sup>+</sup> Confirm Identity of Mixed-Cationic G- Quadruplexes. ....	43
2.4.2. Determination of the First Intermediate in Na <sup>+</sup> / <sup>15</sup> NH <sub>4</sub> <sup>+</sup> Cation Exchange.....	46
2.4.3. Characterization of the Second Intermediate in the Na <sup>+</sup> / <sup>15</sup> NH <sub>4</sub> <sup>+</sup> Cation Exchange Process.....	48
2.5 Cation Exchange Pathway in the Lipophilic G-Quadruplex .....	50
2.6 The Larger Cs <sup>+</sup> Cation, But Not the Smaller Li <sup>+</sup> , Can Displace the Central Cation	

in the Na <sup>+</sup> G-Quadruplex. ....	53
2.7 Conclusion .....	54
<b>Chapter 3. Large and Stable Transmembrane Pores from a Guanosine-Bile Acid Conjugate</b> .....	56
3.1 Introduction:.....	56
3.1.1 G-Quartet/Folate-Quartet as a Motif for Transmembrane Ion Transporter .....	58
3.2. Design of G-quartet Ion Channels Using a Ditopic Guanosine with a Covalent Linker .....	61
3.3 Design of Guanosine-Sterol Conjugate .....	64
3.4 Synthesis of Guanosine-Sterol Conjugate .....	67
3.5 Synthesis of Bis-lithocholamide for Control Experiment.....	71
3.6 Self-Assembly Property Study of Guanosine-Sterol Conjugate.....	72
3.7 Guanosine-Sterol Conjugate Forms Transmembrane Ion Channels (Pores) .....	75
3.7.1 Ion Selectivity of the Synthetic Ion Channels.....	80
3.7.2 Proposed Active Structure of the Synthetic Ion Channel .....	83
3.8 Conclusion .....	87
<b>Chapter 4. Synthetic Ion Channel from Ditopic Sterol-Guanosines with Bis-urea Linker</b> .....	89
4.1 Introduction.....	89
4.2 Bis-urea Macrocycles are Known to Form Self-Assembled Cylinders.....	91
4.3 Synthesis of Bis-urea Guanosine-Sterol Conjugate 4-1 .....	95
4.4 Solution Study of Self-Assembly: Bis-Urea Modified Lithocholate vs. Bis-	

Carbamate Analogue.....	99
4.4.1. <sup>1</sup> H NMR Spectroscopy Provides Evidence of Intermolecular Hydrogen Bonding Between Bis-Urea Linker Units. ....	99
4.4.2. Intermolecular Hydrogen Bonding Study by FT-IR Spectroscopy .....	101
4.5 Large and Stable Ion Channel From Guanosine-Sterol Conjugate With Bis-Urea Modified Linker .....	104
4.6 Structural Study of Guanosine-Sterol Conjugate With the Bis-Urea Linker.....	108
4.7 Guanosine-Sterol Conjugates Cause Release of Carboxyfluorescein from Liposomes.....	110
4.8 Conclusion .....	113
<b>Chapter 5. Final Conclusion and Future Directions .....</b>	<b>114</b>
<b>Chapter 6. Experimental and References .....</b>	<b>118</b>
6.1 General Experimental .....	118
6.2 Synthesis .....	119
6.3 ESI-MS Experiment of G-quadruplex .....	128
6.4 NMR Titration .....	129
6.5 <sup>15</sup> N Filtered <sup>1</sup> H NMR Experiment .....	129
6.6 NOESY Experiment .....	130
6.7 Selective NOE Experiment.....	130
6.8 Planar Bilayer Conductance Experiments .....	131
6.9 Reversal Potential Measurements.....	131

6.10 Liposome Preparation .....	132
<b>References</b> .....	<b>133</b>

## List of Tables

<b>Table 3.1</b> Hille's diameter of ion channels formed from <b>3-1</b> .....	85
<b>Table 4.1</b> FT-IR frequencies for bis-urea <b>4-10</b> and bis-carbamate lithocholate <b>3-13</b> .....	103
<b>Table 4.2</b> Frequency of Events for Channels formed from <b>4-1</b> and <b>3-1</b> . .....	106

## List of Figures

<b>Figure 1.1</b> a) Natural Nucleobase; b) Watson-Crick base pairing motif; c) Hoogsteen base- pairing motif. ....	4
<b>Figure 1.2</b> Self-assembled structures of guanine: a) G-ribbon and b) G-quartet. ....	5
<b>Figure 1.3</b> a) Example of phospholipid: phosphatidylcholine; b) A phospholipid bilayer with their polar head groups exposed to water and their hydrophobic tails buried in the interior of the membrane. ....	6
<b>Figure 1.4</b> Chemical structure of cytidinediphosphatediacylglycerol 1-6. ....	8
<b>Figure 1.5</b> Chemical structure of the nucleolipid antibiotic: tunicamycins. ....	9
<b>Figure 1.6</b> Some examples of nucleolipids. ....	13
<b>Figure 1.7</b> The representation of the incorporation of lipophilic (thyminyloctyl) ammonium bromide or alkylthymine into SDS micelles and the hydrogen bond formation between lipophilic thymine derivatives and lipophilic alkyladenine inside micelles. ....	16
<b>Figure 1.8</b> a) Chemical structure of the lipophilic anchor of the oligonucleotides LT 23mer. b) The sequence of the LT23mer on the membrane surface can recognize the complementary oligonucleotides A 20mer to form DNA double helix. ....	19
<b>Figure 1.9</b> a) Chemical structures of complementary oligonucleotide amphiphiles ONA <sub>1</sub> and ONA <sub>2</sub> , control DNA sequences A <sub>1</sub> and A <sub>2</sub> , fluorescent 14mer and 9mer DNA probes. b) A liposome anchored ONA can function as either the thermo-controlled reversible switch or the chemical irreversible switch. Below the melting temperature of the duplex, the probe is centered onto the liposome surface (on state). Above melting temperature or	

in the presence of a competitive complementary ON), the fluorescent probe is expelled from the surface (off state)..... 20

**Figure 1.10** a) Chemical structures of the cationic nucleolipids for 5'-DMP or 5'-AMP transport. b) A cartoon of transport of 5'-DMP or 5'-AMP by a carrier mechanism. The formation of carrier/substrate complex through complementary hydrogen bonding and electrostatic interaction contribute to the transmembrane transport. .... 23

**Figure 1.11** a) Chemical structures of uridine-based cationic nucleolipid; b) Schematic drawing of lipoplexes formed by CL-DNA and uridine-based nucleolipid, where DNA rods are intercalated between nucleolipid bilayers. .... 24

**Figure 1.12** The crystal structure of DNA G-quadruplex formed from oligonucleotides (TG<sub>4</sub>T) in the presence of Na<sup>+</sup> in the solution, which provide a nature ion channel model. .... 26

**Figure 1.13** Some examples of lipophilic guanosine. .... 27

**Figure 1.14** Crystal structure of a lipophilic G-quadruplex [G]<sub>16</sub>•4K<sup>+</sup>•4Pic<sup>-</sup> ..... 28

**Figure 2.1** ESI-MS from titration of KPh<sub>4</sub>B into a solution of [G **1**]<sub>16</sub>•4Na<sup>+</sup>•4DNP<sup>-</sup> in 1:1 CD<sub>2</sub>Cl<sub>2</sub>/CD<sub>3</sub>CN. a) [G **1**]<sub>16</sub>•4Na<sup>+</sup>•4DNP<sup>-</sup>; b) after addition of 1 equivalents of KPh<sub>4</sub>B; c) after addition of 2 equivalents of KPh<sub>4</sub>B; d) after addition of 4 equivalents of KPh<sub>4</sub>B; and e) [G **1**]<sub>16</sub>•4K<sup>+</sup>•4DNP<sup>-</sup>. The diagram illustrates the possible mixed-cation G-quadruplexes that could be formed in the cation exchange process.....40

**Figure 2.2** Region of the <sup>1</sup>H NMR spectra (400 MHz) showing the G-quartet NH<sub>1</sub> amide protons during titration of [G **1**]<sub>16</sub>•4Na<sup>+</sup>•4DNP<sup>-</sup> with KPh<sub>4</sub>B in 1:1 CD<sub>2</sub>Cl<sub>2</sub>/CD<sub>3</sub>CN. (a) [G **1**]<sub>16</sub>•4Na<sup>+</sup>•4DNP<sup>-</sup>. The molar ratio of added KPh<sub>4</sub>B to the [G **1**]<sub>16</sub>•4Na<sup>+</sup>•4DNP<sup>-</sup> G-quadruplex, is (b) 0.5:1; (c) 1:1; (d) 2:1; (e) 3:1; (f) 4:1; and (g) 12:1..... 42

**Figure 2.3** A region of the <sup>1</sup>H NMR spectra (400 MHz) for titration of <sup>15</sup>NH<sub>4</sub>Ph<sub>4</sub>B into a solution of (G **1**)<sub>16</sub>• 4Na<sup>+</sup>• 4DNP<sup>-</sup> in 1:1 CD<sub>2</sub>Cl<sub>2</sub>:CD<sub>3</sub>CN at 20 °C. The signals for the amide N<sub>1</sub>H protons of the G-quartets are shown. a) (G **1**)<sub>16</sub>• 4Na<sup>+</sup>• 4DNP<sup>-</sup>. The mole ratio of <sup>15</sup>NH<sub>4</sub><sup>+</sup> to (G **1**)<sub>16</sub>•4Na<sup>+</sup>•4DNP<sup>-</sup> is b) 0.5:1; c) 1:1; d) 2:1; e) 3:1; f) 4:1; g) 12:1..... 544

**Figure 2.4** a) Region from the 2-D <sup>15</sup>N-<sup>1</sup>H HSQC-ROESY NMR spectrum of [G **1**]<sub>16</sub>•4NH<sub>4</sub><sup>+</sup>•4DNP<sup>-</sup> in 1:1 CD<sub>2</sub>Cl<sub>2</sub>/CD<sub>3</sub>CN showing cross-peaks between the <sup>15</sup>N NMR resonances and the <sup>15</sup>N-filtered <sup>1</sup>H resonances. b) Region of the 2-D <sup>1</sup>H-<sup>1</sup>H NOESY NMR



spectra of  $[G\ 1]_{16}\cdot 4NH_4^+\cdot 4DNP^-$  in 1:1  $CD_2Cl_2/CD_3CN$  showing cross-peaks between the  $N_1H$  amide resonances and the  $^1H$  resonances for the bound  $NH_4^+$  cations. Both spectra were recorded on a 1 mM sample at 20 °C using a 500 MHz NMR spectrometer. .... 45

**Figure 2.5**  $^{15}N$ -filtered  $^1H$  NMR (500 MHz) spectra of  $^{15}NH_4Ph_4B$  titration the solution of  $[G\ 1]_{16}\cdot 4Na^+\cdot 4DNP^-$  in 1:1  $CD_2Cl_2/CD_3CN$  with mol ratio at (a) 0:1; (b) 1:1; (c) 2:1; (d) 3:1; (e) 4:1; (f) 12:1; and (g)  $[G\ 1]_{16}\cdot 4^{15}NH_4^+\cdot 4DNP^-$  ..... 47

**Figure 2.6** Portion of a NOESY spectrum of a 1:1  $^{15}NH_4\ Ph_4B$  titration into  $[G\ 1]_{16}\cdot 4Na^+\cdot 4DNP^-$  in 1:1  $CD_2Cl_2/CD_3CN$ . The 2-D spectrum shows the NOE cross-peak between the  $^{15}NH_4^+H$  resonance with the  $N_1H$  of the inner G-quartet layer. The chemical shifts of  $\delta\ 11.79$  and  $11.40$  ppm correspond to the  $N_1H$  amide protons for the outer and inner G-quartet layers. The chemical shift of the  $^{15}NH_4^+$  proton was confirmed from the  $^{15}N$  decoupled  $^1H$  NMR spectrum showing a single peak at  $\delta\ 7.10$  ppm. .... 48

**Figure 2.7** Selective NOE spectra for amide  $N_1H$  peaks of  $(G\ 1)_{16}\cdot 4Na^+\cdot 4DNP^-$  titrated with 2 equivalents of  $^{15}NH_4Ph_4B$  in 1:1 $CD_2Cl_2:CD_3CN$ . Left: a)  $N_1H$  region of  $^1H$  NMR spectrum (green dots indicate the  $N_1H$  amide proton from the first intermediate; blue dots indicate the  $N_1H$  amide proton from the second intermediate); b)  $^{15}NH_4^+$  proton region showing selective NOE correlation to amide proton at  $\delta\ 11.51$ ,  $\delta\ 11.35$ ,  $\delta\ 11.40$  and  $\delta\ 11.79$  ppm, respectively. Right: structural scheme for the second intermediate  $[G_4(o)\cdot Na^+\cdot G_4(i)\cdot ^{15}NH_4^+\cdot G_4(i)\cdot ^{15}NH_4^+\cdot G_4(o)]$  formed during the  $Na^+ / NH_4^+$  exchange process, with the assignments for the different G-quartet  $N_1H$  amide protons..... 50

**Figure 2.8**  $^1H$  NMR spectra of  $N_1H$  region of different G-quadruplex solutions in  $CD_2Cl_2/CD_3CN$  at 20 °C. (a)  $[G1]_{16}\cdot 4Na^+\cdot 4DNP^-$ ; (b) 10:1 mol ratio of  $LiPh_4B$  and  $[G1]_{16}\cdot 4Na^+\cdot 4DNP^-$ ; (c) 8:1 mol ratio of  $CsPh_4B$ ; and  $[G1]_{16}\cdot 4Na^+\cdot 4DNP^-$ . .... 54

**Figure 3.1** Ditopic G-sterol **3-1** and control bis-lithocholamide **3-16**. Typical traces of conductance vs. time, after addition of **3-1** or **3-16**, are depicted.....56

**Figure 3.2** Hypothetical structure of a self-assembled barrel-stave ion channel formed from compound **1**. The wedge represents guanosine moiety, the line represents the bis-lithocholic acid linker. Channel formation would be controlled by the self-assembly of guanosine head groups to give a G-quartet based structure..... 58

**Figure 3.3** The unimolecular G-quadruplex stabilized by post-covalent modification that can function as a transmembrane  $Na^+$  transporter. .... 59

**Figure 3.4** Chemical structure of the folate dendrimer **3-5**, the building block for the “folate-quartet” ion channel. .... 60

**Figure 3.5** Schematic illustration of two types of “cation channel” formed from a G-quadruplex. a) “Barrel Rosette” G-quadruplex formed by 16 lipophilic guanosine

subunits. b) “Barrel Stave” G-quadruplex from by 4 ditopic ligands. The ball stands for a cation and the stave stand for the ligand. .... 62

**Figure 3.6** Possible supramolecular structure formed by **3-6** through association into G-quartets stabilized by  $K^+$  binding: a) internally-bridged  $[(3-6)_2 K^+]$  assembly; b) linear chain of doubly bridged  $G_4$  units; c) fully cross-linked regular array of  $G_4$  units..... 63

**Figure 3.7** Structure of bis-iminoboronate-guanosine **3-7** used to form  $G_4$ -quartet based membrane. .... 64

**Figure 3.8** The structure of cholic acid **3-8** and lithocholic acid **3-9**. .... 65

**Figure 3.9** Top: structures of bis-cholic acid derivatives **3-11** with methoxy group on the concave  $\alpha$ -face; **3** with hydroxyl group on the concave  $\alpha$ -face. Below: Kobuke’s proposed cross section image of ion channel, constructed from a bis-cholic acid derivative trimer/water and bis-cholic acid derivative tetramer/water.. .... 66

**Figure 3.10** a).  $^1H$ -NMR spectrum of guanosine-bislithocholate conjugate **3-1** in  $DMSO-d_6$ . b). Selective NOE experiment was carried out by irradiating new amide proton peak at  $\delta$  8.08 ppm. .... 69

**Figure 3.11**  $^1H$ -  $^1H$ NOESY spectrum of guanosine-bislithocholic acid conjugate **3-1** in  $DMSO-d_6$ . The expansion of the F1 (vertical) axis correlations near  $\delta$  8.08 ppm showing NOE of amide N-H proton is correlated with  $H_a'$ ,  $H_a''$ ,  $H_5'$ ,  $H_5''$ ,  $H_4'$ ,  $H_3'$  ..... 70

**Figure 3.12** ESI-Mass spectrum of guanosine-sterol conjugate **3-1**. .... 71

**Figure 3.13** a).  $^1H$ -NMR spectrum of guanosine-bislithocholic acid conjugate **3-1** in  $DMSO-d_6$  and  $CDCl_3$ . b).  $^1H$ -NMR spectrum of bis-lithocholamide control compound **3-16** in  $CDCl_3$ ..... 73

**Figure 3.14** CD spectra of guanosine-sterol conjugate **3-1** (blue line); **3-1** mixed with an equiv of [2, 2, 2]-cryptand (green line); **3-1** after solid-liquid extraction of  $K^+$  DNP $^-$ . All spectra were obtained in  $CDCl_3$ . .... 75

**Figure 3.15** The setup of voltage clamp experiment. The bilayer membrane was prepared with soybean phospholipid supplemented with 0.5% asolectin, 0.5% DPPC and 0.1% cholesterol. The buffer solution is 1M KCl, 2mM  $MgCl_2$ , and 5mM Pipes. All the measurements were done at 25 °C. .... 76

**Figure 3.16** Representative traces from voltage-clamp experiments. The distinct conductance values were recorded in the presence of **3-1** at -10 mV in 1 M KCl. The number of open events was counted from a total of six experiments. Three of the experiment results were from method A, another three were from method B. .... 78

<b>Figure 3.17</b> Distribution of conductance change. The frequency was calculated based on the total number of increment (channel open) events or decrement (channel close) events. .....	80
<b>Figure 3.18</b> The data analysis showed that ion selectivity ( $P_{K^+} / P_{Cl^-}$ ) decreases with a corresponding increase in conductance of ion channels. These results suggested guanosine-sterol conjugate <b>1</b> forms a variety of ion channels with different sizes. Panel A, Panel B showed the ion selectivity data obtained by applying guanosine-sterol conjugate <b>3-1</b> using the sample loading method A and method B, respectively.....	82
<b>Figure 3.19</b> Barrel-stave ion channel formed from guanosine-sterol conjugate <b>3-1</b> . The central G-quartet pore is responsible for the <0.1 nS conductance during voltage clamp experiment.....	84
<b>Figure 3.20</b> Left: Hille's cylinder model of ion channel; Right: Hille's Equation, where L is the length of the channel, r is the radius of the channel and $\rho$ is the resistivity of the solution. Under our planar voltage experiment condition, the resistivity of 1.0 M KCl solution is 89 $\Omega \cdot m$ . The length of the channel is estimated as the thickness of the phospholipid bilayer membrane, which is approximately 50 Å. ....	85
<b>Figure 3.21</b> Molecular modeling of one possible self-assembly of two molecules of guanosine-lithocholate <b>3-1</b> ( Modeling was made by Dr. Monica Melegari).....	86
<b>Figure 3.22</b> Possible G <sub>4</sub> -quartet stacks formed by bis-G-lithocholate <b>1</b> within bilayer membrane.....	87
<b>Figure 4.1</b> a) Structure represents the modification of sterol linker. b) Scheme depicting the one possible self-assembled structure from bis-urea <b>4-1</b> . The bis-urea modified sterol linker might introduce additional hydrogen bonding through urea stacking to stabilize this synthetic ion channel.....	90
<b>Figure 4.2</b> a).Examples of macrocyclic urea derivatives in the development of nanotubes. b) Bis-urea macrocycle <b>4-4</b> designed by Shimizu. c) X-ray crystal structure of the self-assembled bis-urea <b>4-4</b> , including the 3-centered hydrogen bonding patterns and the skewed orientation of monomers. ....	93
<b>Figure 4.3</b> Dynamic self-organization of heteroditopic receptors <b>4-5</b> . ....	94
<b>Figure 4.4</b> a) Crystal structures of lipophilic G-quadruplex templated by the sodium cation. b) One of the proposed ion channels from self-assembled bis-urea modified guanosine-sterol conjugate. The urea-urea hydrogen bond between the linkers was envisioned to improve the stability of the pore.....	95
<b>Figure 4.5</b> <sup>1</sup> H NMR spectrum of 3 $\alpha$ -amino lithocholate <b>4-9</b> in CDCl <sub>3</sub> . ....	96
<b>Figure 4.6</b> <sup>1</sup> H NMR and ESI-MS Spectra of Bis-Urea <b>4-1</b> in DMSO- <i>d</i> <sub>6</sub> . ....	98

<b>Figure 4.7</b> $^1\text{H}$ NMR spectra of N-H proton of bis-urea lithocholate <b>4-10</b> (blue line) and bis-carbamate lithocholate <b>3-13</b> (red line) in $\text{CDCl}_3$ . a) at room temperature, the chemical shift of NH proton is plotted against concentration; b) at 10 mM concentration, the chemical shift of NH proton is plotted against temperature. ....	101
<b>Figure 4.8</b> N-H stretching region of the IR spectra as a function of concentration for a) bis-urea lithocholate <b>4-10</b> ; b) bis-carbamate lithocholate <b>3-13</b> in $\text{CDCl}_3$ at $25^\circ\text{C}$ . ....	102
<b>Figure 4.9</b> Representative conductance records from voltage clamp experiment. Ion channels formed by <b>4-1</b> in a planar bilayer at an applied voltage of -10 mV in 1M KCl ( <i>trans</i> ) / KCl ( <i>cis</i> ) solution (pH 7.0). ....	104
<b>Figure 4.10</b> Distribution of conductance change for the ion channels from guanosine-sterol conjugate <b>4-1</b> and <b>3-1</b> . The frequency was calculated based on the total number of increment (channel open) events or decrement (channel close) events. a) data from compound <b>4-1</b> ; b) data from compound <b>3-1</b> . ....	106
<b>Figure 4.11</b> Histogram showing the various open lifetimes for 1-5 nS channels formed from <b>3-1</b> and <b>4-1</b> . Distribution of conductance change, the frequency was calculated based on the total number of increment (channel open) events. ....	108
<b>Figure 4.12</b> a) Chemical structure of carboxyfluorescein. b) Scheme of a fluorescent assay of carboxyfluorescein release from liposome. ....	111
<b>Figure 4.13</b> Carboxyfluorescein release assay confirmed the pore formation mediated by guanosine-sterol conjugate <b>3-1</b> and <b>4-1</b> . ....	112

## List of Schemes

<b>Scheme 2.1</b> Schematic structure of (A) G-quartet and (B) G <sub>8</sub> -octamer. ....	32
<b>Scheme 2.2</b> High-resolution crystal structure of a DNA G-quadruplex formed by oligonucleotide [d(TG <sub>4</sub> T)] <sub>4</sub> . b) Natural potassium ion channel. ....	34
<b>Scheme 2.3</b> Schematic representation of <sup>15</sup> NH <sub>4</sub> <sup>+</sup> movement through the Oxy-1.5 quadruplex. a) bulk NH <sub>4</sub> <sup>+</sup> cation only exchanges with the outer <sup>15</sup> NH <sub>4</sub> <sup>+</sup> . b) exchange of two bound <sup>15</sup> NH <sub>4</sub> <sup>+</sup> cations are random. Black, yellow and red ball represent the bulk ammonium ion, and the bound ammonium ions located in outer and inner binding site of the G-quadruplex. ....	35
<b>Scheme 2.4</b> G-quadruplex formed through self-assembly of G <b>1</b> in the presence of K <sup>+</sup> DNP <sup>-</sup> . ....	36
<b>Scheme 2.5</b> Proposed central insertion pathway for cation exchange in the lipophilic G-quadruplex system. ....	51
<b>Scheme 2.6</b> These depictions are taken from the crystal structure for [G <b>1</b> ] <sub>16</sub> ·4Na <sup>+</sup> ·4pic <sup>-</sup> . The illustrations show the octahedral coordination geometry for one of the outer Na <sup>+</sup> cations (on the left) and for the central Na <sup>+</sup> (right). The central Na <sup>+</sup> has a almost cubic coordination geometry, whereas the oxygen ligands are twisted toward the energetically more favorable square anti-prism geometry for the outer Na <sup>+</sup> . ....	52
<b>Scheme 3.1</b> Synthesis of bis-guanosine-lithocholic acid conjugate <b>3-1</b> . ....	68
<b>Scheme 3.2</b> Synthesis of control compound bis-lithocholamide <b>3-16</b> . ....	72
<b>Scheme 4.1</b> Three center hydrogen bonding net-work formed by urea derivative. ....	92
<b>Scheme 4.2</b> Synthesis of 3α-amino lithocholate <b>4-9</b> . ....	96
<b>Scheme 4.3</b> Synthesis of bis-urea modified guanosine-sterol conjugate <b>4-1</b> . ....	97
<b>Scheme 4.4</b> Synthesis of bis-urea lithocholamide <b>4-12</b> for the control experiment. ....	109

# Chapter 1. Introduction

## 1.1 Introduction

Molecular self-assembly plays a fundamental role in Nature, and is a widely used principle to build supramolecular structures from individual molecular components.<sup>1-3</sup> For example, self-assembly has been a useful tool to mimic biological functions and fabricate nanomaterials.<sup>4,5</sup> In recent years, many research activities have focused on the development of novel functional materials using well-defined building blocks. This thesis, “*Synthetic Ion Channels from Lipophilic Guanosine Derivatives*” describes the design and development of amphiphilic building blocks for the self-assembly of functional structures.

## 1.2 Thesis Organization

This thesis is organized into six chapters. The overall goal of this research was to develop trans-membrane synthetic ion channels using lipophilic guanosine as building blocks. **Chapter 1** briefly discusses the molecular recognition properties of the naturally occurring nucleobases and then goes on to review the potential use of lipophilic nucleobases, nucleosides and oligonucleotides as functional nanostructures and biomaterials. The cation exchange studies in **Chapter 2** give insight into the stability of self-assembled lipophilic G-quadruplex in solution. The kinetic lability of lipophilic G-quadruplex inspired the design of a ditopic lipophilic guanosine to build trans-membrane ion channels. **Chapter 3** describes large and stable ion channels formed from a ditopic

guanosine-lithocholic acid conjugate. The ion channel activity and structure-properties characterization suggested the key role of the guanosine subunit in the formation of ion channels. **Chapter 4** explores the enhanced stability and activity of ion channels through the modification of guanosine-sterol building blocks. **Chapter 5** describes the conclusion and directions of future research. Finally, **Chapter 6** contains the experimental protocols for the research described in **Chapters 2-4**.

### **1.3 Nucleobases and Lipids as Building Motifs for Supramolecular Structures**

#### **1.3.1 Nucleobases: Molecular Recognition Motif**

In Nature, the self-assembly of single strand DNA into double helix and other higher order structures is mediated by many noncovalent interactions, such as hydrogen bonding,  $\pi$ - $\pi$  stacking, and van der Waals forces. Among these intermolecular interactions, complementary hydrogen bonding *via* nucleobase-pairing is of primary importance in the molecular recognition of DNA and RNA sequences. Thus, the molecular recognition capability of nucleobases *via* specific hydrogen-bonding pattern is considered to play an essential role in the storage, translation and replication of genetic information.<sup>6-8</sup>

The naturally occurring nucleobases are nitrogen-containing aromatic heterocycles, including the double-ringed purines (adenine **1-1**, guanine **1-2**) and single-ringed pyrimidines (cytosine **1-3**, thymine **1-4**, and uracil **1-5**). They are the key constituents of DNA and RNA that are involved in molecular recognition. Cytosine **1-3**,

guanine **1-2**, adenine **1-1** and thymine **1-4** are found in DNA, while uracil **1-5** replaces thymine **1-4** in RNA. Nucleobases are able to recognize each other through a complementary hydrogen bonding interaction, known as Watson-Crick pairing.<sup>9</sup> Watson-Crick pairing is one of the most recognized observations in a variety of DNA- and RNA-structures. In this specific hydrogen-bonding motif, guanine **1-2** pairs with cytosine **1-3** through a three-point hydrogen bonding, while adenine **1-1** interacts with thymine **1-4** (or uracil in RNA) in a two-point hydrogen bonding fashion (**Figure 1.1**).

Furthermore, various alternative hydrogen-bonding motifs are also possible.<sup>7,10,11</sup> These non-Watson-Crick pairings include mismatch-pairing, nucleobase self-dimerization, and Hoogsteen base pairing that associates the C6 and N7 binding sites of purine nucleobases. Hoogsteen base pairing through the self-association of guanosine **1-2** is another prevalent hydrogen bonding motif found in a variety of G-rich DNA and RNA suprastructures.<sup>12</sup>



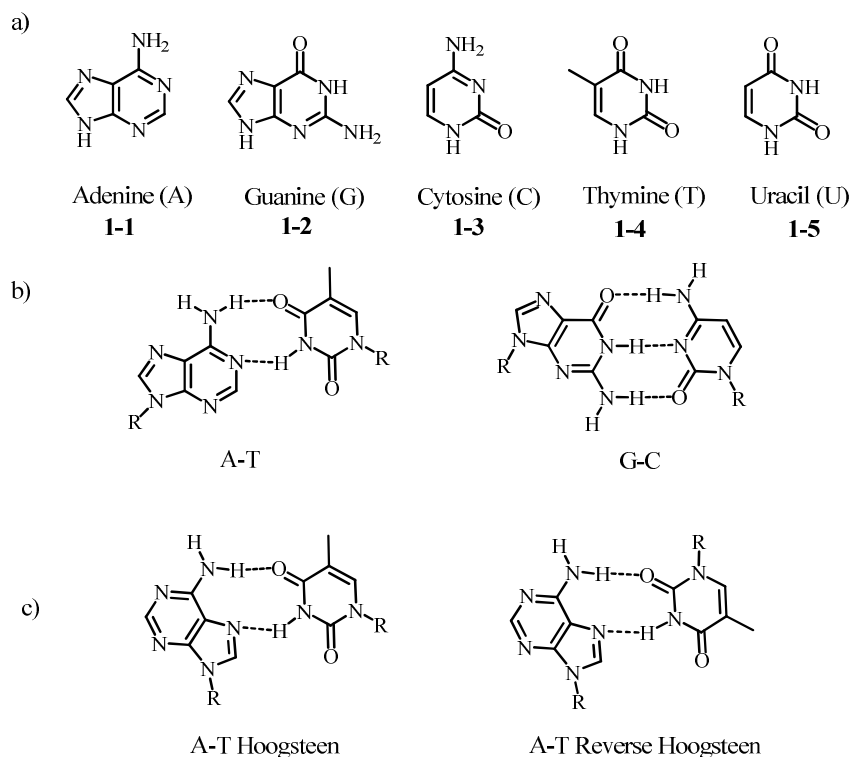


**Figure 1.1** a) Natural Nucleobase; b) Watson-Crick base pairing motif; c) Hoogsteen base-pairing motif.

Of the natural nucleobases, guanosine **1-2** possesses a unique self-association property, since it incorporates both Watson-Crick and Hoogsteen edges for the self-complementary hydrogen bonding. The guanine-guanine interactions involve the two Hoogsteen pairings between hydrogen bonding acceptor O6 and N7 at Hoogsteen edges and hydrogen bonding donor N1H amide and N2H amine at Watson-Crick edges. Under certain conditions, guanine self-assembles into several suprastructures that differ from the classic nucleobase dimers.<sup>13-17</sup> These higher-ordered structures include the G-ribbon structure or cyclic structure, known as the G-quartet (**Figure 1.2b**). **Figure 1.2a** shows the hydrogen-bonded ribbon G-structure in the absence of cations. Whereas, the G-quartet is a preferential self-assembled structure in the presence of cations, since cations

stabilize this cyclic tetramer through the electrostatic interaction between cation and the carbonyl oxygens (Figure 1.3b).

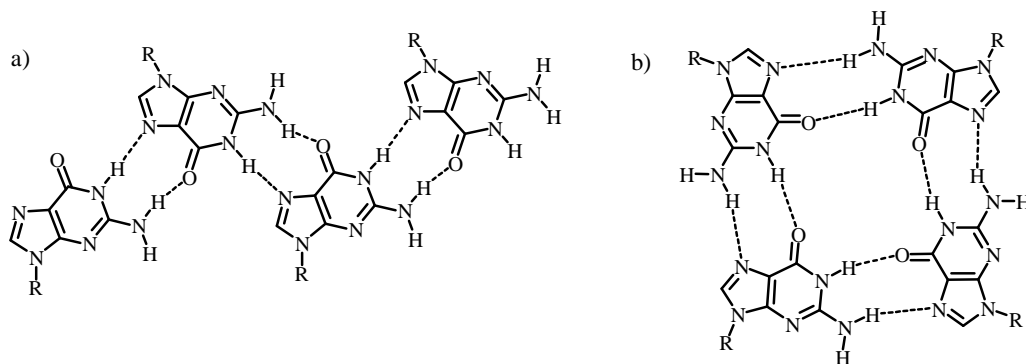


**Figure 1.2** Self-assembled structures of guanine: a) G-ribbon and b) G-quartet.

### 1.3.2 Lipid Bilayer: Structural Unit of Functional Biological Membrane

The lipid bilayer is the basic structural unit of all biological membranes.<sup>18,19</sup> It acts as the hydrophobic barrier that segregates cellular compartments and isolates the cells from the extracellular environment. As shown in **Figure 1.3**, phospholipids, the fundamental building blocks of all cell membranes, consist of a polar phosphate-containing head group and two nonpolar hydrocarbon tails. These amphiphilic molecules self-assemble in a tail-to-tail fashion to form a lipid bilayer with a hydrophobic interior and a hydrophilic surface. Lipid bilayers are versatile structures that can be formed by a number of phospholipids and other lipid molecules such as cholesterol and glycolipids.

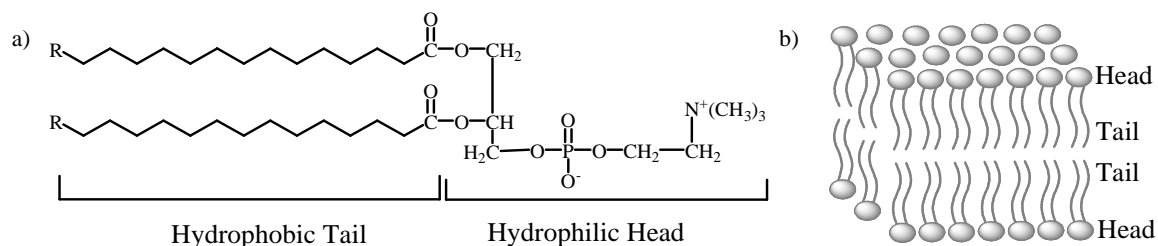


**Figure 1.3** a) Example of phospholipid: phosphatidylcholine; b) A phospholipid bilayer with their polar head groups exposed to water and their hydrophobic tails buried in the interior of the membrane.

In addition, lipid bilayers can also accommodate or bind to a variety of biological molecules.<sup>20,21</sup> For example, proteins are the other major constituent of cell membranes. They are either embedded within the lipid bilayer or surface-adsorbed on the lipid bilayer. These different species of proteins and lipids can recognize specifically with other another by their individual chemical nature. As a result, the lipids associated with proteins are involved in a wide array of cellular processes and specialized membrane functions such as cell adhesion, selective transport of molecules across membranes and cell signaling.

## 1.4 Lipophilic Nucleobases, Nucleosides and Oligonucleotides: The Nucleolipids

### 1.4.1 Natural Nucleolipids

Nature has utilized the nucleobase-derived building molecules to develop functional self-assemblies with specificity and control. One class of extremely promising and interesting biomolecules are nucleolipids, the nucleobase-derived amphiphiles obtained by covalently linking a lipophilic moiety with a nucleobase, a nucleoside or an oligonucleotide.<sup>22</sup> Nucleolipids have been found to be involved in biosynthesis

processes,<sup>14</sup> and a variety of biological activities, such as antimicrobial, antiviral, anti-tumor activities in eukaryotic and prokaryotic cells.<sup>23,24</sup>

Cytidinediphosphatediacylglycerol (CDP-diacylglycerol) **1-6** is one of the most ubiquitous nucleolipids present in cells (**Figure 1.4**).<sup>25</sup> It plays an essential role in the biosynthesis of the membrane phospholipids. In mammalian cells, CDP-diacylglycerol **1-6** is formed from cytidinetriphosphate and phosphatidic acid and serves as an activated, energy-rich intermediate. Catalyzed by different specific membrane-bound enzymes, CDP-diacylglycerol **1-6** is able to transfer a phosphatidic acid to a hydroxyl group of a carbohydrate or glycolipid to generate phospholipids. The specific enzymes are located in mitochondria for the biosynthesis of phosphatidylglycerol, the precursor of cardiolipin, or in microsomes for the biosynthesis of phosphatidylinositol.<sup>26,27</sup> This indicates that nucleoside-based lipid can be incorporated into a variety of phospholipids in the cell membrane. In prokaryotes, CDP-diacylglycerol **1-6** functions as the precursor for the biosynthesis of phosphatidylserine as well.<sup>28</sup>

Moreover, CDP-diacylglycerol **1-6** is involved in the enzymatic activities of phosphatidylserine synthases occurring in gram-negative bacteria, such as *E. coli*, *Salmonella typhimurium*, *Serratiamarcescense*, etc. The membrane association of these phosphatidylserine synthases is induced by the lipid substrate CDP-diacylglycerol **1-6**.<sup>18,19</sup> The CDP-diacylglycerol-dependent activity of phosphatidylserine suggested that phosphatidylserine synthases are peripheral membrane proteins that specifically bind to the nucleolipid CDP-diacylglycerol **1-6** via an intermolecular interaction, such as

nucleobase-pairing, hydrophobic interactions and/or van der Waals interactions. Nucleolipid CDP-diacylglycerol **1-6** can reside in the membrane, due to its high degree of amphiphilicity.

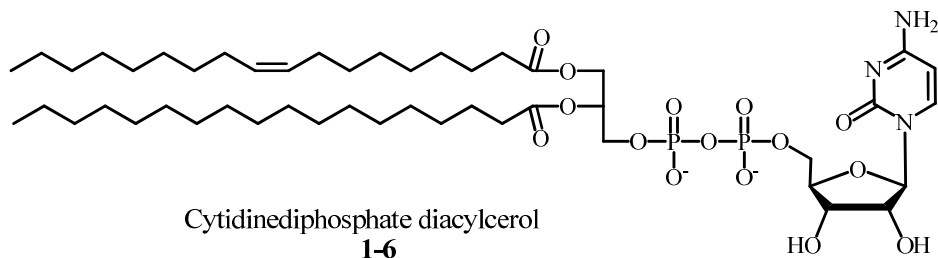
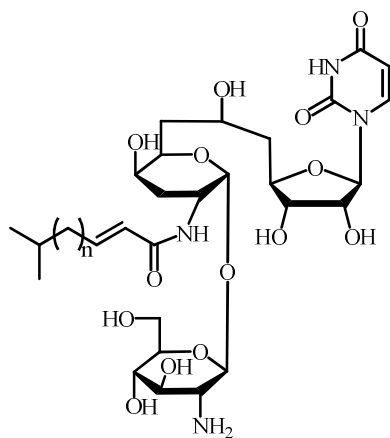


**Figure 1.4** Chemical structure of cytidinediphosphatediacylglycerol 1-6.

Tunicamycins **1-7** was the first discovered nucleolipid antibiotic that was produced from the fermentation broths of *Streptomyceslysosuperificus* (**Figure 1.5**). Tunicamycins**1-7** is composed of the heterocyclic nucleobase uracil and a branched fatty acid side chain, and it has demonstrated the ability to inhibit a variety of biosynthesis of oligosaccharide, thus preventing the glycosylation of proteins in both prokaryotic and eukaryotic cells.<sup>21-24</sup> The antibiotic can function as an irreversible inhibitor for the GlcNAc-1-phosphate transferase. GlcNAc-1-phosphate transferase is the eukaryotic enzyme that catalyzes the transfer of N-acetylglucosamine1-phosphate from UDP-N-acetylglucosamine to dolichylphosphate to generate N-acetylglucosaminylpyrophosphoryldolichol. Mechanistic studies on the actions of tunicamycin **1-7** have revealed that these nucleolipids bind preferentially to the GlcNAc-1-phosphate transferase, and also interact with the membrane phospholipid.<sup>29,30</sup> The binding of the tunicamycins **1-7** to transferase occurs when tunicamycins **1-7** is incorporated into biological membranes. Tunicamycins **1-7** also acts as reversible inhibitors for the phospho-N-acetylmuramyl-pentapeptidetranslocase (translocase I) in

the peptidoglycan biosynthesis as well. Translocase I is the specific enzyme that catalyzes the relocation of phospho-MurNAc-L-Ala-g-D-Glum-DAP-D-Ala-D-Ala from UMP to a membrane-bound carrier, undecaprenyl phosphate. The studies of actions of tunicamycins have showed that the inhibition by tunicamycins **1-7** is competitive with regard to the substrate UDP-MurNAc-pentapeptide, since both molecules share the same uridine subunit. This result demonstrated the recognition characteristic of nucleobase in the observed bioactivity. The capability of tunicamycins **1-7** to locate within the membrane bilayer can be attributed to the hydrophobicity of the tunicamycins.



Tunicamycin A-D (n = 9 - 11)  
**1-7**

**Figure 1.5** Chemical structure of the nucleolipid antibiotic: tunicamycins.

### 1.4.2 Molecular Recognition of Synthetic Nucleolipids

The design of synthetic amphiphiles that are derived from biologically functional nucleobases, nucleosides and oligonucleotides has become a major strategy to build interesting self-assembled structures with complex and desirable properties. Like the typical amphiphiles, nucleolipid amphiphiles will self-assemble in aqueous solution to

form distinct structures such as micelles, vesicles and other self-aggregates.<sup>31-33</sup> However, nucleolipids have unique physicochemical properties due to their informative nucleobase constituents. The specific base-pairing of nucleobases through hydrogen bonding and  $\pi$ - $\pi$  stacking is cooperative with the hydrophobic effect from the lipid segment, contributing to the self-assembly.

In the 1980s, the molecular recognition between two complementary nucleolipids **1-8** and **1-9** was first reported by Ringsdorf and coworkers.<sup>34</sup> Using surface pressure measurements, UV, and DSC techniques, they found that adenine- and thymine-nucleolipids base-paired at the air-water interface. Afterward, numerous techniques, including Langmuir-Blodgett, NMR, FTIR, RA, ATR, fluorescent probes, *etc.*, have provided direct evidence of the complementary hydrogen bonding between nucleolipids at the air-water interface.<sup>35-38</sup>

The base pairing of nucleolipid was also observed at the mesoscopic interfaces of the self-assembly of nucleolipids in either micellar or vesicular structures.<sup>39</sup> For instance, it was reported by Berti and Baglioni that short-chain phospholiponucleosides, diC<sub>8</sub>P-adenosine **1-10** and diC<sub>8</sub>P-uridine **1-11** self-assembled into mixed micelles with CMC values around  $10^{-3}$  M.<sup>40</sup> The data from NMR, UV-Vis, and CD spectroscopies revealed the stacking and hydrogen-bonding of the complementary adenosine and uridine occurred at the micellar surface. The continued study of phospholiponucleosides with longer alkyl chain (DOP-adenosine **1-12**, DOP-uridine **1-13**, and DOP-cytosine **1-14**) demonstrated that these nucleolipids are able to self-assemble into liposomes.<sup>41</sup> The liposomes formed

from a mixture of DOP-adenosine **1-12** and DOP-uridine **1-13** showed the UV, CD and NMR properties for base-pairing, while the liposome formed from a mixture of DOP-adenosine **1-12** and DOP-cytosine **1-14** failed to give any spectroscopic change. These data supporting that the molecular recognition properties of nucleolipids are controlled by specific Watson-Crick base pairing.

Specific base pairing that resembles biofunctional supramolecular structures has been found for certain nucleolipids. Itojima and coworkers reported that lipophilic dimyristoyl-5'-phosphatidyl nucleosides **1-15** can self-assemble into helical strands that are similar to DNA duplex in aqueous solution.<sup>42</sup> Dimyristoyl-5'-phosphatidyladenosine **1-15** can form various self-assemblies, including multi-helical strands, or tubular structure, depending on the pH and alkalinity of the solution. The formation of a hybrid helix from the equimolar mixture of dimyristoyl-5'-phosphatidyladenosine **1-15** and dimyristoyl-5'-phosphatidyluridine **1-16** suggested that the specific hydrogen bonding between nucleobases directs the self-assembly of nucleolipids. The research of Gottarelli and Spada established that in the presence of certain cations, lipophilic guanosine **1-17** can self-associate into columnar structures that contain stacked G-quartet in organic solution.<sup>14,43,44</sup> The self-assembly is driven by Watson-Crick and Hoogsteen base pairing of guanine,  $\pi$ - $\pi$  stacking and cation-dipole interactions. Similar to the liquid crystals formed from guanosine oligonucleotides in aqueous solution, the G-quartet is the fundamental building block for these supramolecular structures. Such a G-quartet was also found in the DNA secondary structure that regulates the telomerase activity in chromosomes.



The molecular recognition characteristics of nucleolipids have attracted substantial research, including attention to the design and synthesis of novel amphiphilics derived from nucleobases for both the fundamental aspects and application purposes. For these reasons, a wide range of nucleolipids have been synthesized by covalently linking the hydrophobic segment to nucleobases, nucleosides, and oligonucleotides. The lipophilic moieties, such as alkyl chain, cholesterol, glycerol, *etc*, are attached either directly to the nucleobase or to the sugar moiety of nucleoside or oligonucleotides. Nucleolipid structures can be classified as either neutral, cationic, anionic or zwitterionic nucleolipids, depending on their charge properties. **Figure 1.6** lists the nucleolipids reported in the literature mentioned in section 1.4.

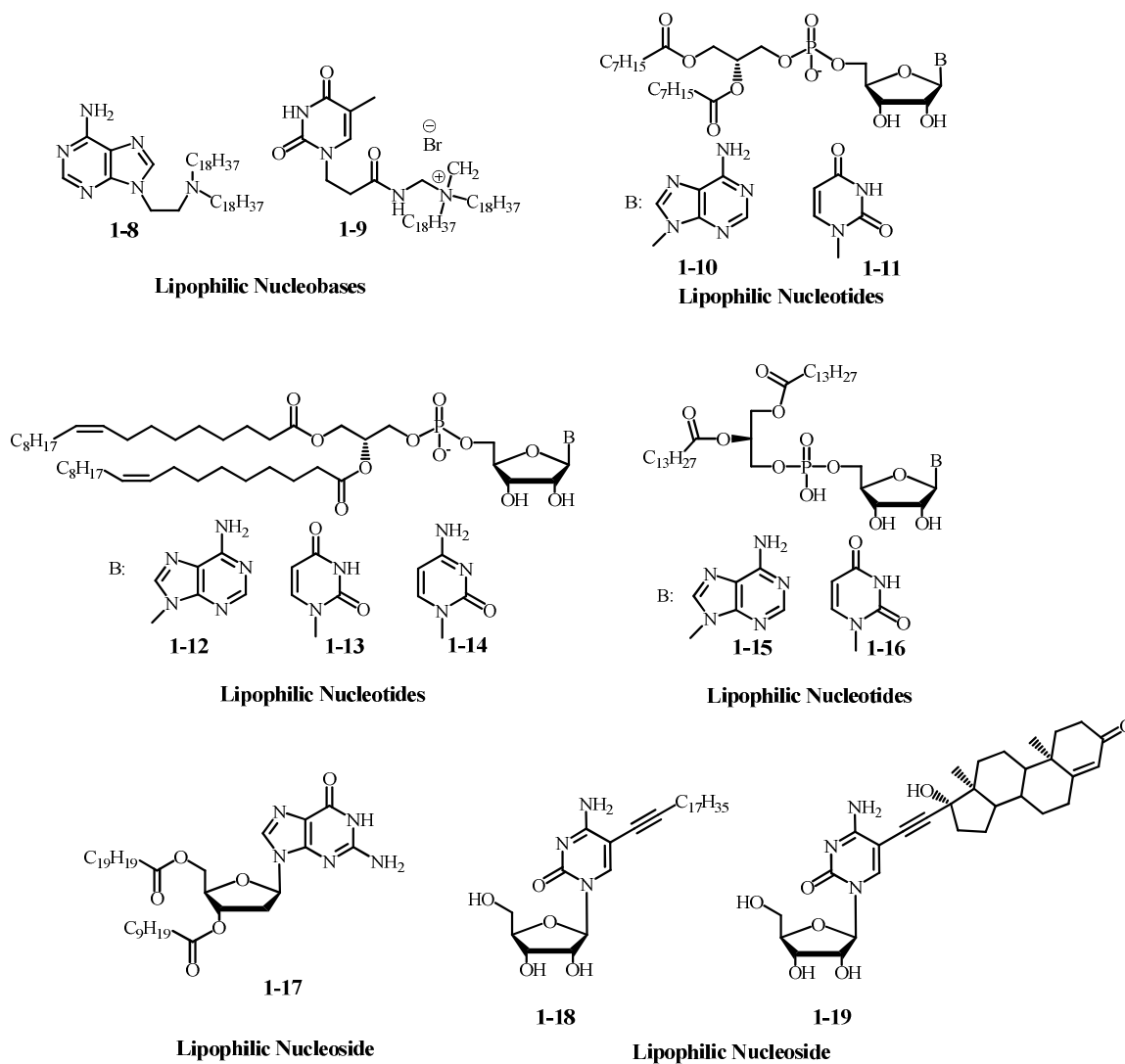


**Figure 1.6** Some examples of nucleolipids.

### 1.4.3 Membrane Association Properties of Nucleolipids

The lipophilic moiety of certain nucleolipids provides another important feature for these compounds: namely, membrane association. A variety of nucleolipids have been found to be lipophilic components that can serve as an anchor to attach lipophilic nucleobase, nucleosides and oligonucleotides into the lipid membrane.<sup>45-48</sup> For the membrane incorporation purpose, the lipid anchor should be sufficiently hydrophobic to

overcome the self-association propensity of the amphiphiles and also allow it to be stable in the membrane. The Huster and Liebscher groups have designed lipophilic nucleosides that conjugate adenine and uracil nucleobases with 1-octadecynyl or sterol hydrophobic moiety **1-18**, **1-19**.<sup>49</sup> Using solid-state, <sup>2</sup>H and <sup>31</sup>P, <sup>1</sup>H MAS NMR spectroscopy, they identified the membrane location of the functional groups of these nucleolipids. The lipid moieties are incorporated into the phospholipid membrane, while the nucleobase functional groups are exposed on the surface of the membrane. The effects of the inserted hydrophobic moiety on the membrane show that the steroidal ring of **1-19** causes the decrease of lipid order parameters and packing density, while the alkyl chain of **1-18** has no pronounced influence on the structure of lipid membrane. Compound **1-18** was proposed as an ideal nucleolipid for building the functional membrane surface. This result suggested that nucleolipids can be used to build functionalized membrane surfaces. In addition, lipophilic moieties are implicated to associate the membrane permeation for the antiviral and antitumor activities of nucleolipid antibiotics.<sup>50-52</sup>

## **1.5 Functional Nanostructures from Amphiphilic Nucleobases**

Various researches on the lipophilic nucleobases, nucleosides and oligonucleotides have demonstrated their very interesting and unique properties.<sup>53,54</sup> The combination of molecular recognition and hydrophobic characteristics of nucleolipids may allow them to target specific lipid membrane or deliver biologically active molecules, which provides a wide opening for the development of bio-devices, drug delivery, biosensor and therapeutic strategy. This section will describe a few, but promising,

nucleolipid systems that can base-pair within membranes or function as membrane transporters.

### **1.5.1 Molecular Recognition in Aqueous Solution: Amphiphilic Nucleobase-Derived Supramolecular Receptors**

The molecular recognition of lipophilic nucleobases through base-pairing in aqueous environment was first reported by Nowick and co-workers.<sup>55-57</sup> In their pioneering work, lipophilic (thyminyloctyl)ammonium bromide **1-20** and sodium dodecyl sulfate (SDS) self-assembled into micelles and served as supramolecular receptors.<sup>55</sup> The resulting receptor, consisting of thymine functionality, was able to recognize *N*<sup>6</sup>-actyle-9-alkyladenine **1-21** in aqueous solution through an A-T base-pair (**Figure1.7**). The incorporation of (thyminyloctyl) ammonium bromide **1-20** into SDS micelles was assisted by the electrostatic interaction between the positive-charged ammonium group of **1-20** and the negatively charged sulfate group of SDS, and the hydrophobic interaction between alkyl chain of **1-20** and SDS. The complete incorporation of 1.0mM of **1-20** into micelles was achieved at an SDS concentration of 20 mM. NMR titration studies showed that thymine derivative **1-20** can bind to alkyladenine derivative **1-21** by means of intermolecular hydrogen bonding in the presence of SDS. This specific binding was determined to be 1:1 stoichiometry by a Job's plot, which is consistent with a 1:1 adenine-thymine base-pairing pattern. It was also found that when SDS is absent in the aqueous solution, only aromatic stacking exists between **1-20** and **1-21**. This result suggests that the presence of SDS is crucial for the hydrogen bond formation, and that the adenine-thymine base-pairing occurs within the hydrophobic core of SDS micelles. The author also investigated the effect of lipophilicity

of adenine derivatives **1-21** on the hydrogen binding between **1-20** and **1-21**. By varying the length of alkyl chain on adenine derivatives **1-21**, the binding constants were measured and compared. The adenine derivatives **1-21** bearing longer alkyl-chains exhibited a larger binding affinity with thymine derivatives **1-20**, indicating that the hydrophobicity of adenine derivatives **1-21** is required for micellar incorporation and base pairing.

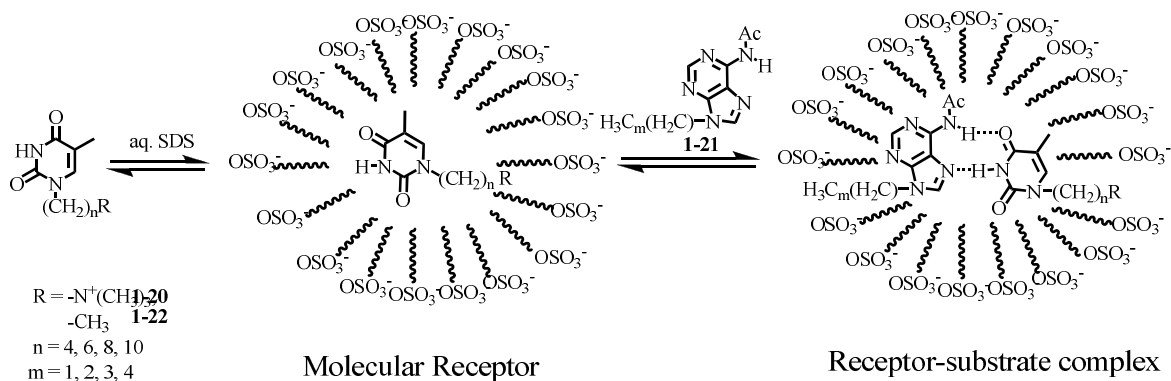


**Figure 1.7** The representation of the incorporation of lipophilic (thyminyloctyl) ammonium bromide or alkylthymine into SDS micelles and the hydrogen bond formation between lipophilic thymine derivatives and lipophilic alkyladenine inside micelles.

The continued effort by the Nowick group provided another successful example of molecular recognition between neutral lipophilic nucleobases in SDS micelles.<sup>57</sup> Here the neutral 1-alkylthymine derivative **1-22** incorporated into SDS micelles functioned as supramolecular receptors. Likewise, the receptors can bind *N*<sup>6</sup>-acyl-9-alkyladenine **1-21** through base-pairing in aqueous solution. Nowick found that 1-alkylthymine derivative **1-22** must be sufficiently hydrophobic to be incorporated within SDS micelles. The incorporation of **1-22** into micelles plays a critical role in the adenine-thymine base-pairing within micelles. The studies on molecular recognition between neutral lipophilic

nucleobases in aqueous SDS micelles confirmed the model of supramolecular receptor proposed in their previous study. The hydrophobic core of SDS micelles provides a suitable environment for hydrogen bonding between the complementary lipophilic nucleobases. The hydrophobic interaction between lipophilic nucleobases and SDS and the base-pairing between two complementary nucleobases moieties provides a driving force for molecular recognition in water. By means of micelles, Nowick's strategy should have a wide application in the recognition or transport of nucleobase related biomolecules.

### **1.5.2 Lipophilic Nucleobases Approach Toward Functional Biological Surfaces**

In biological systems, phospholipid membrane surfaces represent one of the active microscopic interfaces for molecular recognition. As we mentioned before, membranes are versatile structures that are composed of lipids and a variety of biological molecules. For example, proteins embedded within the lipid bilayer or surface adsorbed on the lipid bilayer are involved in most biological activities, such as signal transduction, enzymatic reaction, etc. To mimic and understand the natural recognition and binding process on the membrane surface, a number of researchers have focused on the development of functional membranes using nucleolipids.

Liebecher, Huster, and Herrmann reported an oligonucleotide (LT 23mer) **1-23** that anchors into the lipid membrane and forms a DNA duplex.<sup>58</sup> LT-23mer is designed as an amphiphile that consists of 21 thymidine (T) units and two lipophilic nucleotides L in at positions 1 and 8. The  $\alpha$ -tocopherol subunit located in the 1-position of cytosine serves as a lipophilic anchor (**Figure 1.8**). A doubly lipophilic anchor separated by 6 nucleotides was designed to prevent the oligonucleotide from self-associating in aqueous

environment, which improved the membrane insertion. The membrane incorporation of lipophilic LT 23mer **1-23** was studied by incubating LT 23mer and fluorescently labeled 3'Rh-or 5'Rh-A20mer **1-24** with giant unilamellar vesicles (GUVs) using fluorescence microscopy. Rh fluorescence was detected over the entire membrane, indicating the complementary binding of LT 23mer **1-23** to 3'Rh- or 5'Rh-A20mer **1-24** occurs on the GUV surface. By means of  $^1\text{H}$ ,  $^{31}\text{P}$ ,  $^1\text{H}$  NMR, EPR, DSC and fluorescence techniques, Huster *et al* established that LT 23mer **1-23** are enriched in the liquid-disordered membrane domains.<sup>59</sup> LT 23mer **1-23** inserts stably into lipid membranes and imposes insignificant modification to the bilayer membrane structure. The ribose/cytosine moiety of LT 23mer is located in the lipid-water interface, while the non-lipidated nucleotide end is exposed to the aqueous environment. This result suggests that the nucleolipids could be used to build a functional surface on the membrane surface.

After LT 23mer **1-23** anchored into the lipid membrane, NMR and FRET techniques were used to characterize the functionality of the membrane surface. The GUVs containing LT 23mer and fluorescent phospholipid N-NBD-PE were incubated with 3'Rh-A20mer **1-24**. The resulting strong FRET was attributed to the efficient complementary binding between membrane-bound LT 23mers**1-23**and lipophilic 3'Rh-A20mer**1-24**. The formation of Watson-Crick A-T base pairs, which was confirmed by  $^1\text{H}$  NMR chemical shifts, suggested that the oligonucleotides exposed to the aqueous media are capable of recognizing the complementary oligonucleotide to form the DNA double helix. This membrane-bound DNA double strand presents similar structural feature and melting properties as the free double-stranded DNA, indicating that neither

the lipophilic anchor nor the membrane proximity interferes with the DNA duplex formation. Thus, the membrane-anchored oligonucleotide may function to provide a broad range of cell biological and medical applications, such as biosensor, receptor, *etc.*

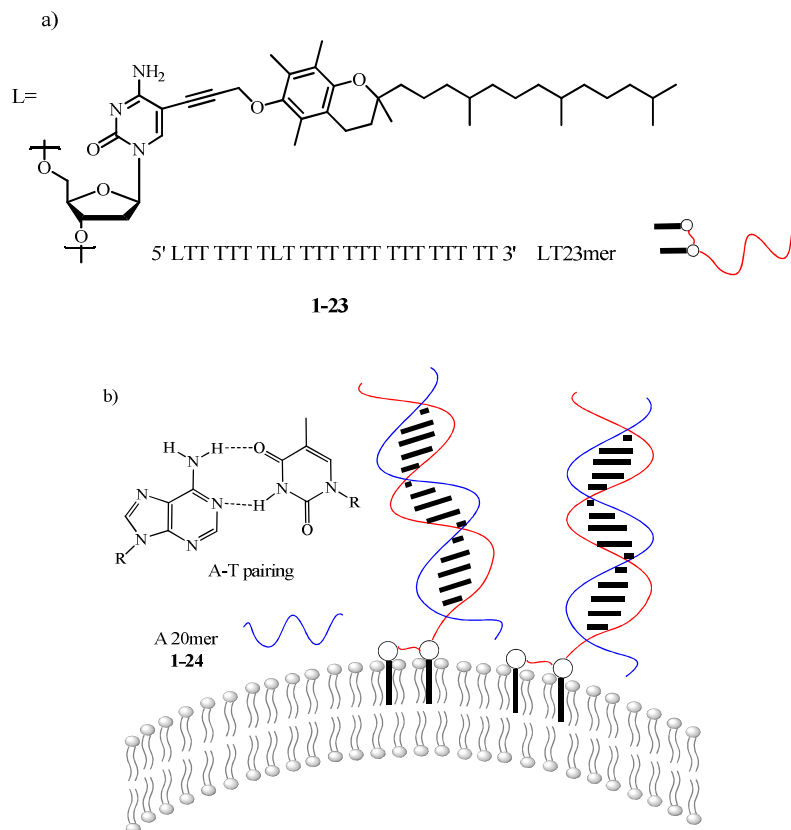


**Figure 1.8** a) Chemical structure of the lipophilic anchor of the oligonucleotides LT 23mer. b) The sequence of the LT23mer on the membrane surface can recognize the complementary oligonucleotides A 20mer to form DNA double helix.

Recently, Barthelemy and coworkers designed and synthesized membrane-anchored lipophilic oligonucleotides (ONA) **1-25** that serve as biocompatible switches (**Figure 1.10**).<sup>60</sup> The incorporation of the lipophilic ONA **1-25** into a zwitterionic DOPC liposome was assisted by a lipophilic di-C<sub>15</sub> ketal anchor. A kinetic study of DNA duplex formation, using the surface plasmon resonance (SPR) technique, suggested that these



lipophilic membrane-bound ONA recognize their complementary sequences (ON) **1-26** or fluorescent-labeled complementary sequences (fONA) **1-27** *via* Watson-Crick base pairings. The DOPC lipid membrane has no effect on this DNA duplex formation. Thus, the oligonucleotide-tagged liposome can function as a supramolecular platform for detection and delivery of bioactive molecules.

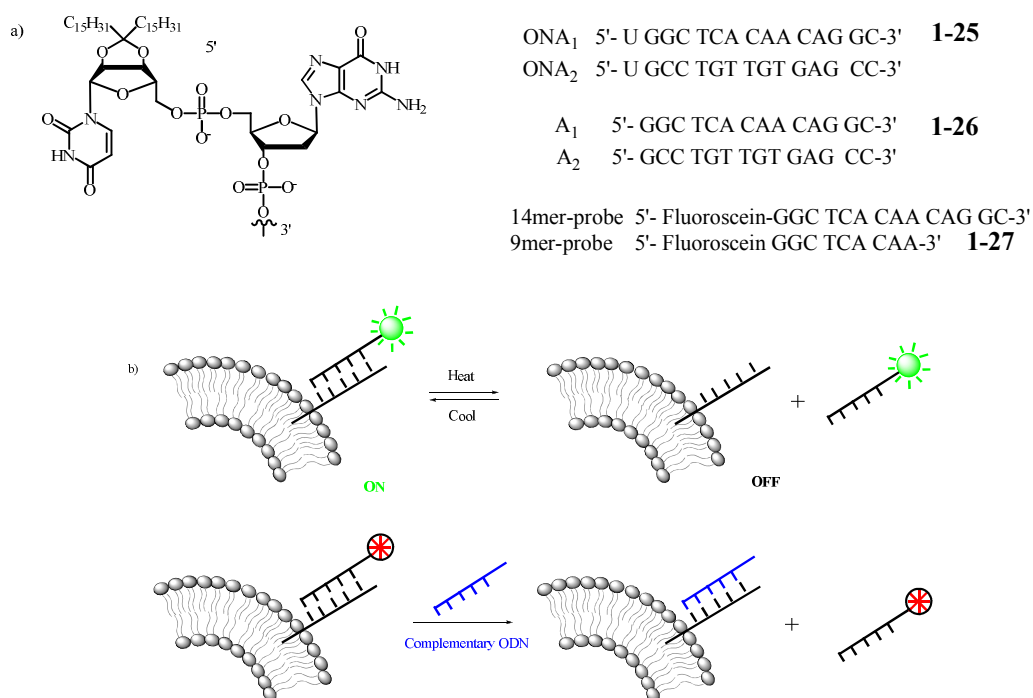


**Figure 1.9** a) Chemical structures of complementary oligonucleotide amphiphiles  $\text{ONA}_1$  and  $\text{ONA}_2$ , control DNA sequences  $\text{A}_1$  and  $\text{A}_2$ , fluorescent 14mer and 9mer DNA probes. b) A liposome anchored ONA can function as either the thermo-controlled reversible switch or the chemical irreversible switch. Below the melting temperature of the duplex, the probe is centered onto the liposome surface (on state). Above melting temperature or in the presence of a competitive complementary ON), the fluorescent probe is expelled from the surface (off state).

Barthelemy demonstrated that liposome-anchored ONA **1-25** can be fluorescently switched “on” or “off”, depending on the stability of DNA duplex formed from ONA and

its fluorescent labeled complementary sequences (fONA) **1-27**. The formation/dissociation of ONA-fONA could be tuned by certain physical (temperature) or chemical (presence of competitive complementary ON sequences) stimuli. They found ONA-tagged liposomes serve as a reversible thermal switch. At temperatures above  $T_m$  (melting temperature of ONA-fONA duplex), the ONA-fONA duplex melts and the switch is turned “off”, while at temperatures below  $T_m$ , the ONA-fONA duplex anneals at the surface of liposome and the switch is “on”. On the other hand, ONA-tagged liposome was demonstrated to be irreversibly switched “off”, when the competitive ON sequences **1-26** to either ONA or fONA **1-27** are present in the system. However, this switch was not sensitive to the scrambled ON complementary to ONA **1-25**, indicating that the switching process is driven by specific Watson-Crick base pairing. These findings suggested that the oligonucleotide-tagged liposome may provide a potential delivery system for drug or other biological molecules. The release of drug or other biological molecules could be triggered by a temperature change or the presence of a competitive RNA or DNA.

## **1.6 Synthetic Nucleolipid for Transport of Biomolecules**

### **1.6.1 Lipophilic Nucleobase as Carrier for Nucleotide Monophosphate Transport**

Hong and colleagues described that lipophilic phosphonium-nucleobase conjugates **1-28** and **1-29** can function as carriers for the trans-membrane transport of 5'-AMP or 5'-GMP.<sup>61,62</sup> The combination of phosphonium and lipophilic nucleobase thymine or cytosine rendered phosphonium-nucleobase **1-28** or **1-29** an ideal structure to

recognize 5'-AMP or 5'-GMP in aqueous solution. The extraction and transport activity showed that phosphonium-nucleobase conjugates **1-28** and **1-29** transport their complementary nucleotide monophosphate much more efficiently than their nucleobase-free analogues. The transport rates were increased by a factor of ~100 for 5'-AMP and 5'-GMP, respectively. The control experiment using non-complementary nucleobase-phosphonium conjugates resulted in the decreased transport of 5'-AMP or 5'-GMP. These data suggested that the base pairing between nucleolipid **1-28** or **1-29** and their complementary nucleotide monophosphate can be attributed to the increased transport. The concentration-dependent extraction study provided a proposed carrier mechanism for 5'-AMP or 5'-GMP transport. The electrostatic interaction between phosphonium and phosphate, and the hydrogen bonding and  $\pi$ - $\pi$  stacking between two complementary nucleobases allowed for the formation of nucleolipid/nucleotide monophosphate complex in aqueous solution, thus leading to the transmembrane transport (Figure 1.10). Based on the same design strategy, Hong prepared lipophilic thiouronium-thymine conjugate **1-30** for 5'-AMP transport. Likewise, thiouronium-thymine demonstrated the enhanced nucleotide monophosphate transport ability. The structure-related transport activity studies confirmed that the complementary Watson-Crick base pairing between lipophilic thiouronium-thymine (carrier) and 5'-AMP (substrate) contributed to the increased transport.

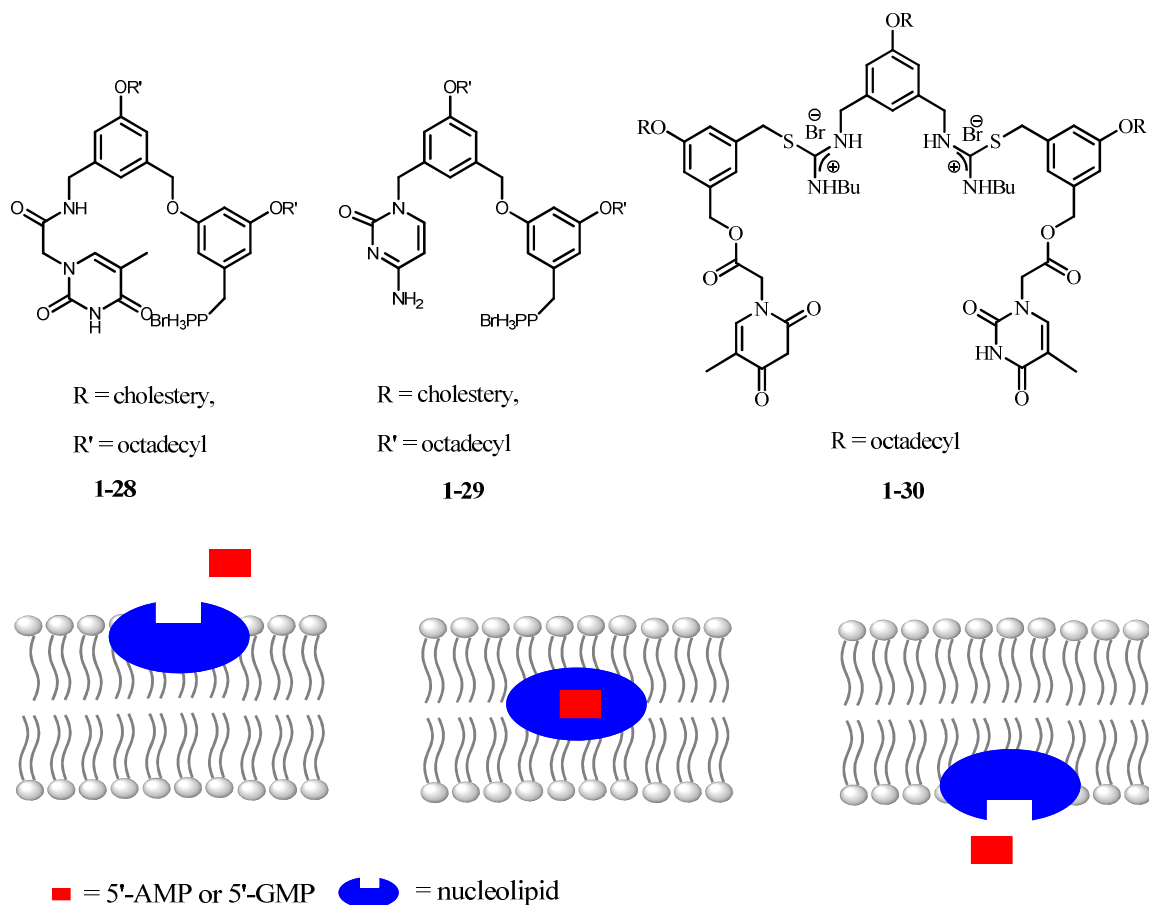


**Figure 1.10** a) Chemical structures of the cationic nucleolipids for 5'-GMP or 5'-AMP transport. b) A cartoon of transport of 5'-GMP or 5'-AMP by a carrier mechanism. The formation of carrier/substrate complex through complementary hydrogen bonding and electrostatic interaction contribute to the transmembrane transport.

## 1.6.2 Nucleolipids for DNA Transfection

The Barthelemy group has pioneered the development of synthetic vectors using cationic lipophilic uridine.<sup>64</sup> The nucleolipids O-Et-DOUPC **1-31** are composed of positive-charged ammonium group, a nucleobase (e.g., uridine) and a lipophilic oleyl alkyl group attached at the 2', 3' position of ribose by an ester linkage (**Figure 1.11**). O-Et-DOUPC **1-31** is able to self-aggregate into unilamellar vesicles. Its positive-charge and nucleobase components enable the formation of nucleolipoplexes (vector/DNA

assembly). Data from TEM, SAXS experiments established that O-Et-DOUPC/calf-thymus DNA (CT-DNA) lipoplexes formed as a multilamellar structure, where DNA is intercalated in the lipid bilayer. The binding of nucleolipid to DNA was confirmed by an ethidium bromide (EB, 3,8-diamino-5-ethyl-6-phenylphenanthridinium bromide) fluorescence assay. The fluorescence change of EB was observed when O-Et-DOUPC **1-31** displaced CT-DNA bound EB in the solution. This result indicated competitive binding of O-Et-DOUPC **1-31** to CT-DNA.

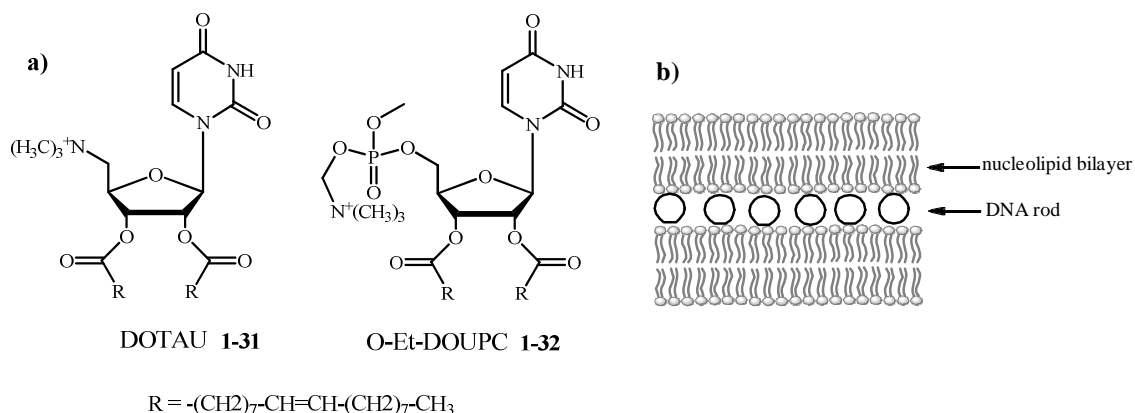


**Figure 1.11** a) Chemical structures of uridine-based cationic nucleolipid; b) Schematic drawing of lipoplexes formed by CL-DNA and uridine-based nucleolipid, where DNA rods are intercalated between nucleolipid bilayers.

The reporter  $\beta$ -gal gene assay revealed that O-Et-DOUPC **1-31** at high nucleolipid:DNA (w : w) ratios (18:1–36:1) can efficiently transport plasmid DNA to Chinese hamster ovarian (CHO) cells. While transfection assays of mammalian cell lines ((HeLa and MCF-7) indicated that DOTAU can transfect expression vector (pEGFP) encoding GFP efficiently. The *in vitro* cytotoxicity measurement results showed that O-Et-DOUPC **1-31** does not inhibit the proliferation of CHO cell line, suggesting the non-toxic nature of this nucleolipid.

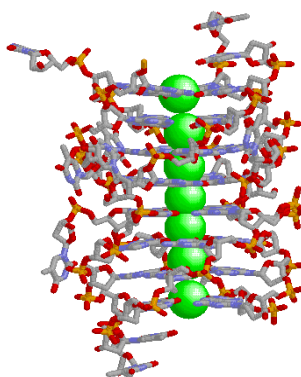
Shortly thereafter, Grinstaff and Barthelemy reported an efficient delivery of a gene using a similar uridine-based nucleolipid, *N*-[5'-(2',3'-dioleoyl)uridine]-*N,N,N*-trimethylammoniumtosylate (DOTAU) **1-32**. Transfection assays of mammalian cell lines (HeLa and MCF-7) suggested that DOTAU is an efficient transfection reagent for an expression vector (pEGFP) encoding GFP. Structural characterization by TEM, SAXS, IR and ethidium bromide fluorescence assays showed typical multilamellar lipoplexes formation from DOTAU vesicles and calf-thymus DNA. The compact structure of lipoplexes of DOTAU/poly A suggests that a uracil moiety is involved in the stabilization of complex through specific U-A base pairing. The proliferation assays on mammalian cell lines showed that the toxicity of DOTAU **1-32** is insignificant compared with the commercially-available Lipofectamine. The cationic nucleolipids provide a future trend for the development of synthetic transfection agent.

## **1.7 Lipophilic Guanosine: Building Block of Transmembrane Ion Channels**

### **1.7.1 Ion Channel Model from DNA G-quadruplex**

As mentioned previously, guanine is able to self-assemble into G-quartets through Watson-Crick and Hoogsteen hydrogen bonding. In nature, guanine-rich sequences of DNA and RNA can fold into G-quadruplexes. These supramolecular structures are involved in the inhibition of telomerase activity in cancer cells, playing an important role in the biology of cancer and ageing.<sup>65-67</sup> Numerous NMR, biophysical and crystallography studies have established that the G-quartet serves as an essential building unit of the DNA G-quadruplex.<sup>68,69</sup> In addition, certain cations (e.g. Na<sup>+</sup>, K<sup>+</sup>) are

important for the stabilization of this supramolecular structure.<sup>70-72</sup> Self-assembly of the G-quadruplex is driven by the specific guanine base pairing,  $\pi$ - $\pi$  stacking and cation-dipole interactions. **Figure 1.12** shows the crystal structure of the G-quadruplex formed by the hexanucleotide [d(TGGGGT)]<sub>4</sub> in the presence of Na<sup>+</sup> cations.<sup>73</sup> In this four-stranded DNA G-quadruplex, the G-quartets are found stacked on top of each other with a space of 3.13 Å and 30° twist angle. It is noteworthy that monovalent Na<sup>+</sup> ions are either located in the central cavity of G-quartet or sandwiched between the stacked G-quartet.



[d(TG<sub>4</sub>T)]<sub>4</sub>

**Figure 1.12** The crystal structure of DNA G-quadruplex formed from oligonucleotides d(TG<sub>4</sub>T) in the presence of Na<sup>+</sup> in the solution, which provide a nature ion channel model.

The alignment of cations along the central tunnels of DNA G-quadruplex is reminiscent of the structure of transmembrane ion channels. That cations can flow through the central channel of DNA G-quadruplex was demonstrated by Feigon's elegant work.<sup>74,75</sup> In this study, oligonucleotide [G<sub>4</sub>T<sub>4</sub>G<sub>4</sub>] (Oxy-1.5) was templated by <sup>15</sup>NH<sub>4</sub><sup>+</sup> ions to form a dimeric G-quadruplex. Utilizing <sup>15</sup>N and <sup>1</sup>H NMR spectroscopy, three ion binding sites within the Oxy-1.5 G-quadruplex were identified. The dynamic analysis revealed that these <sup>15</sup>NH<sub>4</sub><sup>+</sup> ions flow along the central axis of the DNA G-quadruplex.

## 1.7.2 Lipophilic Guanosine Derivatives

A number of research groups have been active in the development of lipophilic guanosine to build functional supramolecular structures. The lipophilic guanosine derivatives can self-assemble into a variety of supramolecular structures, such as organogelators, liquid crystals, nanowires, membrane films *etc.*<sup>43,76-78</sup> In these G-quartet-based assemblies, hydrogen bonding between guanines takes either ribbon-type or stacking nanotube-type structures, depending on experimental condition. For example, lipophilic guanosine **1-33** is an organogelator of alkanes that has a guanine sheet-like structure. The organogel can undergo gel-to-liquid crystal phase transition by heating, due to the selective breakage of hydrogen bonds network in the structure.<sup>79</sup> For lipophilic guanosine **1-34**, in the presence of alkaline cations, NMR and SANS results revealed lipophilic guanosine **1-34** self-assembles into a columnar structure due to G-quartet stacking; while in the absence of cations, NMR and crystal X-ray diffraction data confirmed it only forms ribbon-like structures.<sup>80</sup>

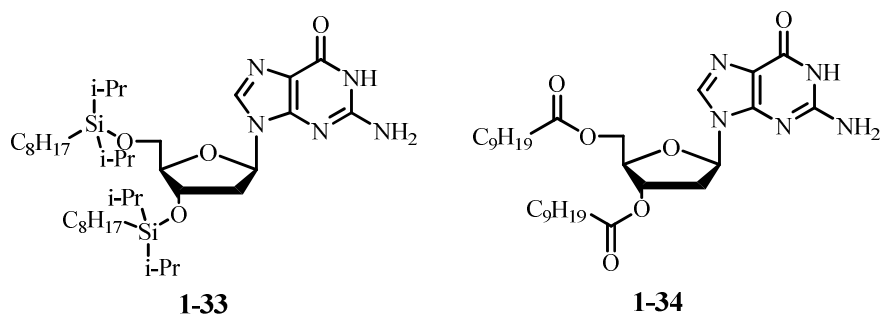


**Figure 1.13** Some examples of lipophilic guanosine.



The Davis group has actively pursued the use of lipophilic G-quadruplexes as supramolecular scaffolds for the construction of ionophores and transmembrane.<sup>81-83</sup> In earlier studies, a series of lipophilic guanosine derivatives were designed and synthesized. These lipophilic guanosine derivatives can recognize each other in organic solvents to self-assemble into G-quadruplexes *via* templating with certain cations. For example, 16 pieces of 5'-silyl-2', 3'-isopropylidene **1-35**, in the presence of K<sup>+</sup>picrate, self-assembled into a lipophilic G-quadruplex (G)<sub>16</sub>·4K<sup>+</sup>·4pic<sup>-</sup> (**Figure 1.14**).<sup>84</sup> NMR and X-ray crystallography data suggested that this supramolecular assembly is composed of two K<sup>+</sup>-sandwiched head-to-tail (G)<sub>8</sub> octamers. There is one central K<sup>+</sup> cation located in between these two (G)<sub>8</sub> octamers and one dynamic Cs<sup>+</sup> ion capping the top of the structure. The structure of lipophilic G-quadruplex, with a hydrophobic exterior and cation-filled hydrophilic interior, resembles a potential transmembrane ion channel.

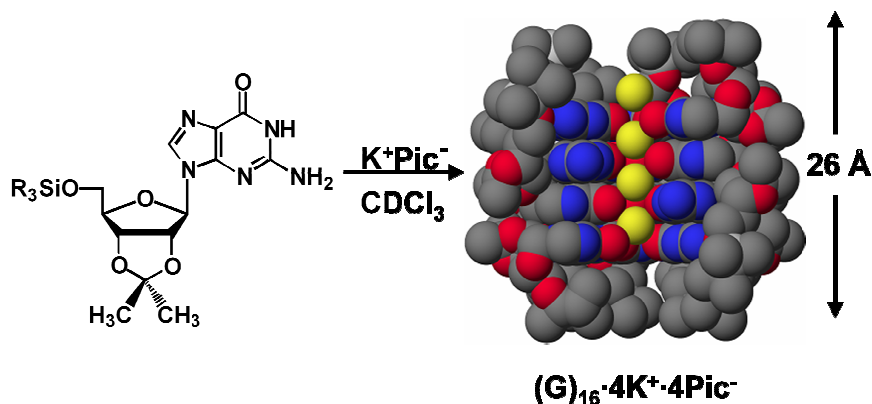


**Figure 1.14** Crystal structure of a lipophilic G-quadruplex (G)<sub>16</sub>·4K<sup>+</sup>·4Pic<sup>-</sup>.

## 1.8 Summary

This chapter has described the self-assembly of lipophobic nucleobases, nucleosides, and oligonucleotides using their molecular recognition properties. In particular, nucleolipids have demonstrated the capability to insert into lipid membranes or function as carriers for membrane transport of biomolecules. The lipophilic G-quadruplexes, bearing the resemblance to the natural DNA G-quadruplex, provide the potential scaffolds to function as synthetic ion channels. My research project described in chapter 2 will focus on whether this lipophilic G-quadruplex can function as a synthetic ion channel.<sup>85</sup> Subsequently, the design and synthesis of lipophilic guanosine derivatives that can form self-assembled ion channels will be described in the following chapters.

## Chapter 2. Cation Exchange in Lipophilic G-Quadruplexes: Not All Ion Binding Sites Are Equal

*The majority of this chapter has been published in reference 85:*

- **Ma, L.;** Iezzi, M. A.; Kaucher, M. S.; Lam, Y-F; Davis, J. T. *J. Am. Chem. Soc.* **2006**, *128*, 15269-15277.

### 2.1 Introduction

The overall goal of the research described in this chapter was to investigate the potential use of lipophilic G-quadruplexes to function as ion channels. Initial studies involved the study of cation exchange between G-quadruplex-bound cations and cations in solution.

In our group, extensive efforts have been made to study the structure and dynamic properties of lipophilic G-quadruplexes with the aim to develop transmembrane synthetic ion channels.<sup>14,82,83,86,87</sup> The diffusion NMR analysis demonstrated that the hexadecameric  $[G\ \mathbf{1}]_{16}\cdot 4K^+\cdot 4pic^-$  (where  $G\ \mathbf{1}$  is 5'-tert-butyltrimethylsilyl-2',3'-isopropylidene guanosine), observed in the solid state, also predominates in organic solution.<sup>82,88</sup> The dynamic study of G-quadruplex showed that the identity of both the bound anions and the bound cations significantly attenuate the kinetic stability of the G-quadruplex and modulate the rate of ligand exchange between G-quadruplex and monomer in solution. In this chapter, we have turned our attention to studying the cation exchange process within the lipophilic G-quadruplex. In short, we would like to determine if the cations exchange through the ends of the G-quadruplex stack, much like

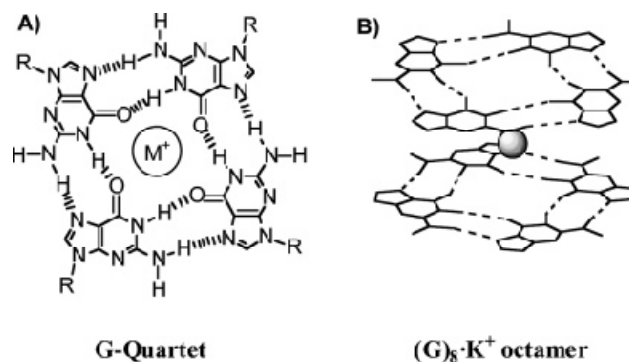
an ion channel, or if cation exchange occurs through the sides of the G-quadruplex, especially since there is no covalent backbone connecting the different G-quartet layers.

The preliminary result of my research has been the identification of the intermediates in the cation exchange process between G-quadruplex bound  $\text{Na}^+$  cation and free  $\text{K}^+$  ( $\text{NH}_4^+$ ) cations in solution. A “central insertion” pathway was proposed for the cation exchange process. This finding suggested that the kinetic lability of the self-assembled hexadecameric G-quadruplex might be too great to function as a synthetic ion channel. The stabilization of this supramolecule by introducing hydrophobic covalent linkers between the individual G-quartet layers will be pursued in the future. Self-assembly of the modified lipophilic G-quadruplex will provide a “DNA-approach” for building supramolecular ion channels.

### 2.1.1 Cation-Dependent Self-Assembly of DNA G-Quadruplex Structures

The G-quartet structure was first discovered by Gellert and co-workers as the fundamental unit in the formation of hydrogels by 5'-GMP.<sup>89</sup> This cyclic structure consists of two hydrogen-bonding arrays from four guanine subunits, where the  $\text{N}_1\text{H}$  amide/ $\text{O}_6$  and  $\text{N}_2\text{H}$  amide/ $\text{N}_7$  are complementary donor/acceptors. Pinnavaia and co-workers later showed that  $\text{Na}^+$  and  $\text{K}^+$  stabilize diastereomeric G8- $\text{M}^+$  octamers by coordinating to the eight carbonyl oxygens of stacked G-quartets (**Scheme 2.1**).<sup>90</sup> This example demonstrated that different cations may selectively bind to a 5'-GMP self-assembled structure. Since those studies, many nucleosides and oligonucleotides have been shown to form the secondary G-quadruplex structures.<sup>77,91,92</sup> In the last decade, the implicated significance of the G-quadruplex in controlling biological functions has driven

considerable research on the stabilization of DNA and RNA G-quadruplexes.<sup>12,93</sup> By means of melting temperature measurement,<sup>90</sup> dehydration energy calculations,<sup>94</sup> X-ray diffraction and NMR studies,<sup>95,96</sup> insight into the cation selectivity of the G-quadruplex has been established. The combination of the correct size for a cation binding pocket and the desolvation energy of cations determine the selectivity trend of monovalent cations in DNA quadruplex structures. In general, monovalent cations stabilize a DNA quadruplex in the following order:  $K^+ > NH_4^+ > Rb^+, Na^+ > Cs^+, Li^+$ . This difference in cation binding affinity can result in the conformational changes within the DNA G-quadruplex, particularly when different competitive cations are present in solution.<sup>97,98</sup>

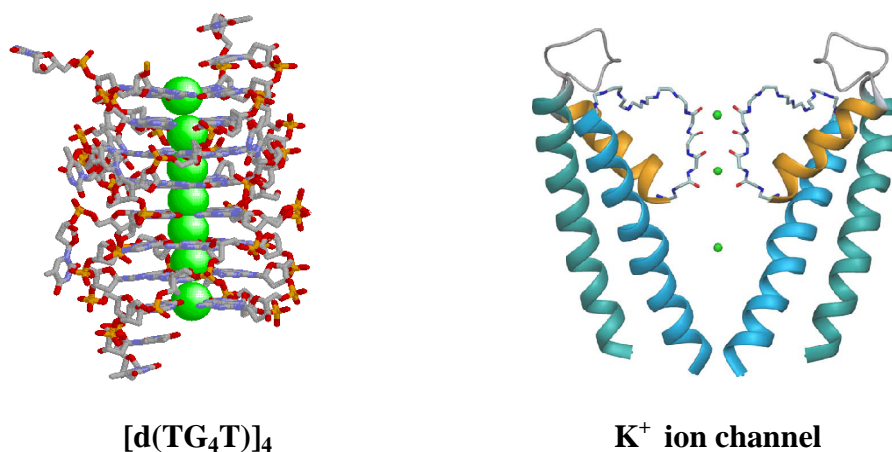


**Scheme 2.1** Schematic structure of (A) G-quartet and (B) G<sub>8</sub>-octamer.

### 2.1.2 DNA G-quadruplex as an Ion Channel Model

The localization of cations bound inside the DNA G-quadruplexes has been achieved directly by crystallography and solid-state NMR. The direct evidence of cation binding site inside a DNA G-quadruplex was reported by Rich and co-workers in their crystallographic study of an *Oxytricha nova* telemetric DNA d(G<sub>4</sub>T<sub>4</sub>G<sub>4</sub>)(Oxy-1.5).<sup>95</sup> The G-quadruplex bound K<sup>+</sup> ions were detected within the central cavity of two G-quartets. Afterward, various crystallographic studies demonstrated that different alkali and alkaline

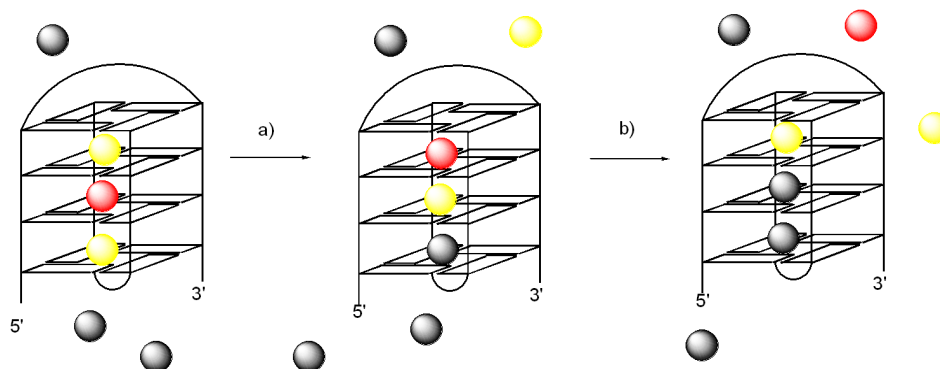
cations, such as  $\text{Na}^+$ ,  $\text{K}^+$ ,  $\text{Ba}^{2+}$ ,  $\text{Sr}^{2+}$ ,  $\text{Pb}^{2+}$ , are sandwiched between two G-quartets.<sup>99,100</sup> One of the excellent examples is Luisi's high-resolution crystal structure of a DNA G-quadruplex formed by oligonucleotide  $[\text{d}(\text{TG}_4\text{T})]_4$  (**Scheme 2.2**).<sup>73</sup> In this parallel-stranded quadruplex, a string of  $\text{Na}^+$  ions located along the central cavities, either within a G-quartet or sandwiched by G-quartets. Solid-state NMR technique also provided complementary evidence of alkali metal cations binding to nucleic acids.<sup>71,101</sup> Griffin and Rovnyak's pioneering work demonstrated the direct observation of  $^{23}\text{Na}^+$  ions bound to the DNA G-quadruplex using  $^{23}\text{Na}$  solid-state NMR.<sup>102</sup> A series of solid-state  $^{23}\text{Na}$  and  $^{39}\text{K}$  NMR methods have been developed by the Wu group that allowed the identification of  $\text{Na}^+$  and  $\text{K}^+$  ions bound to a G-quadruplex, and the determination of cation coordination geometry in a telemetric Oxy-1.5 DNA quadruplex.<sup>101,103</sup> Both crystallography and solid-state NMR studies demonstrated that an array of alkali and alkaline cations can locate within the central channel formed by the stacking G-quartets. The DNA G-quadruplex resembles the crystal structure of natural potassium ion channel formed from *Streptomyces lividans* (**Scheme 2.2**).<sup>104</sup>



**Scheme 2.2** High-resolution crystal structure of a DNA G-quadruplex formed by oligonucleotide [d(TG<sub>4</sub>T)]<sub>4</sub>. b) Natural potassium ion channel.

In addition, solution NMR has been utilized to gain much insight into the structure and dynamics of cation binding by DNA G-quadruplexes.<sup>74,98,105</sup> Pioneering studies by Feigon *et al.* demonstrated the identification of different cation binding sites within the bimolecular G-quadruplex [d(G<sub>4</sub>T<sub>4</sub>G<sub>4</sub>)]<sub>2</sub> in solution.<sup>74,75,106</sup> Using a <sup>15</sup>N-labeled <sup>15</sup>NH<sub>4</sub><sup>+</sup> cation as a probe, they observed three <sup>15</sup>NH<sub>4</sub><sup>+</sup> ions bound in two distinct environments inside the complex: one cation is at the inner binding site, while another two are at the outer binding sites (**Scheme 2.3**). The cation exchange analysis showed that <sup>15</sup>NH<sub>4</sub><sup>+</sup> cations can move in and out of the complex along the central axis of the DNA G-quadruplex. As shown in **scheme 2.3**, in the solution, cation exchange occurred between the inner and outer <sup>15</sup>NH<sub>4</sub><sup>+</sup> ions, as well as between the outer <sup>15</sup>NH<sub>4</sub><sup>+</sup> and solution <sup>15</sup>NH<sub>4</sub><sup>+</sup>. Plavec and co-workers have also used <sup>15</sup>NH<sub>4</sub> as a solution NMR probe to determine the rates of cation exchange within the G-quadruplex formed by [d(G<sub>3</sub>T<sub>4</sub>G<sub>3</sub>)]<sub>2</sub>.<sup>107</sup> They also have used <sup>15</sup>N NMR to identify the formation of mixed-dication intermediates in the <sup>15</sup>NH<sub>4</sub><sup>+</sup>/K<sup>+</sup> ion exchange process that occurs for [d(G<sub>3</sub>T<sub>4</sub>G<sub>3</sub>)]<sub>2</sub>. Recent calculations have predicted that smaller ions such as Li<sup>+</sup> and Na<sup>+</sup>

should move through the DNA G-quadruplex channels with relatively low activation barriers, when compared to the larger  $\text{NH}_4^+$  and  $\text{K}^+$  cations.



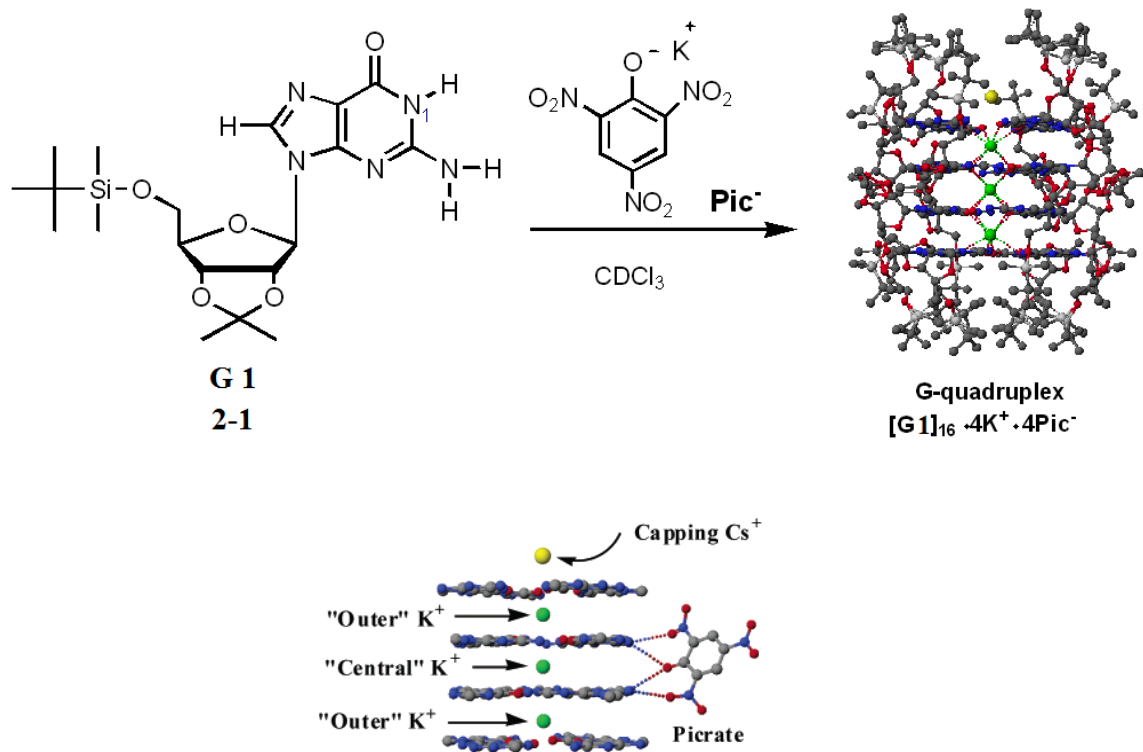
**Scheme 2.3** Schematic representation of  $^{15}\text{NH}_4^+$  movement through the Oxy-1.5 quadruplex. a) bulk  $\text{NH}_4^+$  cation only exchanges with the outer  $^{15}\text{NH}_4^+$ . b) exchange of two bound  $^{15}\text{NH}_4^+$  cations is random. Black, yellow and red ball represent the bulk ammonium ion, and the bound ammonium ions located in outer and inner binding site of the G-quadruplex.

### 2.1.3 Lipophilic G-quadruplexes

The Davis group, and others, have been exploring the properties of lipophilic G-quadruplexes with an eye toward using them as self-assembled ionophores for selective sequestration of radioactive  $^{137}\text{Cs}^+$  and  $^{226}\text{Ra}^{2+}$  and as ion channels for transporting cations across lipid membranes.<sup>108</sup> To design such functional assemblies, it is imperative to understand their structural and dynamic properties. In the presence of cations, 5'-tert-butyltrimethylsilyl-2',3'-isopropylidene guanosine (**G 1**) **2-1** self-assembles into a lipophilic G-quadruplex  $[\text{G } \mathbf{1}]_{16} \cdot 3\text{K}^+ \cdot \text{Cs}^+ \cdot 4\text{pic}^-$  (**Scheme 2.4**). A crystal structure shows the complex to be composed of four stacked G-quartets.<sup>83</sup> This pseudo- $D_4$  symmetric G-quadruplex can be described as a pair of head-to-tail  $C_4$  symmetric  $[\text{G } \mathbf{1}]_8$  octamers that are coaxially stacked on one another in a head-to-head arrangement.<sup>99</sup> The two  $G_8$  octamers use eight carbonyl oxygens to coordinate  $\text{K}^+$  in a square anti-prismatic geometry. A third  $\text{K}^+$ , with a nearly cubic coordination geometry, holds the two  $C_4$



symmetric  $[G\ 1]_8$  octamers together by binding to the two inner G-quartets. A solvated  $Cs^+$  caps the G-quadruplex by sitting in a cavity above one of the outer  $G_4$ -quartets. This capping ion is dynamic in solution since the NMR spectra of the G-quadruplex shows only two sets of signals. If the capping ion was tightly bound, one would expect four sets of NMR signals for the four different G-quartet layers in  $[G\ 1]_{16} \cdot 3K^+ \cdot Cs^+ \cdot 4pic^-$ . The bound cations in these G-quadruplexes have been observed with  $^{23}Na$  and  $^{39}K$  solid-state NMR. For  $^{23}Na$ , all four channel ions (including the capping ion) were resolved. Crystal structures and solution NMR also showed that four phenolate anions hydrogen bond to the two inner G-quartets.



**Scheme 2.4** G-quadruplex formed through self-assembly of **G 1** in the presence of  $K^+DNP^-$ .

Unlike DNA G-quadruplexes, this lipophilic G-quadruplex has no covalent backbone between stacked G-quartet layers. We reasoned that the study of the cation

exchange process between cations in solution and cations bound to the G-quadruplex bound would allow us to evaluate the stability of the G-quadruplex and its potential to function as a transmembrane ion channel.

## **2.2 Mass Spectrometry Shows Mixed-Cation G-Quadruplexes Formed by Sequential Ion Exchange.**

In general, G-quartets are stabilized by monovalent cations in the order  $K^+ > NH_4^+ > Na^+ > Cs^+ > Li^+$ .<sup>5,25</sup> Because of this difference in relative binding strength, the addition of a higher affinity cation to a G-quadruplex containing a weaker binding cation results in replacement of that initially bound ion. Such exchange has been amply demonstrated by solution  $^1H$  NMR in water for  $Na^+/K^+$  exchange in the hairpin G-quadruplex  $d(G_3T_4G_3)_2$ .<sup>94</sup> In that study, exchange between distinct cationic forms of the  $d(G_3T_4G_3)_2$  G-quadruplexes was fast on the NMR chemical shift time scale, giving rise to a single, time-averaged set of signals. In our present case, the different cationic forms of the lipophilic G-quadruplex are in slow exchange on the chemical shift time scale, and what we hypothesized to be mixed-cation intermediates could be readily distinguished from the homomeric all- $Na^+$  and all- $K^+$  G-quadruplexes by solution  $^1H$  NMR (see the following sections). In the DNA study, Feigon and colleagues demonstrated that the free energy of cation dehydration helped determine the relative binding affinity of different ions for DNA G-quartets in water. In an organic solvent, however, free cations are not hydrated, so there may be other factors that determine the cation's binding affinity for the G-quartet in an organic phase. Nonetheless, the mass spectrometric and solution NMR

data, described next, indicate that G-quartets also have a higher affinity for  $K^+$  over  $Na^+$  in organic solvents such as  $CD_2Cl_2$ .

To unequivocally identify mixed-cation G-quadruplexes that form during the  $Na^+/K^+$  ion exchange process, we first used electrospray ionization mass spectrometry (ESI-MS), a powerful method for characterizing noncovalent assemblies.<sup>109</sup> ESI-MS has been used to monitor the formation of G-quadruplexes by a variety of G-nucleosides and G-rich-oligonucleotides.<sup>110,111</sup> To the best of our knowledge, however, the  $Na^+/K^+$  cation exchange process within a G-quadruplex has not been previously characterized by mass spectrometry. Thus, crystalline samples of  $[G1]_{16} \cdot 4 Na^+ \cdot 4 DNP^-$  and  $[G1]_{16} \cdot 4 K^+ \cdot 4 DNP^-$  were prepared according to standard procedures,<sup>83</sup> and their purity was confirmed by both NMR and mass spectrometry. ESI-MS analysis in the positive-ion mode showed distinct peaks for the intact  $Na^+$  and  $K^+$  G-quadruplexes at  $m/z$  7435.3 and 7484.5, respectively (Figure 2.1a,e). These singly charged ions correspond to the molecular weight for the hexadecamer  $[[G \mathbf{1}]_{16} \cdot 3M \cdot 2DNP]^+$ , a species formed in the gas phase by losing one cation (presumably the weakly bound capping ion) and two  $DNP^-$  anions from the starting G-quadruplexes. As depicted in **Figure 2.1b–d**, we then monitored the cation exchange process by adding increasing amounts of  $KPh_4B$  to a solution of  $[G \mathbf{1}]_{16} \cdot 4Na^+ \cdot 4DNP^-$  in 1:1  $CD_2Cl_2/CD_3CN$ . The major peaks in **Figure 2.1b, 2.1c** had  $m/z$  ratios intermediate between the two homomeric species,  $[[G \mathbf{1}]_{16} \cdot 3Na \cdot 2DNP]^+$  and  $[[G \mathbf{1}]_{16} \cdot 3K \cdot 2DNP]^+$ . Significantly, the dominant molecular ion in each titration sample showed a 16 amu increase in mass, corresponding to the sequential displacement of a bound  $Na^+$  by a single  $K^+$  during the titration. For example, **Figure 2.1b**, corresponding to a sample

containing 1 equivalent of  $\text{KPh}_4\text{B}$  for each equivalent of  $[\text{G } \mathbf{1}]_{16}\cdot 4\text{Na}^+\cdot 4\text{DNP}^-$ , showed a significant decrease in the  $[[\text{G } \mathbf{1}]_{16}\cdot 3\text{Na}\cdot 2\text{DNP}]^+$  species ( $m/z$  7435.3) with the concomitant formation of a new major species with  $m/z$  7452.0. This new peak corresponds to a mixed-cation G-quadruplex of formula  $[[\text{G } \mathbf{1}]_{16}\cdot \text{K}\cdot 2\text{Na}\cdot 2\text{DNP}]^+$ . As depicted in **Figure 2.1**, there are two possible isomers for  $[[\text{G } \mathbf{1}]_{16}\cdot \text{K}\cdot 2\text{Na}\cdot 2\text{DNP}]^+$ , depending on whether one of the outer cations or the central cation is first replaced by  $\text{K}^+$ . The addition of a second equivalent of  $\text{KPh}_4\text{B}$  led to the formation of  $[[\text{G } \mathbf{1}]_{16}\cdot 2\text{K}\cdot \text{Na}\cdot 2\text{DNP}]^+$  ( $m/z$  7468.2) as the dominant species in that region of the ESI mass spectrum (Figure 2.1c). Again, as depicted in **Figure 2.1**, there are two possible isomers for this second intermediate. Essentially complete conversion to the  $\text{K}^+$  G-quadruplex ( $m/z$  7484.5) occurred after the addition of just 4 equivalents of  $\text{KPh}_4\text{B}$  to the solution of the  $\text{Na}^+$  G-quadruplex (**Figure 2.1d**). The ESI-MS results depicted in **Figure 2.1** are significant for the following reasons, as this data (1) confirms the pronounced  $\text{K}^+/\text{Na}^+$  binding selectivity shown by this lipophilic G-quadruplex; (2) demonstrate the formation of discrete mixed-cationic assemblies, such as  $[[\text{G } \mathbf{1}]_{16}\cdot \text{K}\cdot 2\text{Na}\cdot 2\text{DNP}]^+$  and  $[[\text{G } \mathbf{1}]_{16}\cdot 2\text{K}\cdot \text{Na}\cdot 2\text{DNP}]^+$ , under conditions where sub-stoichiometric  $\text{K}^+$  is present; and (3) illustrate the stepwise displacement of  $\text{Na}^+$  cations by the stronger binding  $\text{K}^+$  ion. This is the first time, to our knowledge, that mass spectrometric data has revealed the sequential ion exchange process in a G-quadruplex. Such ESI-MS titration experiments should also be informative for understanding the details of structure and ion binding in the rich array of DNA and RNA G-quadruplexes that have been discovered to date.

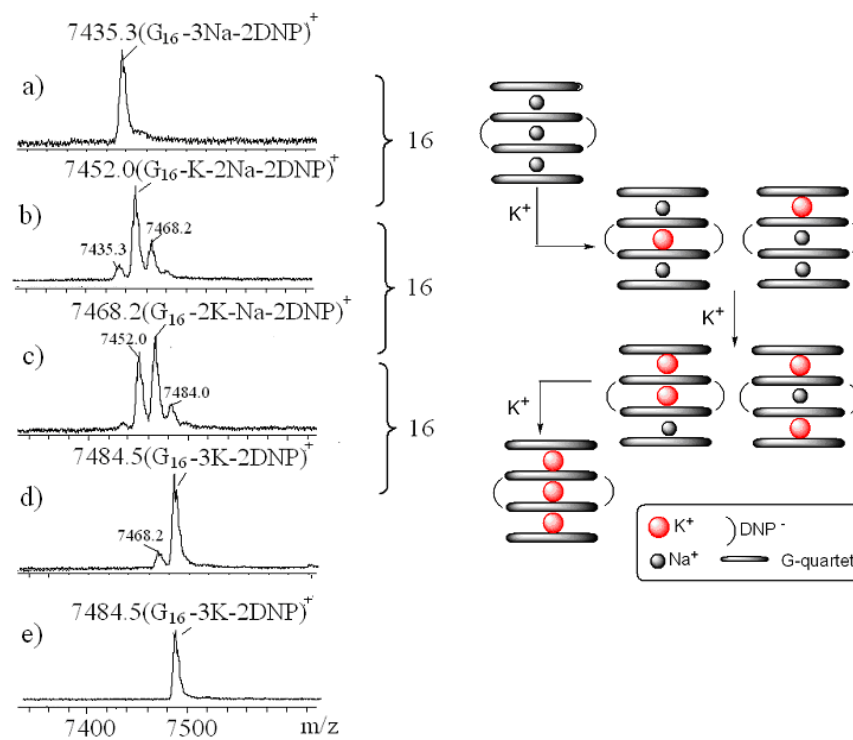


**Figure 2.1** ESI-MS from titration of  $\text{KPh}_4\text{B}$  into a solution of  $[\text{G}1]_{16}\cdot 4\text{Na}^+\cdot 4\text{DNP}^-$  in 1:1  $\text{CD}_2\text{Cl}_2/\text{CD}_3\text{CN}$ . a)  $[\text{G}1]_{16}\cdot 4\text{Na}^+\cdot 4\text{DNP}^-$ ; b) after addition of 1 equivalents of  $\text{KPh}_4\text{B}$ ; c) after addition of 2 equivalents of  $\text{KPh}_4\text{B}$ ; d) after addition of 4 equivalents of  $\text{KPh}_4\text{B}$ ; and e)  $[\text{G}1]_{16}\cdot 4\text{K}^+\cdot 4\text{DNP}^-$ . The diagram illustrates the possible mixed-cation G-quadruplexes that could be formed in the cation exchange process.

### 2.3 Proton NMR Indicates that the Central $\text{Na}^+$ Is the First Cation Exchanged for $\text{K}^+$ in Formation of Mixed $\text{Na}^+$ , $\text{K}^+$ G-Quadruplexes.

ESI-MS analysis of the titration of  $[\text{G}1]_{16}\cdot 4\text{Na}^+\cdot 4\text{DNP}^-$  with  $\text{KPh}_4\text{B}$  provided unequivocal evidence for the formation of the mixed  $\text{Na}^+$ ,  $\text{K}^+$  G-quadruplexes  $[[\text{G}1]_{16}\cdot \text{K}\cdot 2\text{Na}\cdot 2\text{DNP}]^+$  and  $[[\text{G}1]_{16}\cdot 2\text{K}\cdot \text{Na}\cdot 2\text{DNP}]^+$ . However, the isomeric structures of these mixed G-quadruplexes, and the location of bound cations, could not be ascertained from the mass spectrometry data alone. For example, as shown in **Figure 2.1**, the first intermediate formed during  $\text{Na}^+/\text{K}^+$  ion exchange could involve the replacement of either the outer or the centrally bound  $\text{Na}^+$ . In theory, these isomers should be distinguished by

$^1\text{H}$  NMR based on their differences in symmetry. To identify the structures of these discrete intermediates, and to define specific cation exchange pathways, we turned to  $^1\text{H}$  NMR spectroscopy, knowing that the chemical shifts of the G-quartet's amide  $\text{N}_1\text{H}$  protons are sensitive to the identity of the bound cation.<sup>82,94</sup> **Figure 2.2a** shows two distinct  $\text{N}_1\text{H}$  amide peaks for the all- $\text{Na}^+$  G-quadruplex  $[\text{G } \mathbf{1}]_{16}\cdot 4\text{Na}^+\cdot 4\text{DNP}^-$  in 1:1  $\text{CD}_2\text{Cl}_2/\text{CD}_3\text{CN}$ , with the signal at  $\delta$  11.46 ppm corresponding to the  $\text{N}_1\text{H}$  amide for the two inner  $\text{G}_4$ -quartets and the signal at  $\delta$  11.71 ppm due to the outer  $\text{G}_4$ -quartets. In contrast, the G-quartet  $\text{N}_1\text{H}$  amide peaks for the  $\text{K}^+$  G-quadruplex,  $[\text{G } \mathbf{1}]_{16}\cdot 4\text{K}^+\cdot 4\text{DNP}^-$ , occur at  $\delta$  11.35 (inner) and  $\delta$  11.58 ppm (outer), respectively (**Figure 2.2g**).

**Figure 2.2b** shows that two new amide  $\text{N}_1\text{H}$  signals ( $\delta$  11.42 and  $\delta$  11.75 ppm) appear after the addition of 0.5 equivalents of  $\text{KPh}_4\text{B}$  to a solution of  $[\text{G } \mathbf{1}]_{16}\cdot 4\text{Na}^+\cdot 4\text{DNP}^-$ . These new  $\text{N}_1\text{H}$  signals are in slow exchange on the chemical shift time scale with signals for  $[\text{G } \mathbf{1}]_{16}\cdot 4\text{Na}^+\cdot 4\text{DNP}^-$ , a feature that helped us recognize this new species as a mixed  $\text{Na}^+$ ,  $\text{K}^+$  G-quadruplex. Further addition of  $\text{KPh}_4\text{B}$  (1 equivalent) resulted in these new  $\text{N}_1\text{H}$  resonances becoming predominant, while the signals for  $[\text{G } \mathbf{1}]_{16}\cdot 4\text{Na}^+\cdot 4\text{DNP}^-$  greatly diminished (**Figure 2.2c**). The new G-quadruplex in Figure 2.2c has only two  $\text{N}_1\text{H}$  signals (one set for the outer G-quartets and one set for the inner G-quartets), an indication that cation exchange occurred with the central  $\text{Na}^+$  in  $[\text{G } \mathbf{1}]_{16}\cdot 4\text{Na}^+\cdot 4\text{DNP}^-$  to give an intermediate with pseudo- $D_4$  symmetry, namely,  $[[\text{G } \mathbf{1}]_{4(o)}\cdot \text{Na}^+\cdot [\text{G } \mathbf{1}]_{4(i)}\cdot \text{K}^+\cdot [\text{G } \mathbf{1}]_{4(i)}\cdot \text{Na}^+\cdot [\text{G } \mathbf{1}]_{4(o)}]$ . If one of the outer  $\text{Na}^+$  cations had been displaced by the first equivalent of  $\text{K}^+$ , we would expect a lower symmetry hexadecamer,  $[[\text{G } \mathbf{1}]_{4(o)}\cdot \text{K}^+\cdot [\text{G } \mathbf{1}]_{4(i)}\cdot \text{Na}^+\cdot [\text{G } \mathbf{1}]_{4(i)}\cdot \text{Na}^+\cdot [\text{G } \mathbf{1}]_{4(o)}]$ , with four separate signals for its nonequivalent G-quartet layers.

Only after the addition of 2 equivalents of KPh<sub>4</sub>B did the <sup>1</sup>H NMR spectra show that the major G-quadruplex in solution had four new N<sub>1</sub>H amide peaks of similar intensity, consistent with the formation of a mixed hexadecamer of lower symmetry, [[G1]<sub>4(o)</sub>·K<sup>+</sup>·[G1]<sub>4(i)</sub>·K<sup>+</sup>·[G1]<sub>4(i)</sub>·Na<sup>+</sup>·[G1]<sub>4(o)</sub>], where one of the two outer Na<sup>+</sup> cations must have been exchanged for a higher affinity K<sup>+</sup> (see the four labeled peaks in **Figure 2.2d,e**). Conversion into the all-K<sup>+</sup> G-quadruplex was essentially complete after the addition of just 4 equivalents of KPh<sub>4</sub>B (**Figure 2.2f**), a result that was consistent with the ESI-MS titration experiment (**Figure 2.1**).

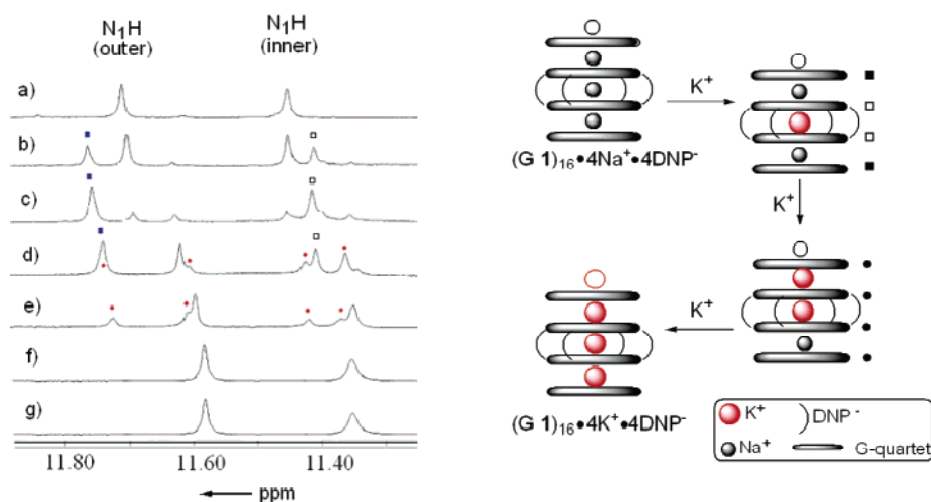


**Figure 2.2** Region of the <sup>1</sup>H NMR spectra (400 MHz) showing the G-quartet NH1 amide protons during titration of [G **1**]<sub>16</sub>·4Na<sup>+</sup>·4DNP<sup>-</sup> with KPh<sub>4</sub>B in 1:1 CD<sub>2</sub>Cl<sub>2</sub>/CD<sub>3</sub>CN. (a) [G **1**]<sub>16</sub>·4Na<sup>+</sup>·4DNP<sup>-</sup>. The mol ratio of added KPh<sub>4</sub>B to the [G **1**]<sub>16</sub>·4Na<sup>+</sup>·4DNP<sup>-</sup> G-quadruplex, is (b) 0.5:1; (c) 1:1; (d) 2:1; (e) 3:1; (f) 4:1; and (g) 12:1.

Both ESI-MS and <sup>1</sup>H NMR titration data indicated that replacement of bound Na<sup>+</sup> by K<sup>+</sup> is a thermodynamically favorable process, particularly since the addition of only 4 equivalents of KPh<sub>4</sub>B led to essentially complete transformation of the all-Na<sup>+</sup> G-quadruplex to the all-K<sup>+</sup> G-quadruplex. In addition, mixed-cationic G-quadruplexes were

detected in conversion of the all- $\text{Na}^+$  G-quadruplex to the all- $\text{K}^+$  G-quadruplex. Since  $\text{Na}^+$  and  $\text{K}^+$  are invisible using standard solution NMR spectroscopy, we were not able to directly detect the different  $\text{Na}^+$  and  $\text{K}^+$  cations bound to various G-quadruplex species during the exchange process. To overcome this limitation, we used the NMR-active  $^{15}\text{NH}_4^+$  as a surrogate for  $\text{K}^+$  to identify the mixed-cation G-quadruplexes formed upon displacement of  $\text{Na}^+$  by a higher affinity cation.

## 2.4 Use of $^{15}\text{NH}_4^+$ Cation to Probe the Cation Exchange Process Within a Lipophilic G-quadruplex

### 2.4.1 NMR Studies with $^{15}\text{NH}_4^+$ Confirm Identity of Mixed-Cationic G-Quadruplexes.

The  $\text{NH}_4^+$  cation has a similar coordination chemistry as  $\text{K}^+$ , and  $^{15}\text{NH}_4^+$  has been used as an NMR probe to localize cations in DNA G-quadruplexes.<sup>74,75</sup> Wong and Wu have also used solid-state  $^{23}\text{Na}$  NMR competition experiments to show that  $\text{K}^+$  and  $\text{NH}_4^+$  have similar free energies of binding to G-quadruplexes.<sup>101,103</sup> NMR titrations indicated that the order of the site exchange between free  $\text{NH}_4^+$  and  $\text{Na}^+$  bound to  $[\text{G } 1]_{16}\cdot 4\text{Na}^+\cdot 4\text{DNP}^-$  was similar to that observed for the  $\text{K}^+/\text{Na}^+$  exchange in Figure 2.2. The  $^1\text{H}$  NMR spectra of various amounts of  $^{15}\text{NH}_4\text{Ph}_4\text{B}$  titrated into a solution of  $[\text{G } 1]_{16}\cdot 4\text{Na}^+\cdot 4\text{DNP}^-$  in 1:1  $\text{CD}_2\text{Cl}_2:\text{CD}_3\text{CN}$  is shown in Figure 2.3. A new set of  $\text{N}_1\text{H}$  amide protons appeared upon addition of one equivalent of  $^{15}\text{NH}_4^+$  to the solution of  $[\text{G } 1]_{16}\cdot 4\text{Na}^+\cdot 4\text{DNP}^-$  (**Figure 2.3c**). This indicates that the first intermediate is a highly symmetric structure. Several new  $\text{N}_1\text{H}$  amide proton peaks appeared as additional



equivalents of  $^{15}\text{NH}_4\text{Ph}_4\text{B}$  were titrated into the solution (**Figure 2.3d-g**). This result indicated that sequential cation exchange continued, and a second, asymmetric G-quadruplex intermediate was formed. Twelve equivalents of  $^{15}\text{NH}_4^+$  cations had to be used to complete the conversion from the all- $\text{Na}^+$  G-quadruplex into the all- $^{15}\text{NH}_4^+$  G-quadruplex (**Figure 2.3g**), providing evidence that  $^{15}\text{NH}_4^+$  cation has a lower preference than does  $\text{K}^+$  for the G-quadruplex. Thus, mixed-cationic species that were in slow exchange with the all- $\text{Na}^+$  and all- $\text{NH}_4^+$  forms of the G-quadruplexes were identified by their separate sets of  $^1\text{H}$  NMR signals.

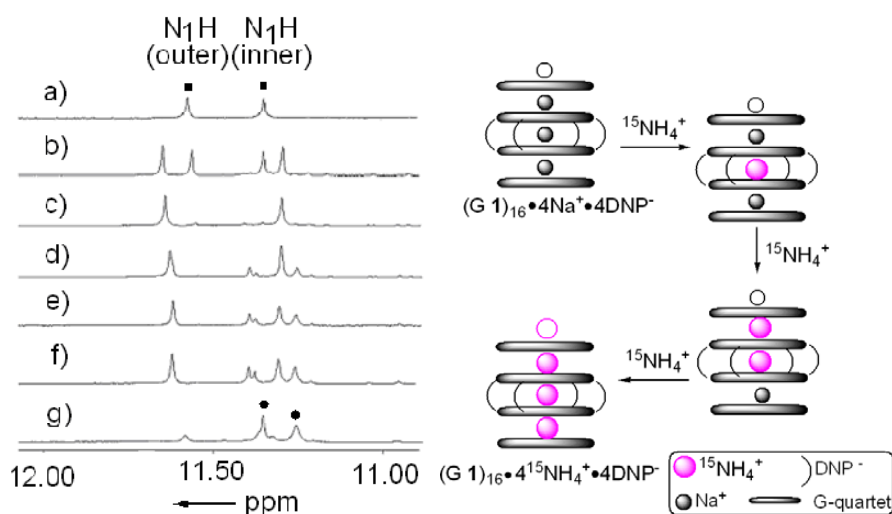


**Figure 2.3** A region of the  $^1\text{H}$  NMR spectra (400 MHz) for titration of  $^{15}\text{NH}_4\text{Ph}_4\text{B}$  into a solution of  $(\text{G } 1)_{16} \cdot 4\text{Na}^+ \cdot 4\text{DNP}^-$  in 1:1  $\text{CD}_2\text{Cl}_2:\text{CD}_3\text{CN}$  at  $20^\circ\text{C}$ . The signals for the amide  $\text{N}_{1\text{H}}$  protons of the G-quartets are shown. a)  $(\text{G } 1)_{16} \cdot 4\text{Na}^+ \cdot 4\text{DNP}^-$ . The mole ratio of  $^{15}\text{NH}_4^+$  to  $(\text{G } 1)_{16} \cdot 4\text{Na}^+ \cdot 4\text{DNP}^-$  is b) 0.5:1; c) 1:1; d) 2:1; e) 3:1; f) 4:1; g) 12:1.

Both 2-D  $^{15}\text{N}-^1\text{H}$  HSQC-ROESY<sup>112</sup> and  $^1\text{H}-^1\text{H}$  NOESY data (**Figure 2.4**) for the all- $\text{NH}_4^+$  species  $[\text{G } 1]_{16} \cdot 4 \text{NH}_4^+ \cdot 4\text{DNP}^-$  showed two types of bound  $^{15}\text{NH}_4^+$ , with one cation occupying the central location between the inner G-quartets and two  $^{15}\text{NH}_4^+$  cations bound to the symmetry-related outer sites. The  $^{15}\text{N}-^1\text{H}$  HSQC spectrum in **Figure 2.4a** shows two cross-peaks between the larger  $^{15}\text{N}$  signal at  $\delta$  30.2 ppm and the larger

$^{15}\text{N}$ -decoupled  $^1\text{H}$  signal at  $\delta$  7.19 ppm. This correlation corresponds to the two  $^{15}\text{NH}_4^+$  cations in the outer cation binding sites. The other cross-peak between the  $^{15}\text{N}$  signal at  $\delta$  27.4 ppm and the  $^1\text{H}$  signal at  $\delta$  7.30 ppm corresponds to  $^{15}\text{NH}_4^+$  in the central binding site. These assignments were confirmed by NOESY (**Figure 2.4b**). NOE cross-peaks are observed between the two different  $^{15}\text{NH}_4^+$  signals and the  $\text{N}_1\text{H}$  amide protons for the inner and outer G-quartets. The  $^{15}\text{NH}_4^+$  cation bound in the central binding site shows cross-peaks only with the  $\text{N}_1\text{H}$  amide of the inner G-quartet ( $\delta$  11.41 ppm). In contrast, the stronger  $^{15}\text{NH}_4^+$  signals show cross-peaks with  $\text{N}_1\text{H}$  amide protons for both the inner and the outer G-quartets, as would be expected for an ammonium cation bound between both types of layers. No  $^{15}\text{NH}_4^+$  binding to the capping site was observed in these solution studies.

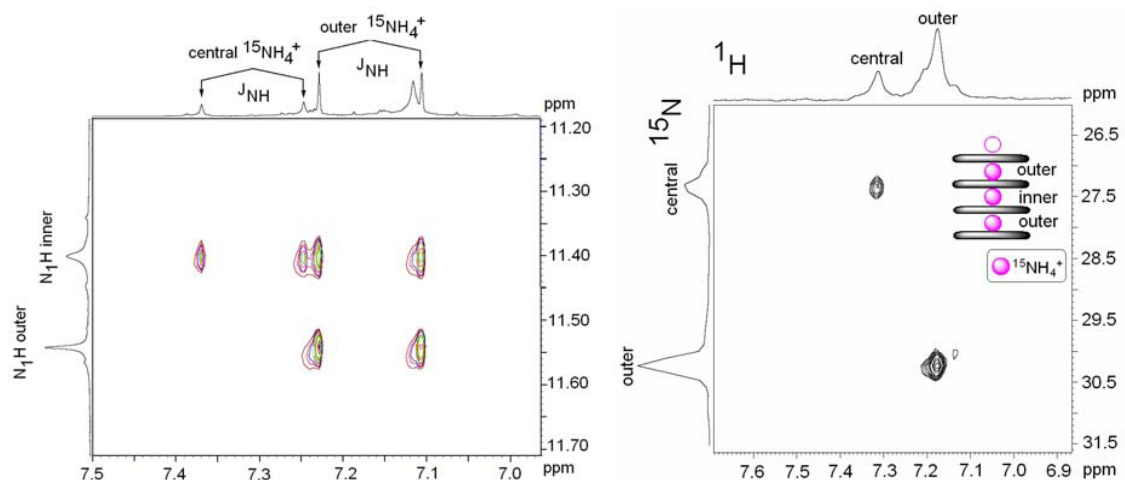


**Figure 2.4** a) Region from the 2-D  $^{15}\text{N}$ - $^1\text{H}$  HSQC-ROESY NMR spectrum of  $[\text{G } 1]_{16}\cdot 4\text{NH}_4^+\cdot 4\text{DNP}^-$  in 1:1  $\text{CD}_2\text{Cl}_2/\text{CD}_3\text{CN}$  showing cross-peaks between the  $^{15}\text{N}$  NMR resonances and the  $^{15}\text{N}$ -filtered  $^1\text{H}$  resonances. b) Region of the 2-D  $^1\text{H}$ - $^1\text{H}$  NOESY NMR spectra of  $[\text{G } 1]_{16}\cdot 4\text{NH}_4^+\cdot 4\text{DNP}^-$  in 1:1  $\text{CD}_2\text{Cl}_2/\text{CD}_3\text{CN}$  showing cross-peaks between the  $\text{N}_1\text{H}$  amide resonances and the  $^1\text{H}$  resonances for the bound  $\text{NH}_4^+$  cations. Both spectra were recorded on a 1 mM sample at 20 °C using a 500 MHz NMR spectrometer.

The  $\text{Na}^+/\text{K}^+$  exchange data in **Figure 2.2** suggest that the central cation in  $(\text{G } \mathbf{1})_{16}\cdot 4\text{Na}^+\cdot 4\text{DNP}^-$ , which exchanges first, is bound less tightly than the outer cations coordinated within  $\text{G}_8$ -octamers. This hypothesis was supported by  $^{15}\text{N}$  longitudinal relaxation measurements for the bound  $\text{NH}_4^+$  cations in  $[\text{G } \mathbf{1}]_{16}\cdot 4\text{NH}_4^+\cdot 4\text{DNP}^-$ . Thus,  $^{15}\text{N}$   $T_1$  spin–lattice relaxation times were found to be 12.5 s for the  $^{15}\text{N}$  signal of the outer ions at  $\delta$  30.2 ppm and just 2.3 s for the central ion at  $\delta$  27.4 ppm. Although there are many factors that influence  $T_1$  relaxation, the much shorter value for the centrally bound  $^{15}\text{NH}_4^+$  may be because it is undergoing chemical exchange with solvated cations more readily than are the more tightly bound  $^{15}\text{NH}_4^+$  cations in the two outer binding sites.

#### 2.4.2 Determination of the First Intermediate in $\text{Na}^+/\text{}^{15}\text{NH}_4^+$ Cation Exchange

Using  $^{15}\text{NH}_4^+$  as a visible replacement ion for  $\text{K}^+$ , we performed a series of  $^{15}\text{N}$ -filtered  $^1\text{H}$  NMR experiments to unambiguously assign the two different cation binding sites within the G-quadruplex.<sup>84</sup> The  $^{15}\text{N}$ -filtered and  $^{15}\text{N}$ -decoupled  $^1\text{H}$  NMR spectra in **Figure 2.5** show the  $^{15}\text{NH}_4^+/\text{Na}^+$  exchange that occurs upon titration of  $^{15}\text{NH}_4\text{Ph}_4\text{B}$  into a solution of  $[\text{G}\mathbf{1}]_{16}\cdot 4\text{Na}^+\cdot 4\text{DNP}^-$ . The composition of mixed-cationic G-quadruplexes varies with added  $^{15}\text{NH}_4^+$ . After the addition of 1 equivalent of  $^{15}\text{NH}_4^+$  to  $[\text{G } \mathbf{1}]_{16}\cdot 4\text{Na}^+\cdot 4\text{DNP}^-$  (**Figure 2.5b**), one resonance ( $\delta$  7.10 ppm) was observed in the  $^{15}\text{N}$ -filtered  $^1\text{H}$  NMR spectra, consistent with  $^{15}\text{NH}_4^+$  being bound to a single site within the hexadecameric G-quadruplex. As the amount of  $^{15}\text{NH}_4^+$  increased, additional  $^{15}\text{N}$ -decoupled signals for  $\text{NH}_4^+$  resonances were observed, indicating further displacement of specific  $\text{Na}^+$  ions by  $^{15}\text{NH}_4^+$ . The titration sample containing 12 equivalents of  $^{15}\text{NH}_4\text{Ph}_4\text{B}$  showed two  $^{15}\text{NH}_4^+$  proton peaks (in a 1:2 ratio) at  $\delta$  7.31 ppm and  $\delta$  7.17

ppm, respectively (**Figure 2.5f**). This pattern is consistent with the structure of the all- $\text{NH}_4^+$  G-quadruplex  $(\text{G } \mathbf{1})_{16} \cdot 4^{15}\text{NH}_4^+ \cdot 4\text{DNP}^-$  (**Figure 2.5g**). The other two equal intensity  $^{15}\text{NH}_4^+$  signals that appear and then disappear during the course of the titration (marked by blue circles in **Figure 2.5c–f**) are due to a G-quadruplex that contains two bound  $^{15}\text{NH}_4^+$  cations and one bound  $\text{Na}^+$  cation, namely,  $[[\text{G } \mathbf{1}]_{4(o)} \cdot ^{15}\text{NH}_4^+ \cdot [\text{G } \mathbf{1}]_{4(i)} \cdot ^{15}\text{NH}_4^+ \cdot [\text{G } \mathbf{1}]_{4(i)} \cdot \text{Na}^+ \cdot [\text{G } \mathbf{1}]_{4(o)}]$ .

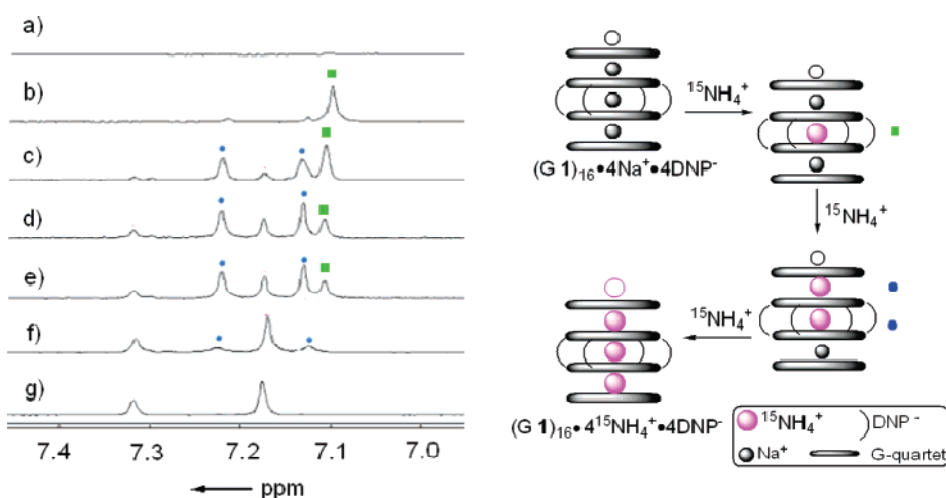


**Figure 2.5**  $^{15}\text{N}$ -filtered  $^1\text{H}$  NMR (500 MHz) spectra of  $^{15}\text{NH}_4\text{Ph}_4\text{B}$  titration the solution of  $[\text{G } \mathbf{1}]_{16} \cdot 4\text{Na}^+ \cdot 4\text{DNP}^-$  in 1:1  $\text{CD}_2\text{Cl}_2/\text{CD}_3\text{CN}$  with mol ratio at (a) 0:1; (b) 1:1; (c) 2:1; (d) 3:1; (e) 4:1; (f) 12:1; and (g)  $[\text{G } \mathbf{1}]_{16} \cdot 4^{15}\text{NH}_4^+ \cdot 4\text{DNP}^-$ .

We reasoned that the species formed in **Figure 2.5b**, after the addition of 1 equivalent of  $^{15}\text{NH}_4\text{Ph}_4\text{B}$  to  $[\text{G } \mathbf{1}]_{16} \cdot 4\text{Na}^+ \cdot 4\text{DNP}^-$ , must be a  $D_4$  symmetric mixed G-quadruplex, with the  $^{15}\text{NH}_4^+$  cation bound in the central cavity between two  $\text{G}_8\text{-Na}^+$ -octamers. This assignment for the species  $[[\text{G } \mathbf{1}]_{4(o)} \cdot \text{Na}^+ \cdot [\text{G } \mathbf{1}]_{4(i)} \cdot ^{15}\text{NH}_4^+ \cdot [\text{G } \mathbf{1}]_{4(i)} \cdot \text{Na}^+ \cdot [\text{G } \mathbf{1}]_{4(o)}]$  was confirmed by a 2-D  $^1\text{H}$ ,  $^1\text{H}$  NOESY experiment. Figure 2.6 shows a cross-peak between the  $^{15}\text{NH}_4^+$  protons centered at  $\delta$  7.10 ppm and the  $\text{N}_1\text{H}$  protons of the inner G-

quartet layers at  $\delta$  11.40 ppm. In marked contrast, there were no  $^1\text{H}$ - $^1\text{H}$  NOEs between this bound  $^{15}\text{NH}_4^+$  and the  $\text{N}_1\text{H}$  amide of the outer G-quartet layers at  $\delta$  11.79 ppm.

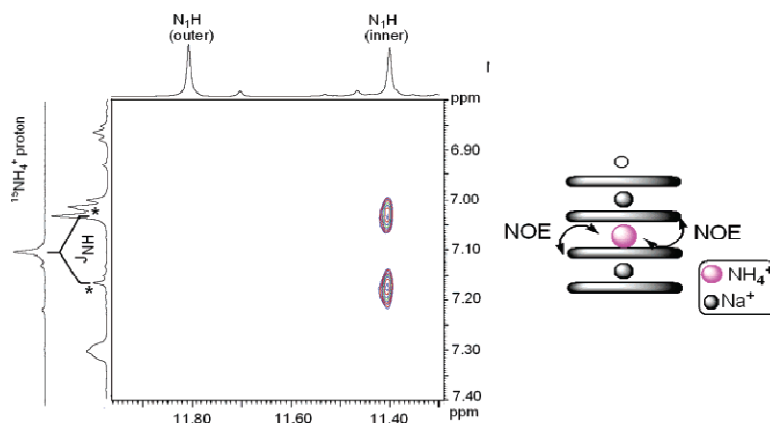


**Figure 2.6** Portion of a NOESY spectrum of a 1:1  $^{15}\text{NH}_4$  Ph<sub>4</sub>B titration into  $[\text{G } \mathbf{1}]_{16} \cdot 4\text{Na}^+ \cdot 4\text{DNP}^-$  in 1:1  $\text{CD}_2\text{Cl}_2/\text{CD}_3\text{CN}$ . The 2-D spectrum shows the NOE cross-peak between the  $^{15}\text{NH}_4^+ \text{H}$  resonance with the  $\text{N}_1\text{H}$  of the inner G-quartet layer. The chemical shifts of  $\delta$  11.79 and 11.40 ppm correspond to the  $\text{N}_1\text{H}$  amide protons for the outer and inner G-quartet layers. The chemical shift of the  $^{15}\text{NH}_4^+$  proton was confirmed from the  $^{15}\text{N}$  decoupled  $^1\text{H}$  NMR spectrum showing a single peak at  $\delta$  7.10 ppm.

The NMR data in **Figures 2.5 and 2.6** conclusively demonstrate that the initial  $\text{NH}_4^+/\text{Na}^+$  cation exchange occurs between solvated  $^{15}\text{NH}_4^+$  and the centrally bound  $D_4$  symmetric  $\text{Na}^+$  cation to give  $[[\text{G } \mathbf{1}]_{4(o)} \cdot \text{Na}^+ \cdot [\text{G } \mathbf{1}]_{4(i)} \cdot ^{15}\text{NH}_4^+ \cdot [\text{G } \mathbf{1}]_{4(i)} \cdot \text{Na}^+ \cdot [\text{G } \mathbf{1}]_{4(o)}]$  as the first discrete intermediate in the cation exchange process.

### 2.4.3 Characterization of the Second Intermediate in the $\text{Na}^+ / ^{15}\text{NH}_4^+$ Cation Exchange Process

A series of 1D selective NOE analyses was carried out on the solution of  $(\text{G } \mathbf{1})_{16} \cdot 4\text{Na}^+ \cdot 4\text{DNP}^-$  that contained 2 equivalents of  $^{15}\text{NH}_4\text{Ph}_4\text{B}$  in 1:1  $\text{CD}_2\text{Cl}_2:\text{CD}_3\text{CN}$ .

**Figure 2.7** shows the selective NOE data that allowed to identify a mixed 2:1  $\text{NH}_4^+/\text{Na}^+$

species,  $[[G \mathbf{1}]_{4(o)} \cdot ^{15}NH_4^+ \cdot [G \mathbf{1}]_{4(i)} \cdot ^{15}NH_4^+ \cdot [G \mathbf{1}]_{4(i)} \cdot Na^+ \cdot [G \mathbf{1}]_{4(o)}]$  as the second intermediate in the exchange process. In the N1H proton region, the two stronger peaks at  $\delta 11.79$  and  $\delta 11.40$  ppm were irradiated first. No NOE was observed between  $^{15}NH_4^+$  and the N1H proton of the outer layer at  $\delta 11.79$  ppm (see bottom trace in **Figure 2.7b**). Only the N1H amide proton of the inner layer at  $\delta 11.40$  ppm had a selective NOE with  $^{15}NH_4^+$  protons, showing a pair of peaks (due to 15N-1H coupling) in the  $^{15}NH_4^+$  region (labeled with green). These data agree with the previous assignment that the first intermediate in the exchange process is asymmetric G-quadruplex  $[G \mathbf{1}]_{4(o)} \cdot Na^+ \cdot [G \mathbf{1}]_{4(o)} \cdot ^{15}NH_4^+ \cdot [G \mathbf{1}]_{4(o)} \cdot Na^+ \cdot [G \mathbf{1}]_{4(o)}$ . It was noticed that the N1H signal at  $\delta 11.40$  ppm also correlated with another  $^{15}NH_4^+$  proton in a different intermediate (blue 'i' label in Figure 2.7b). This finding suggested the overlap of N1H amide protons of the second intermediate with that of the first intermediate at  $\delta 11.40$  ppm. The overlap of N1H peaks probably results from the similar chemical environment of the "inner" G-quartets in these two intermediates. We next irradiated the G-quartet N1H signal at  $\delta 11.35$  ppm, a new peak in the titration solution. Two new  $^{15}NH_4^+$  resonances displayed selective NOEs to this amide peak at  $\delta 11.35$  ppm. One  $^{15}NH_4^+$  was the same as previously identified to be part of the second intermediate (blue 'i' label in Figure 2.7b). The other  $^{15}NH_4^+$  signal corresponded to one that also had an NOE with the N1H proton at  $\delta 11.51$  ppm. Combining all of this information from the selective NOE experiments allowed us to identify the second intermediate as  $[G \mathbf{1}]_{4(o)} \cdot ^{15}NH_4^+ \cdot [G \mathbf{1}]_{4(i)} \cdot ^{15}NH_4^+ \cdot [G \mathbf{1}]_{4(i)} \cdot Na^+ \cdot [G \mathbf{1}]_{4(o)}$ . Because of its asymmetric structure, the four G-quartet layers of this mixed cation G-quadruplex have quite different chemical environments, with four N1H resonances at  $\delta 11.79$ , 11.40, 11.35 and 11.51 ppm, respectively.

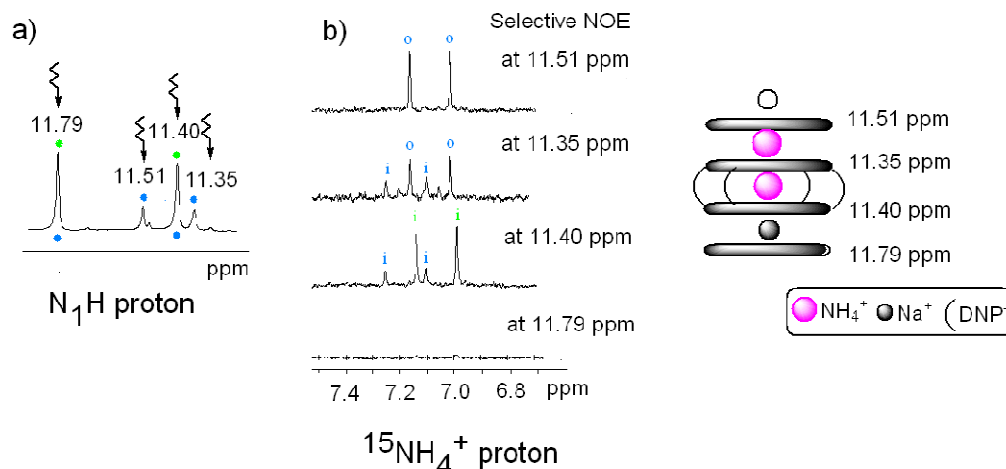
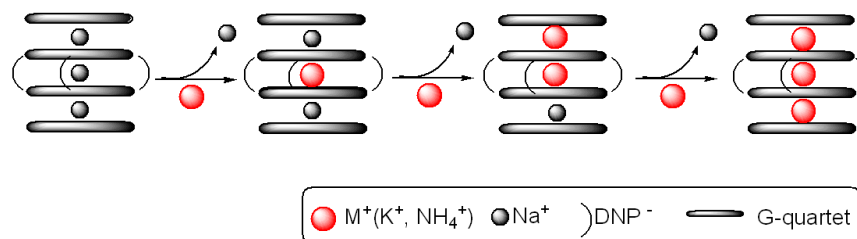


**Figure 2.7** Selective NOE spectra for amide N1H peaks of  $[G \mathbf{1}]_{16} \cdot 4\text{Na}^+ \cdot 4\text{DNP}^-$  titrated with 2 equivalents of  $^{15}\text{NH}_4\text{Ph}_4\text{B}$  in 1:1  $\text{CD}_2\text{Cl}_2:\text{CD}_3\text{CN}$ . Left: a) N1H region of  $^1\text{H}$  NMR spectrum (green dots indicate the N1H amide proton from the first intermediate; blue dots indicate the N1H amide proton from the second intermediate); b)  $^{15}\text{NH}_4^+$  proton region showing selective NOE correlation to amide proton at  $\delta 11.51$ ,  $\delta 11.35$ ,  $\delta 11.40$  and  $\delta 11.79$  ppm, respectively. Right: structural scheme for the second intermediate  $[G \mathbf{1}]_{4(o)} \cdot \text{Na}^+ \cdot [G \mathbf{1}]_{4(i)} \cdot ^{15}\text{NH}_4^+ \cdot [G \mathbf{1}]_{4(i)} \cdot ^{15}\text{NH}_4^+ \cdot [G \mathbf{1}]_{4(o)}$  formed during the  $\text{Na}^+ / \text{NH}_4^+$  exchange process, with the assignments for the different G-quartet N1H amide protons.

## 2.5 Cation Exchange Pathway in the Lipophilic G-Quadruplex

Firm identification of these mixed-cationic G-quadruplexes using the combined ESI-MS and  $^1\text{H}$ ,  $^{15}\text{N}$  NMR data, allowed us to define a pathway for exchange of monovalent cations in this lipophilic G-quadruplex (**Scheme 2.5**). Thus, higher affinity cations such as  $\text{K}^+$  and  $\text{NH}_4^+$  preferentially displace the central  $\text{Na}^+$  cation in the G-quadruplex  $[G \mathbf{1}]_{16} \cdot 4\text{Na}^+ \cdot 4\text{DNP}^-$  to give the pseudo- $D_4$  symmetric mixed-cation G-quadruplex  $[[G \mathbf{1}]_{4(o)} \cdot \text{Na}^+ \cdot [G \mathbf{1}]_{4(i)} \cdot ^{15}\text{NH}_4^+ \cdot [G \mathbf{1}]_{4(i)} \cdot \text{Na}^+ \cdot [G \mathbf{1}]_{4(o)}]$  as the first intermediate. Consequently, sequential exchange of the two tighter-bound outer cations finished the ion exchange process. Control experiments, where components were mixed in the appropriate ratios, confirmed that the process depicted in **Scheme 2.5** is under complete thermodynamic control (data not shown).

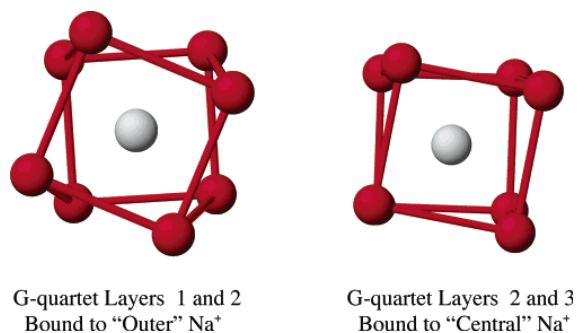


**Scheme 2.5** Proposed central insertion pathway for cation exchange in the lipophilic G-quadruplex system.

Why is it easier to displace the central  $\text{Na}^+$  ion in  $[\text{G } \mathbf{1}]_{16} \cdot 4\text{Na}^+ \cdot 4\text{DNP}^-$ , as opposed to the ions in the outer binding sites of the G-quadruplex? We propose that differences in the cations' octahedral coordination geometries at these separate binding sites may be responsible for the relative facility of cation exchange. Crystal structures for the  $[\text{G } \mathbf{1}]_{16} \cdot 4\text{M}^+ \cdot 4\text{A}^-$  system show that the central cation in this hexadecameric assembly has an almost cubic coordination geometry with the eight oxygen atoms of the two inner G-quartets.<sup>113</sup> In contrast, the oxygen ligands that sandwich the outer  $\text{Na}^+$  cations are twisted more toward square anti-prismatic coordination geometry. Cubic coordination geometry is relatively rare because of the electrostatic repulsion that occurs between the ligand atoms that eclipse each other.<sup>114</sup> The anti-prismatic geometry, on the other hand, is usually more favorable since the ligand atoms are twisted, so as to minimize ligand–ligand contacts while maintaining an optimum ligand– $\text{M}^+$  distance (Scheme 2.6). This influence of coordination geometry on the interaction energy of cations within  $\text{G}_8\text{–M}^+$  octamers has been addressed recently by Meyer and co-workers using DFT calculations.<sup>115</sup> They found that a  $\text{G}_8\text{–Na}^+$  octamer with square anti-prismatic coordination was more stable (by about 9 kcal/mol) than a  $\text{G}_8\text{–Na}^+$  octamer with a cubic coordination environment. We propose that, because of these differences in coordination geometry in  $[\text{G } \mathbf{1}]_{16} \cdot 4\text{Na}^+ \cdot 4\text{DNP}^-$ , the central cation is bound less strongly than are the



outer cations and, therefore, exchanges more readily with the higher affinity  $K^+$  or  $NH_4^+$ . Indeed, X-ray data show that the separation between the two inner G-quartets is greater than the average separation between the inner and the outer G-quartet layers. There is more space in the central ion binding site than in the outer sites.



**Scheme 2.6** These depictions are taken from the crystal structure for  $[G\ 1]_{16} \cdot 4Na^+ \cdot 4pic^-$  (ref 16). The illustrations show the octahedral coordination geometry for one of the outer  $Na^+$  cations (on the left) and for the central  $Na^+$  (right). The central  $Na^+$  has a almost cubic coordination geometry, whereas the oxygen ligands are twisted toward the energetically more favorable square anti-prism geometry for the outer  $Na^+$ .

This central cation may serve to help dimerize discrete  $G_8-M^+$  octamer units into more highly ordered superstructures. Indeed, we have previously shown for another lipophilic G-quadruplex that the  $K^+$  ion concentration can influence the degree of self-association.<sup>21</sup> Thus, at low  $K^+$  concentrations, 5'-(3,5-bis(methoxy)benzoyl)-2',3'-isopropylidene (**G 2**) forms an octamer. Upon the addition of extra  $K^+$ , these  $[G\ 2]_8 \cdot K^+$  octamers dimerize to form a stable  $[G\ 2]_{16}$ -hexadecamer in solution. A similar phenomenon has been seen for the tetrahymena telomere sequence d(T<sub>2</sub>G<sub>4</sub>) and for the human telomere sequence d(TTAGGG), which are both monomeric G-quadruplexes at lower  $K^+$  ion concentrations but form head-to-head G-quadruplex dimers at higher  $K^+$  ion concentrations.

## 2.6 The Larger Cs<sup>+</sup> Cation, But Not the Smaller Li<sup>+</sup>, Can Displace the Central Cation in the Na<sup>+</sup> G-Quadruplex.

The final experiments in this study were based on the hypothesis that the near cubic coordination geometry for the central cation binding site should accommodate a larger cation much more readily than a smaller cation. We reasoned that a larger cation should maximize the separation between the eclipsing oxygen atoms within the central ion binding site. As shown in **Figure 2.8**, this hypothesis appears reasonable, as we could substitute this position with Cs<sup>+</sup> ( $r = 1.67 \text{ \AA}$ ), a large cation that typically is not thought to stabilize G<sub>8</sub>-octamers. Thus, the addition of 8 equivalents of CsPh<sub>4</sub>B to a solution of the Na<sup>+</sup> G-quadruplex led to the telltale formation of two new G-quartet N<sub>1</sub>H amide signals, consistent with displacement of the central Na<sup>+</sup> cation and formation of a pseudo-*D*<sub>4</sub> symmetric G-quadruplex  $[[\text{G } \mathbf{1}]_{4(o)} \cdot \text{Na}^+ \cdot [\text{G } \mathbf{1}]_{4(i)} \cdot \text{Cs}^+ \cdot [\text{G } \mathbf{1}]_{4(i)} \cdot \text{Na}^+ \cdot [\text{G } \mathbf{1}]_{4(o)}]$ . In marked contrast, the addition of 10 equivalents of LiPh<sub>4</sub>B to the same Na<sup>+</sup> G-quadruplex gave no noticeable formation of any mixed-cationic species. Thus, unlike Cs<sup>+</sup> ( $r = 1.67 \text{ \AA}$ ), the smaller Li<sup>+</sup> ( $r = 0.59 \text{ \AA}$ ) does not displace Na<sup>+</sup> ( $r = 0.97 \text{ \AA}$ ) from the central ion binding site in this G-quadruplex. These experiments show that new, mixed-cationic G-quadruplexes can be rationally prepared based on the combined structural information from X-ray crystallography, ESI mass spectrometry, and solution NMR spectroscopy. These results also suggest that large ions such as Cs<sup>+</sup> may well stabilize higher ordered DNA G-quadruplexes that are capable of forming head-to-head dimers with a cubic coordination geometry.<sup>116</sup>

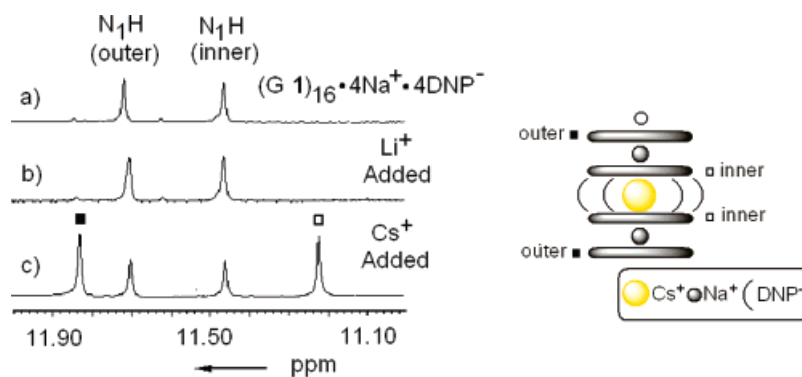


**Figure 2.8**  $^1\text{H}$  NMR spectra of  $\text{N}_1\text{H}$  region of different G-quadruplex solutions in  $\text{CD}_2\text{Cl}_2/\text{CD}_3\text{CN}$  at  $20^\circ\text{C}$ . (a)  $[\text{G } \mathbf{1}]_{16}\cdot 4\text{Na}^+\cdot 4\text{DNP}^-$ ; (b) 10:1 mol ratio of  $\text{LiPh}_4\text{B}$  and  $[\text{G } \mathbf{1}]_{16}\cdot 4\text{Na}^+\cdot 4\text{DNP}^-$ ; (c) 8:1 mol ratio of  $\text{CsPh}_4\text{B}$ ; and  $[\text{G } \mathbf{1}]_{16}\cdot 4\text{Na}^+\cdot 4\text{DNP}^-$ .

## 2.7 Conclusion

In summary, we have studied the cation exchange between competitive cations in solution and  $\text{Na}^+$  ions bound to the lipophilic G-quadruplex  $[\text{G } \mathbf{1}]_{16}\cdot 4\text{Na}^+\cdot 4\text{DNP}^-$ . Cations with a stronger binding affinity for G-quadruplexes, such as  $\text{K}^+$ , drive the cation exchange process. Both ESI-MS and NMR measurements of the  $\text{K}^+$  titration into  $[\text{G } \mathbf{1}]_{16}\cdot 4\text{Na}^+\cdot 4\text{DNP}^-$  revealed that cation exchange is a sequential process, as discrete mixed-cation intermediates were detected. Using the  $^{15}\text{NH}_4^+$  cation as a probe, the identity of these mixed-cation G-quadruplex isomers was determined by  $^{15}\text{N}$ -filtered  $^1\text{H}$  NMR, NOESY, and selective NOE experiments. A central insertion pathway, in which free cations first replace the central cation in  $[\text{G } \mathbf{1}]_{16}\cdot 4\text{Na}^+\cdot 4\text{DNP}^-$ , is operative in this lipophilic G-quadruplex. A structural rationale, based on the different solid-state octahedral coordination geometries in  $[\text{G } \mathbf{1}]_{16}\cdot 4\text{Na}^+\cdot 4\text{DNP}^-$ , was proposed to explain the differences in site exchange between the central and the outer binding sites for these lipophilic G-quadruplexes.

The strategy that we have outlined in this chapter may also be useful for identification of specific ion exchange pathways in G-quadruplexes formed by DNA and RNA oligonucleotides, particularly for those systems that have been shown to form dimeric G-quadruplexes either in the solid-state or in solution. Finally, these mechanistic studies on cation exchange, which clearly couple aspects of the crystal structure to solution state properties, should help us better understand the factors that control assembly and disassembly of lipophilic G-quadruplexes. Such knowledge will guide our future efforts to build selective ionophores and synthetic ion channels. For example, unlike in DNA G-quadruplexes, the cations in these lipophilic G-quadruplexes apparently do not move through the ends of the central channel. In fact, the cation in the middle of the assembly is the easiest to displace. Thus, it is likely that covalent side chains will be needed to link together lipophilic G-units so as to generate an appropriate building block for a synthetic ion channel. Such covalent linkages should stabilize these G-quadruplex structures.

## Chapter 3. Large and Stable Transmembrane Pores from a Guanosine-Bile Acid Conjugate

The majority of this chapter has been published in reference 117:

- Ma, L.; Melegari, M.; Colombini, M.; Davis, J. T. “Large and Stable Transmembrane Pores from Guanosine-Bile Acid Conjugates” *J. Am. Chem. Soc.* **2008**, *130*, 2938-2939.

### 3.1 Introduction:

The research in this chapter reports that the guanosine-lithocholate **3-1** is able to self-assemble into discrete synthetic ion channels in phospholipid membranes (**Figure 3.1**).<sup>117</sup> The pores are large (nS conductance) and stable, with “open” times of seconds, distinguishing them from most synthetic channels, which typically conduct in the pS range with millisecond lifetimes.

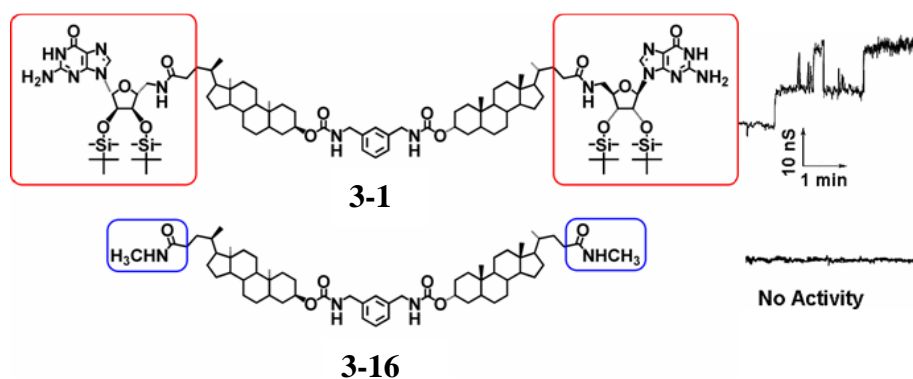


**Figure 3.1** Ditopic G-sterol **3-1** and control bis-lithocholamide **3-16**. Typical traces of conductance vs. time, after addition of **3-1** or **3-16**, are depicted. See Reference 115 for detail.

The preliminary results reported in chapter 2 indicate that cation exchange between cations bound to a lipophilic G-quadruplex and free cations in solution proceed

through a “central channel” pathway. The data suggest that the cation sandwiched between two  $(G\ 1)_8 \cdot M^+$  octamers within the lipophilic G-quadruplex is more dynamic than the “outer” cations located inside the individual  $(G\ 1)_8 \cdot M^+$  octamers. This finding was consistent with our group’s previous results that  $(G\ 1)_8 \cdot M^+$  octamers are building blocks for the self-assembled lipophilic G-quadruplex.<sup>113,118</sup> Under typical experimental conditions, the lipophilic G-quadruplexes are thermodynamically stable, but they are kinetically labile. The G-quadruplex is a self-assembly of 16 subunits held together through the non-covalent interactions, such as hydrogen bonds,  $\pi$ - $\pi$  stacking and cation-dipole interactions. Thus these structures would be much more vulnerable to dissociate than their covalent analogs.

A ditopic design strategy was employed to develop transmembrane ion channel. A hybrid molecule that conjugates a hydrophobic linker with two capping guanosine units could provide an ideal structure for membrane insertion and self-assembly of guanosine. In this research, a bis-lithocholate linker was chosen to build a guanosine-sterol conjugate. The structure of target molecule **3-1** is shown in **Figure 3.1**. The covalent bis-lithocholate backbone in **3-1** has a proper length to match that of the hydrophobic portion of lipid bilayer. Additionally, the high lipophilicity of **3-1** should allow for membrane permeability. We hypothesized that guanosine-sterol conjugate **3-1** might be able to form a barrel-stave-type superstructure by means of self-assembly of guanosine into G-quartet assemblies (**Figure 3.2**). This chapter will describe the ion compound **3-1** does form transmembrane ion channels. Even though, the channel activities of compound **3-1** suggest that active channel structures should be different from our hypothetical structure shown in **Figure 3.2**.

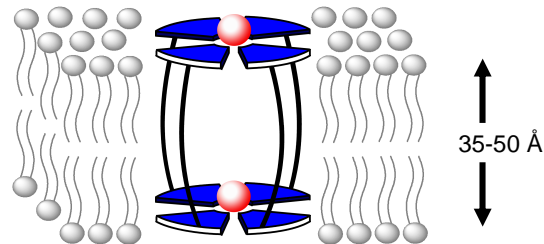


**Figure 3.2** Hypothetical structure of a self-assembled barrel-stave ion channel formed from compound **1**. The wedge represents guanosine moiety, the line represents the bis-lithocholic acid linker. Channel formation would be controlled by the self-assembly of guanosine head groups to give a G-quartet based structure.

### 3.1.1 G-Quartet/Folate-Quartet as a Motif for Transmembrane Ion Transporter

As a hydrogen-bonded macrocyclic array with ionophore properties, the G-quartet represents a promising scaffold on which to build synthetic ion channels. A variety of lipophilic guanosine derivatives have been designed as self-assembled ionophores. They all combine a central hydrophilic cation binding pore with hydrophobic periphery. Several previous efforts include Matile's rigid-rods attached guanosine on their periphery,<sup>119</sup> and Davis' guanosine-calix[4]arene conjugate.<sup>87</sup> These synthetic strategies have been used to stabilize the formation of G-quartets. In all these cases, the resulting self-assembled G-quartet exhibited the tubular architecture that resembles an ion channel. However, there was no evidence in any of these systems that they function as transmembrane ion channels.

The first synthetic ion transporter containing G-quartet units was developed by the Davis group using a synthetic strategy based on the "covalent capture" of a self-assembled G-quadruplex (**Figure 3.3**).<sup>120</sup> In this case, lipophilic guanosine **3-2** was

designed with terminal alkene attachments. This new lipophilic guanosine readily forms a G-quadruplex **3-3** in the presence of a  $K^+$  template. Then, postmodification of the G-quadruplex **3-3** via olefin metathesis yields a unimolecular G-quadruplex **3-4**. This covalently modified supramolecule **3-4** acts as a transmembrane  $Na^+$  transporter in phospholipid liposomes. This unimolecular approach suggests that the self-assembled G-quadruplex **3-3** was stabilized by post-covalent modification.

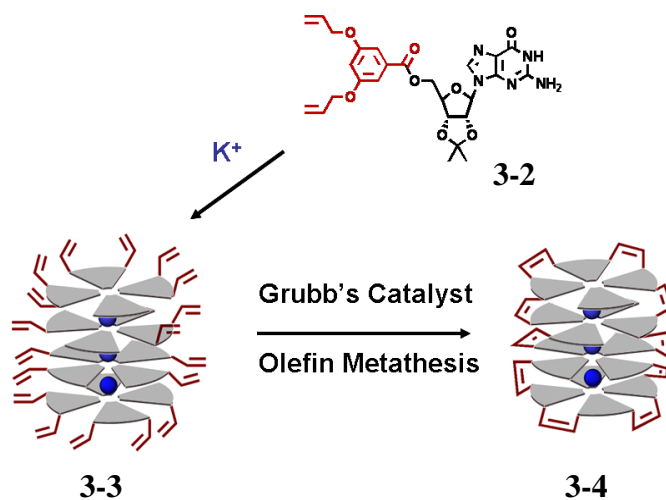


**Figure 3.3** The unimolecular G-quadruplex stabilized by post-covalent modification that can function as a transmembrane  $Na^+$  transporter.<sup>120</sup>

Recently, synthetic transmembrane ion channels built from folate dendrimers **3-5** were reported by the Matile and Kato groups (**Figure 3.4**).<sup>121</sup> Folic acid and guanine base have similar hydrogen bonding motif. Folic acid self-assembles into a folic acid quartet that is similar to the G-quartet. Serving as the central core of the folate dendrimer, the folate analog is surrounded by a hydrogen-bonded amide network, phenyl ring, and alkyl dendritic periphery. The report from Matile and Kato revealed that the folate dendrimer could self-assemble into  $\pi$ -stacked folate rosettes in hydrophobic media with or without a cation template. The ion channel activity of these dendritic folate rosettes shows that the



central pore of “folate-quartet” functions as an ion channel. Compared to the dynamic G-quadruplex system made from lipophilic 5'-tert-butyltrimethylsilyl-2',3'-isopropylidene guanosine **2-1**, these  $\pi$ -stacked folate rosettes are more robust. Apparently, the extra hydrophobic interactions and  $\pi$ - $\pi$  interactions of the dendritic periphery help to stabilize the supramolecular architecture of the folate quartets within a phospholipid bilayer.

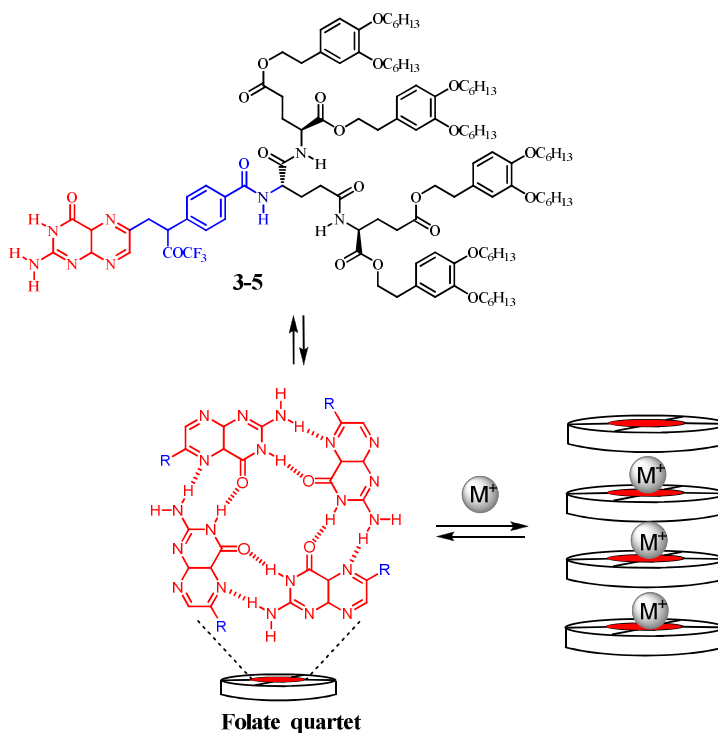


**Figure 3.4** Chemical structure of the folate dendrimer **3-5**, the building block for the “folate-quartet” ion channel.<sup>13</sup>

### 3.2 Design of G-quartet Ion Channels Using a Ditopic Guanosine with a Covalent Linker

Based on the crystal structures of the lipophilic G-quadruplex,<sup>83</sup> the structural requirements for the skeleton of the ditopic guanosine monomer can be conceived. The design strategy for the backbone will focus on the following factors: 1) proper length that matches the width of the hydrophobic portion of a lipid membrane; 2) high lipophilicity to help with membrane permeability. Such a ditopic guanosine analog may provide a better system to study the structure related properties of the lipophilic G-quadruplex and its function as transmembrane ion channel. In addition, the backbone length and functionality of the covalent linker can be adjusted by organic synthesis. Therefore, the self-assembly of an optimized pre-organized ditopic guanosine monomer may result in synthetic ion channels.

In this work, a ditopic lipophilic guanosine **3-1** with a hydrophobic covalent linker was the initial design for the ion channel precursor. We reasoned that the kinetic instability of a completely non-covalent assembly would be overcome by the covalent backbone that connects two guanosine monomers. In the presence of monovalent cations, we hypothesized that the self-association of the guanosine moieties into a G-quartet would transform four building blocks into a columnar supramolecular structure. In this case, a “barrel-stave” type of ion channel would be formed, instead of the “barrel-rosette” channel represented by the hexadecameric G-quadruplex (**Figure 3.5**). Furthermore, this self-assembly strategy to build synthetic ion channels should have several advantages over the covalent synthesis. Self-assembled ion channels can be prepared from molecules

with high synthetic efficiency; the size and functionality of those ion channels can be manipulated by adjusting the building subunits.

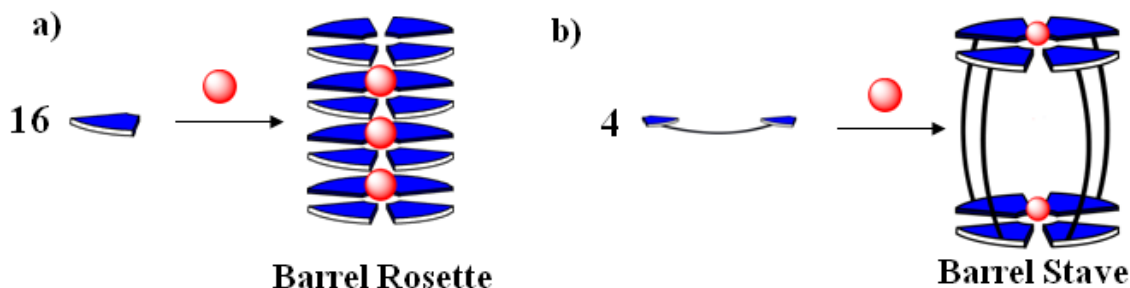


**Figure 3.5** Schematic illustration of two types of “cation channel” formed from a G-quadruplex. a) “Barrel Rosette” G-quadruplex formed by 16 lipophilic guanosine subunits. b) “Barrel Stave” G-quadruplex formed by 4 ditopic ligands. The ball stands for a cation and the stave stand for the ligand.

Various ditopic guanosine derivatives have been designed and used to develop functional supramolecular materials.<sup>78,122</sup> As shown in **Figure 3.6**, Lehn used the ditopic  $\alpha,\omega$ -bis-guanine monomer **3-6** to study the reversible sol-gel interconversion of self-assembled polymer hydrogels *via* a  $K^+$  template and a  $K^+$  release pathway.<sup>78</sup> Their results show that supramolecular polymer forms gel through the self-complementary hydrogen bonding of guanine units. They proposed that supramolecular macrocycles with a G-quartet core were stabilized by  $K^+$  complexation.

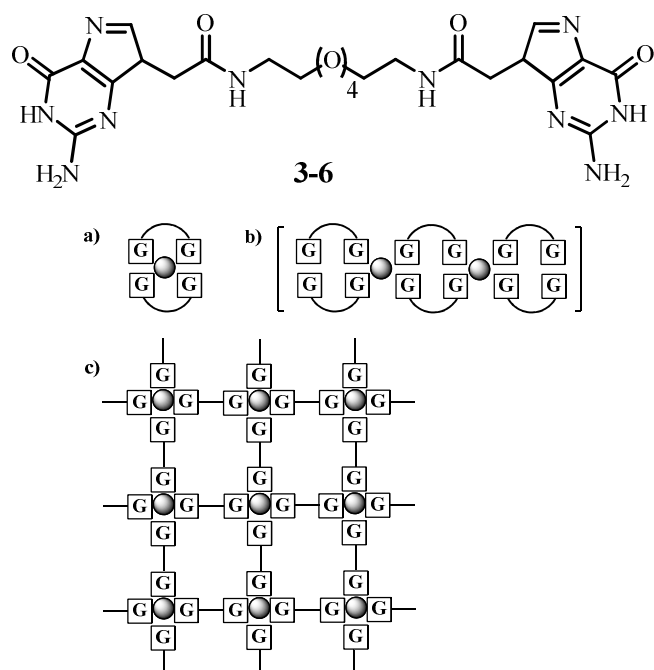


**Figure 3.6** Possible supramolecular structure formed by **3-6** through association into G-quartets stabilized by  $K^+$  binding: a) internally-bridged  $[(3-6)_2 K^+]$  assembly; b) linear chain of doubly bridged  $G_4$  units; c) fully cross-linked regular array of  $G_4$  units. For more details, see ref 78.

More recently, the Barboiu group reported a functional membrane material that was made from a ditopic bis-iminoboronate-guanosine monomer **3-7** (**Figure 3.7**).<sup>122</sup> This strategy involves the stabilization of the G-quadruplex structure through a so-called “double dynamic” connection, which incorporated both non-covalent and reversible covalent connections. This had the effect of combining polyassociation (G-quadruplex aggregation) and polycondensation (iminoboronate formation) process. With a  $K^+$  template, bis-iminoboronate-guanosine **3-7** produced a polymeric G-quartets film. With the conformation shown in **Figure 3.7**, the formation of the covalent N-B bond contributes extra stabilization to the boronate-guanosine ester. In brief, the cation templated self-assembly of bis-iminoboronate-guanosine **3-7** gave rise to a G-quartet network that was implanted in the polymeric membrane film. This G-quartet polymeric

membrane demonstrates both electron/proton transfer and cation transport properties. In spite of the impressive progress mentioned above, there are still considerable challenges to meet to develop stable self-assembled structures that can function as discrete ion channels.

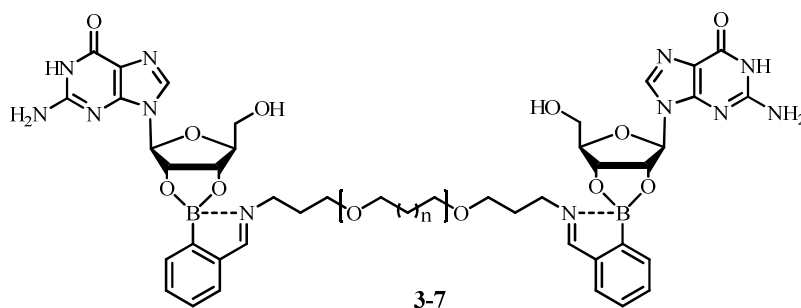


**Figure 3.7** Structure of bis-iminoboronate-guanosine **3-7** used to form  $G_4$ -quartet based membrane.<sup>14</sup>

### 3.3 Design of Guanosine-Sterol Conjugate

Bile acids are cholesterol-derived amphiphilic molecules that facilitate dietary fat processing through formation of mixed micelles.<sup>123</sup> All bile acids are composed of a rigid steroid skeleton and an alkyl side-chain with a terminal carboxylic acid group. The bile acids are structurally distinguished from each other by their side-chain structure, the stereochemistry of the steroid ring and the number and position of hydroxyl groups on the steroid ring. **Figure 3.8** shows the structure of cholic acid **3-8**, one of the most prevalent bile acid in humans, and lithocholic acid **3-9**, the compound we chose as the hydrophobic backbone for the ditopic guanosine **3-1**. Due to the rigidity of their concave skeletons and the ability of variable functionalization, bile acids and their analogues have been promising building blocks used extensively in molecular recognition, host-guest chemistry and biomimetic chemistry.<sup>124,125</sup>

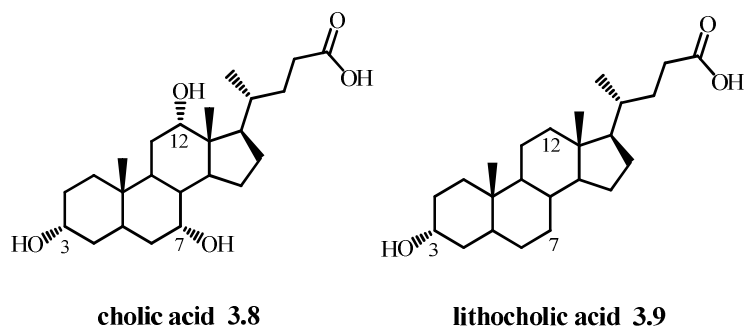


**Figure 3.8** The structure of cholic acid **3-8** and lithocholic acid **3-9**.

The Kobuke group reported that bischolic acid derivatives with methoxy group **3-10** (**Figure 3.9**) are able to form stable single ion channels with conductance values in the picosiemens (pS) range.<sup>126,127</sup> Kobuke's structural study showed that the charge on the external headgroups only influenced the cation/anion selectivity of the channels. They found that the hydrophilic groups on the concave  $\alpha$ -face of cholic acid were crucial for the stability of the ion channels. They proposed that hydrogen-bonding of hydroxyl and methyl ether groups with water determined the channel's pore size and its conductance level. Kobuke *et al* also showed bischololate acid derivative **3-11** with hydroxyl groups can form two discrete channels. The dependence of conductance on the concentration of **3-11** indicates these two ion channels are self-assembled with different number of building molecules. Kobuke proposed two possible aggregation structures to explain the specific conductance of these two channel states (**Figure 3.9**). A self-associated trimer interacting with water molecules was proposed to form one type of ion channel. The self-assembly of bischolic acid derivative **3-11** into a tetramer, giving an ion channel with a larger pore than the trimer, was proposed as the second active channel structure.

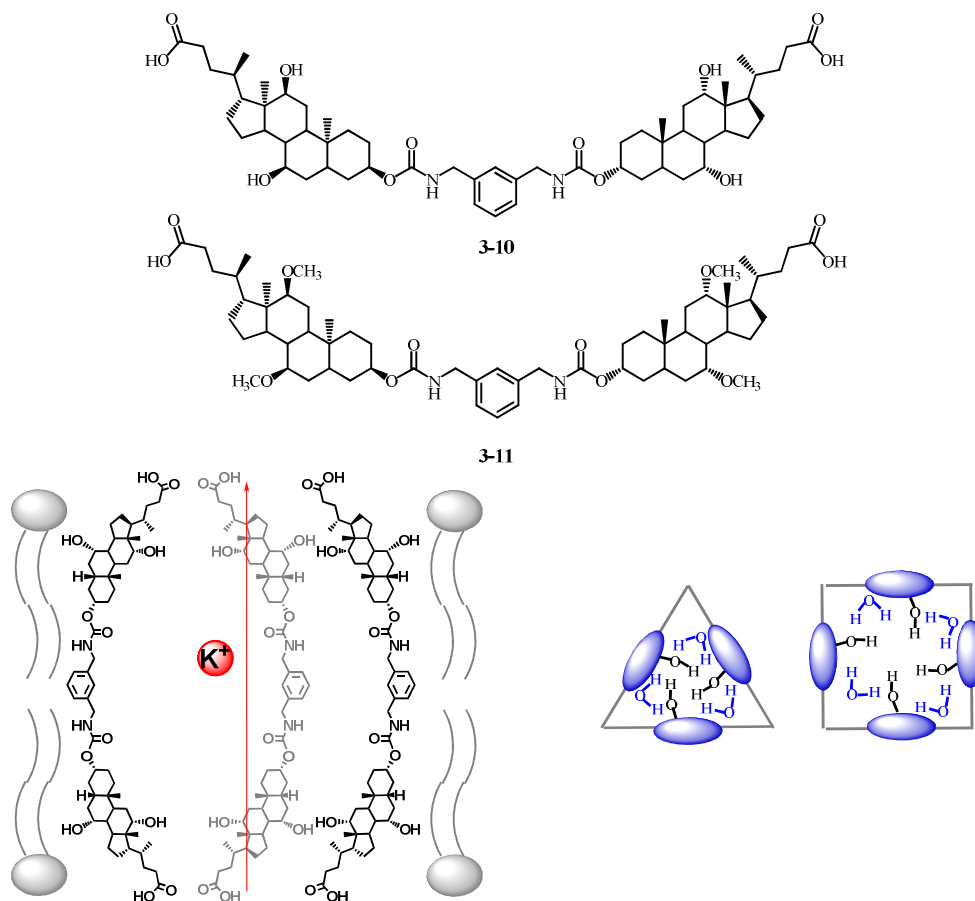


**Figure 3.9** Top: structures of bis-cholic acid derivatives **3-11** with methoxy group on the concave  $\alpha$ -face; **3** with hydroxyl group on the concave  $\alpha$ -face. Below: Kobuke's proposed cross section image of ion channel, constructed from a bis-cholic acid derivative trimer/water and bis-cholic acid derivative tetramer/water. For more detail, see reference 126, 127.

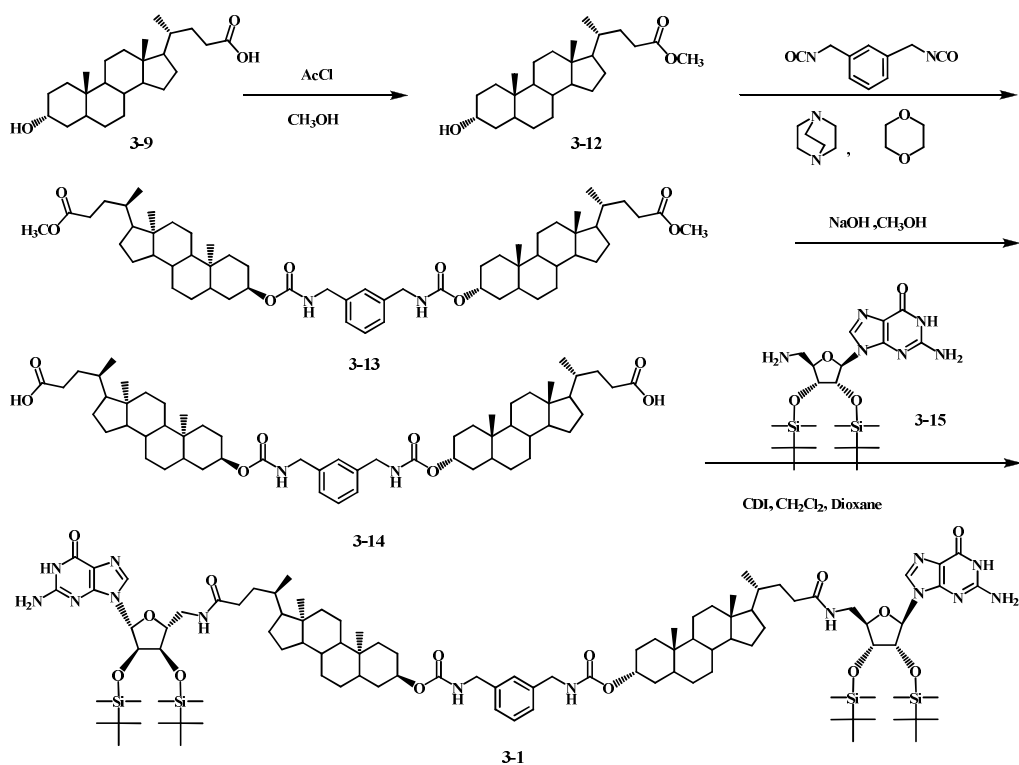
Inspired by Kobuke's bis-cholic acid ion channels, we decided to use bis-lithocholic acid as a covalent linker to connect two guanosine end-groups. Lithocholic acid **3-9** is different from cholic acid **3-8** in that it has no hydroxyl groups at the 7 and 12 positions of the steroid skeleton (see **Figure 3.8**). This lack of  $-\text{OH}$  groups excludes the possibility that self-association of lithocholate derivatives is driven by any interactions of hydrophilic groups on the concave  $\alpha$ -face. In addition, the bis-lithocholic acid backbone in the ditopic guanosine derivatives **3-1** has a proper length to match the hydrophobic

portion of lipid bilayer; its lipophilicity should also allow guanosine-sterol conjugate **3-1** to partition into the phospholipid bilayer. Using guanosine-sterol conjugate as a building block, it was expected that the guanosine head group might control the self-association of ligands to give transmembrane ion channels based on G<sub>4</sub>-quartet pores. We expected that the self-assembly of guanosine into a G-quartet based structure would direct the ion channels to take a barrel-stave type supramolecular structure within the bilayer membrane (See **Figure 3.2**).

### **3.4 Synthesis of Guanosine-Sterol Conjugate**

The synthesis of guanosine-bislithocholic acid conjugate **3-1** is outlined in **Scheme 3.1**. Esterification of lithocholic acid **3-9** was achieved by using acetyl chloride in MeOH. Two equivalents of the resulting ester **3-12** reacted with one equivalent of xylylene diisocyanate, in the presence of diazabicyclo[2,2,2]octane, provided a bis-lithocholate **3-13** with a bis-urethane linkage. The subsequent hydrolysis of diester resulted in bis-lithocholic acid precursor **3-14**. The coupling of diacid linker **3-14** with the known 2', 3'-bis-tBDMSi-5'-amino guanosine **3-15**<sup>83</sup> gave the final target compound **3-1**.





**Scheme 3.1** Synthesis of bis-guanosine-lithocholic acid conjugate **3-1**.

Characterization of the desired final product was carried out by  $^1\text{H}$  NMR spectroscopy and by ESI-mass spectrometry. The  $^1\text{H}$ NMR spectrum of compound **3-1** in  $\text{DMSO}-d_6$  gave a well-resolved set of signals. This spectrum showed a new amide N-H proton at  $\delta$  8.08 ppm (**Figure 3.10a**). Since there are two amino groups in 2', 3'-bis-tBDMSi-5'-amino guanosine **3-15**, at the C2 and C5' positions, it was necessary to clarify the regioselectivity of the coupling reaction between 5'-amino guanosine **3-15** and bis-lithocholic acid **3-14**. A selective NOE experiment was carried out in order to assign the new amide N-H signal in conjugate **3-1**. As shown in **Figure 3.10b**, irradiating the N-H proton peak at  $\delta$  8.08 ppm showed characteristic NOE signal to the  $\alpha$ -proton of carbonyl on the lithocholate side chain, as well as NOEs to the protons on the C5', C4', C3' carbon

of the ribose moiety. These NOEs are characteristic features that indicated that amide formation had occurred, as desired, by coupling bis-lithocholic acid **3-14** with the 5'-amino group of guanosine **3-15**.

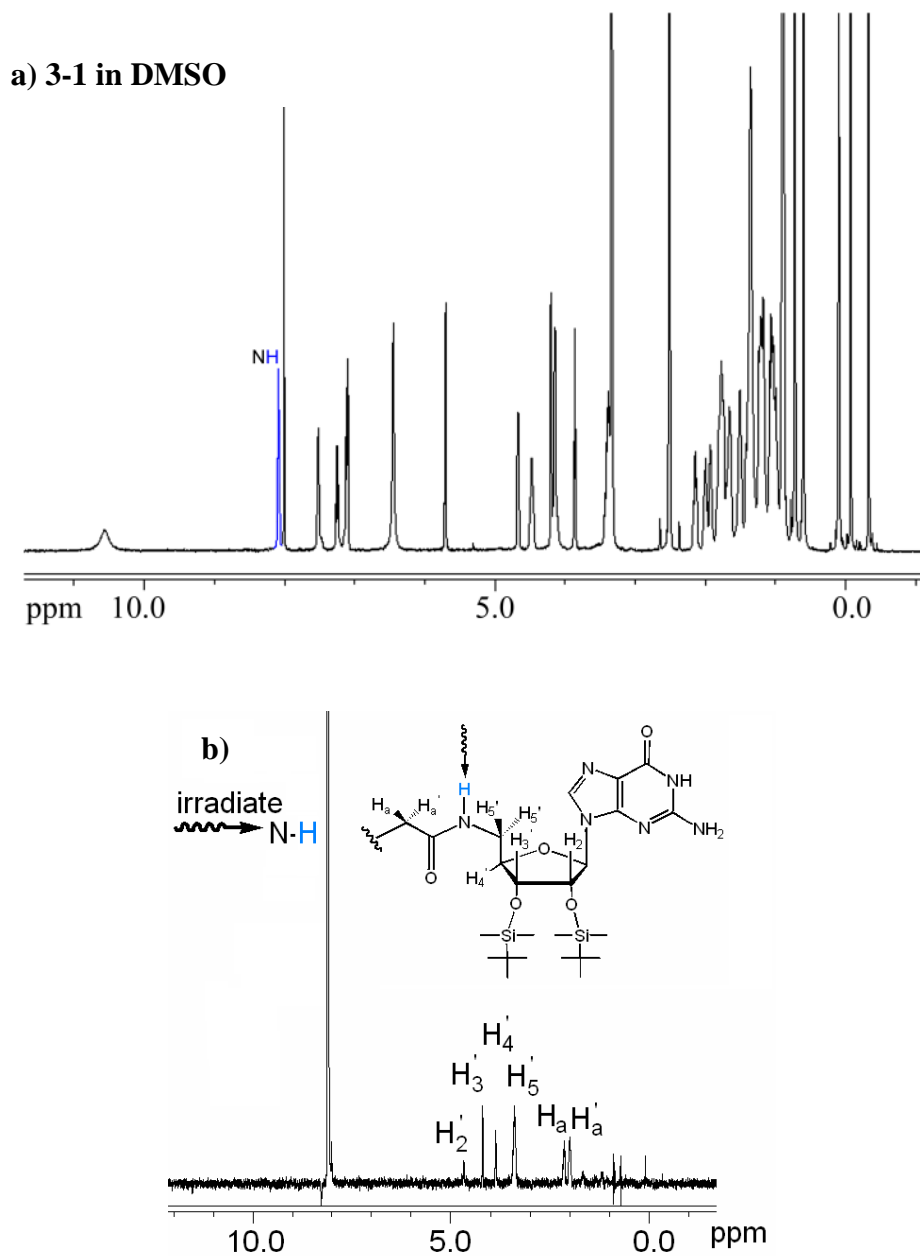


**Figure 3.10** a).  $^1\text{H}$ NMR spectrum of guanosine-bislithocholate conjugate **3-1** in  $\text{DMSO-}d_6$ . b). Selective NOE experiment was carried out by irradiating new amide proton peak at  $\delta$  8.08 ppm.

Further structural evidence for the identity of **3-1** was obtained from a series of COSY and NOESY experiments. **Figure 3.11** exhibits the 2D NOESY of guanosine-sterol conjugate **3-1**. Consistent with the selective NOE result in **Figure 3.10b**, the expansion of the F1 (vertical) axis correlations near  $\delta$  8.08 ppm show NOE correlation of the 5'-amide proton with carbonyl  $\alpha$ -proton, (CONH---H<sub>a</sub>' , H<sub>a</sub>'') and guanosine ribose C 5', C 4', C 3' protons. The new amide bond forms from coupling of bis-lithocholic acid derivative **3-15** with the 5'-amino group of 2',3'-bis-TBDMS,5'-amino guanosine **3-15**.

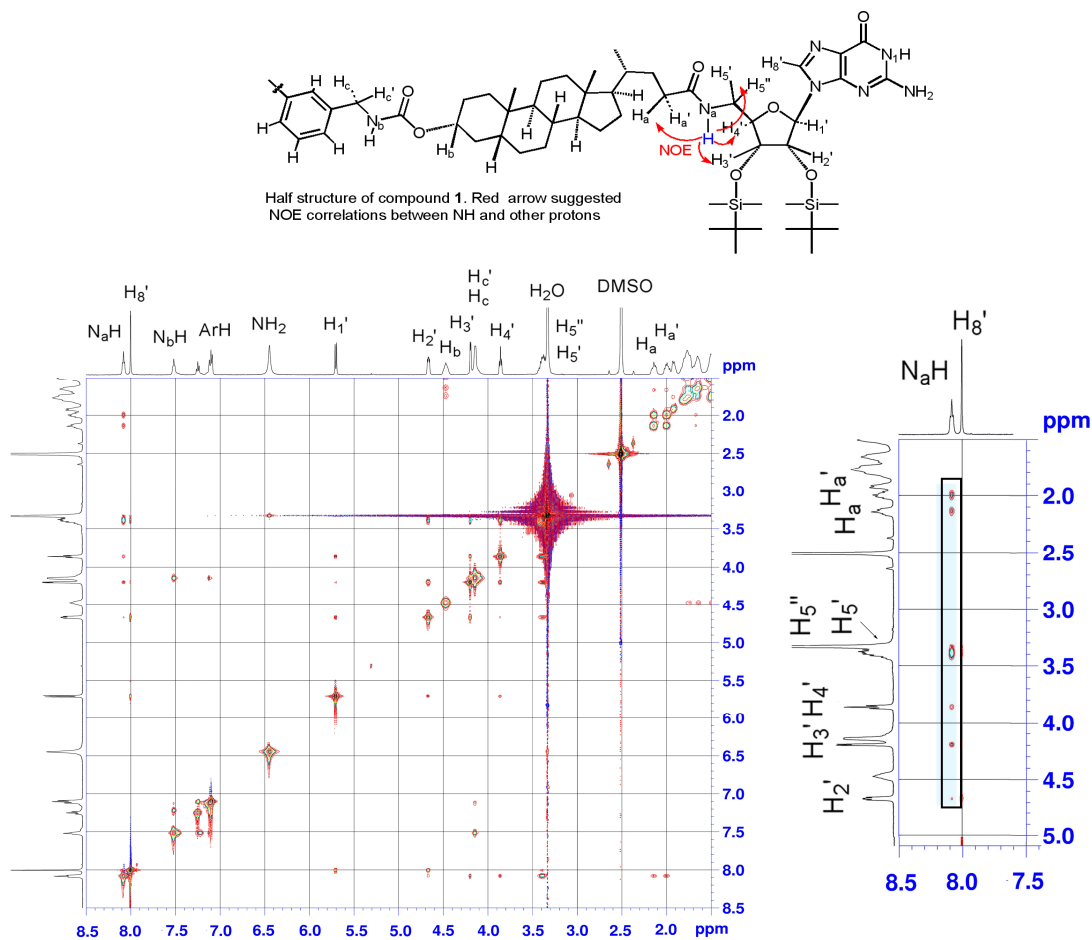


**Figure 3.11**  $^1\text{H}$ - $^1\text{H}$ NOESY spectrum of guanosine-bislithocholic acid conjugate **3-1** in  $\text{MSO-d}_6$ . The expansion of the F1 (vertical) axis correlations near  $\delta$  8.08 ppm showing NOE of amide N-H proton is correlated with H<sub>a</sub>' , H<sub>a</sub>'', H<sub>5</sub>' , H<sub>5</sub>'', H<sub>4</sub>' , H<sub>3</sub>' .

The ESI-MS characterization of **3-1** showed the (M-H)<sup>+</sup> peak at m/z 1926.2, which is consistent with the theoretical calculation (M.W.= 1926.2) (**Figure 3.12**). These NMR and MS characterization confirmed the formation of ditopic guanosine-sterol conjugate **3-1**.

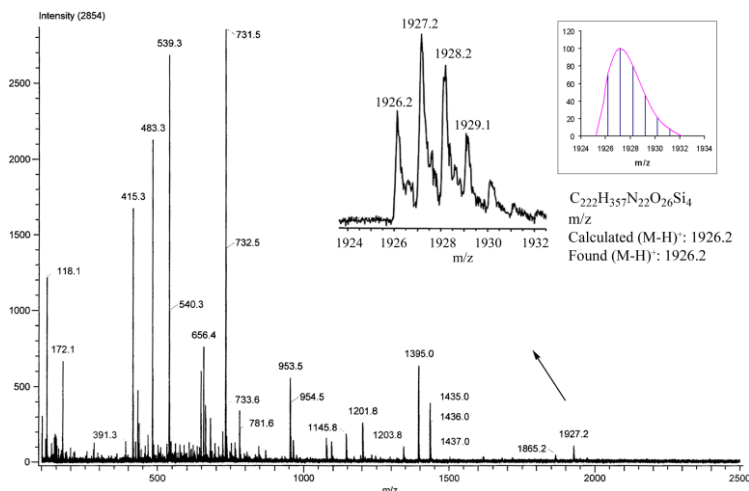
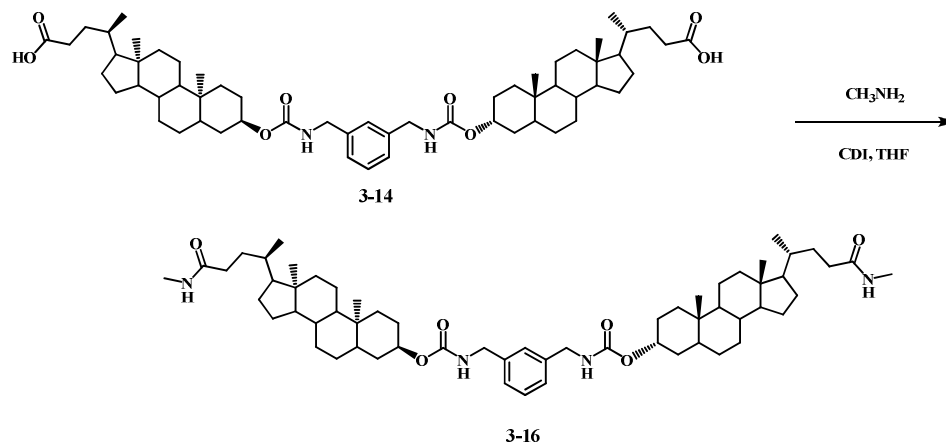


**Figure 3.12** ESI-Mass spectrum of guanosine-sterol conjugate **3-1**.

### 3.5 Synthesis of Bis-lithocholamide for Control Experiment

To understand the importance of the guanosine end-groups in the self-assembly of ion channels made from guanosine-sterol conjugate **3-16**, we decided to prepare bis-lithocholamide **3-16** with -NHCH<sub>3</sub> end groups as a control compound. Comparing the ion channel activity of both compound **3-1** and **3-16** would allow us to distinguish the contribution of the guanosine subunits to any active ion channels. The synthesis of **3-16** in Scheme 3.2 was based on the similar synthetic strategy as described in the bis-lithocholate formation (**Scheme 3.1**), the only difference is introducing methylamine

instead 5'-amino-2',3'-DMTBSi-Guanosine **3-15** in the last coupling step. The synthesis is shown in **Scheme 3.2**.



**Scheme 3.2** Synthesis of control compound bis-lithocholamide **3-16**.

### 3.6 Self-Assembly Property Study of Guanosine-Sterol Conjugate

Before testing for ion channel activity for guanosine-sterol conjugate **3-1** and its control compound **3-16**, we first studied the self-assembly properties of these compounds in the presence of  $\text{K}^+$  cations. The solution properties of compound **3-1** and **3-16** were characterized by  $^1\text{H}$  NMR spectroscopy. As shown in **Figure 3.13**, the  $^1\text{H}$  NMR spectrum of guanosine-lithocholate **3-1** gave sharp peaks in  $\text{DMSO-d}_6$ . Apparently, any self-assembly mediated by hydrogen bonding of guanosine moiety is inhibited since  $\text{DMSO-d}_6$  strongly competes for hydrogen bonding. In contrast, the  $^1\text{H}$  NMR spectrum of **3-1** in  $\text{CDCl}_3$  gave very broad signals, which is consistent with self-association of **3-1** in non-polar media. The control compound **3-16** had a well-resolved spectrum in  $\text{CDCl}_3$ , as expected for a hydrophobic compound with little propensity to self-associate in a non-polar environment.

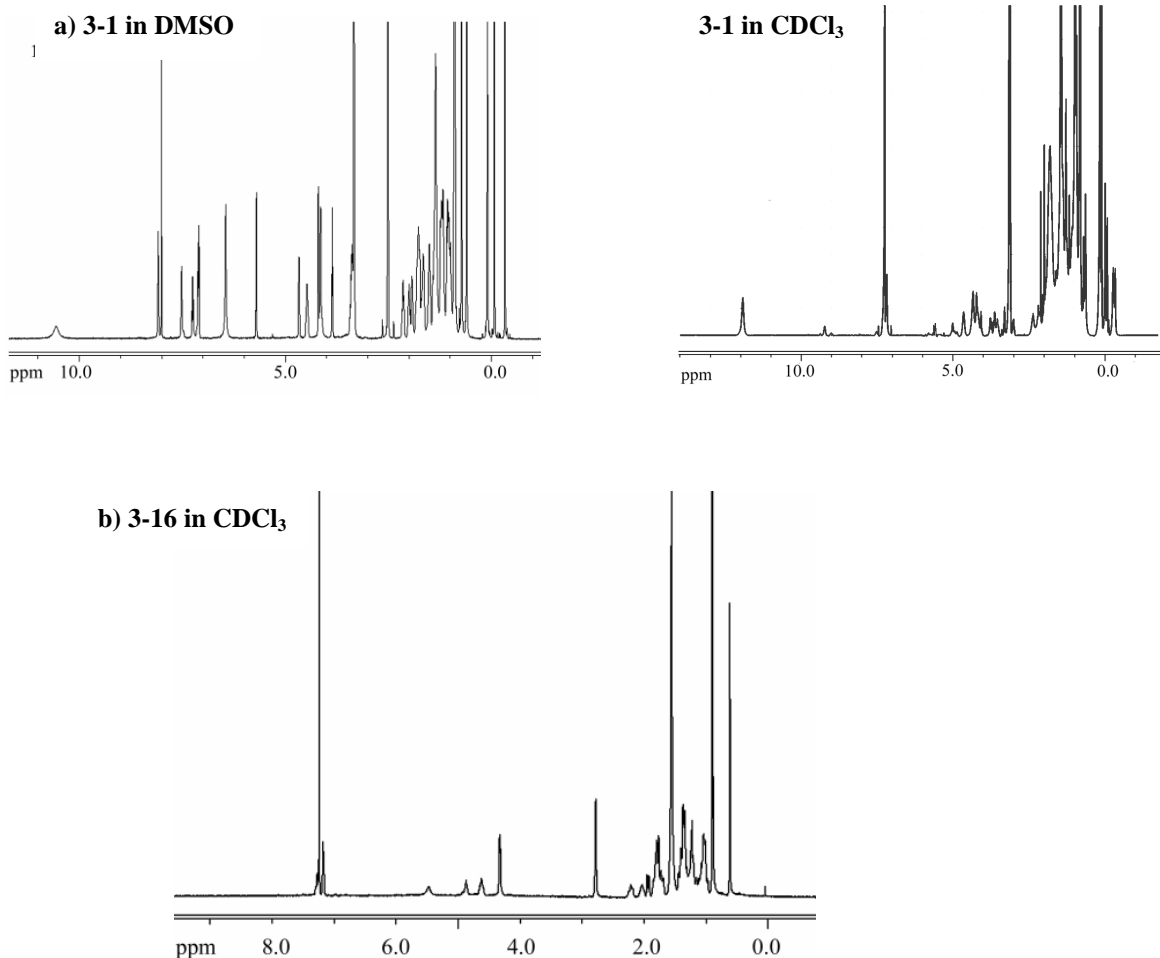


**Figure 3.13** a)  $^1\text{H}$ NMR spectrum of guanosine-bislithocholic acid conjugate **3-1** in  $\text{DMSO-}d_6$  and  $\text{CDCl}_3$ . b)  $^1\text{H}$ NMR spectrum of bis-lithocholamide control compound **3-16** in  $\text{CDCl}_3$ .

The self-assembly property of guanosine-sterol conjugate **3-1** in the presence of  $\text{K}^+$  cations was further characterized by circular dichroism (CD) spectroscopy. CD spectroscopy has been widely used to characterize the structures of both DNA G-quadruplexes and lipophilic G-quadruplexes.<sup>128</sup> In the presence of certain templating cations, the stacking of G-quartets give rise to characteristic CD bands, representing formation of self-assembled structures.

In this study, CD spectroscopy showed compound **3-1** can form stacked G-quartets in a non-polar environment. **Figure 3.14** shows a series of CD spectra for different samples of **3-1** in  $\text{CHCl}_3$ . First, the CD spectrum of **3-1** (blue line) was taken after its isolation from a silica gel column. This sample showed some CD activity in the 200-280 nm region, suggesting that there might be stacked G-quartets that are templated by the trace cations in solution. Then, one equivalent of [2.2.2]-cryptand was added to remove any adventitious cations that were bound to **3-1**. The resulting CD spectrum (green line) showed less CD activity after addition of the ionophore. Finally, we stirred the solution of **3-1** and [2.2.2]-cryptand in the presence of excess  $\text{K}^+\text{DNP}^-$  salt. After extraction of  $\text{K}^+\text{DNP}^-$ , the CD spectrum of the guanosine-lithocholate **3-1** (red line) showed a CD signature that was diagnostic for stacked G-quartets, with a positive band at  $\lambda = 266$  nm and a negative peak at  $\lambda = 240$  nm.<sup>128</sup> In addition, the complex formed by ditopic conjugate **3-1** and  $\text{K}^+$  showed a strong negative band at  $\lambda = 296$  nm, a signal that has been observed for DNA G-quadruplexes.<sup>43</sup> As expected, the control compound, bis-lithocholamide **3-16**, showed no CD activity under identical conditions. Overall, the CD data indicate that  $\text{K}^+$  can template the formation of stacked G-quartets by compound **3-1** in a non-polar environment.

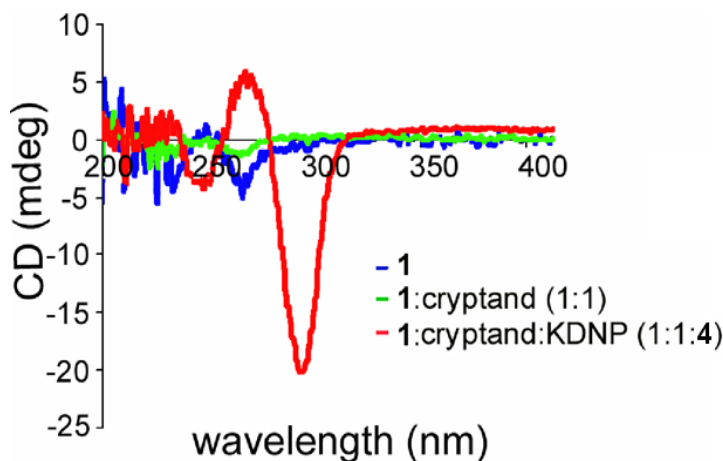


**Figure 3.14** CD spectra of guanosine-sterol conjugate **3-1** (blue line); **3-1** mixed with an equiv of [2, 2, 2]-cryptand (green line); **3-1** after solid-liquid extraction of  $K^+$  DNP. All spectra were obtained in  $CDCl_3$ .

### 3.7 Guanosine-Sterol Conjugate Forms Transmembrane Ion Channels (Pores)

There are two main experimental approaches to characterize synthetic ion channels: liposomes or planar bilayer membranes.<sup>129</sup> Liposomes are spherical closed-shell structures formed by dispersing phospholipids into an aqueous solution. They are bilayer structures that separate the interior aqueous solution from the external media. The formation of ion channels (or pores) provides a means for passive transport of ions and organic molecules to diffuse from one side of a membrane to another. The analytical liposome assays that are sensitive to change in concentration of ions or organic molecules have been developed to measure the transport activities.<sup>130</sup> These assays include tests based on  $^{23}Na$  NMR spectroscopy, pH-sensitive or ion selective fluorescent assay, and fluorescent dye release assay. Liposome methods are powerful means to assess the activity of a transporter. However, additional technical evidence is needed to confirm the ion channel formation, since transmembrane transport of ions or organic molecules can



occur via either a carrier or channel mechanism. Alternatively, planar bilayer membranes measurement is an electrophysiological method for the study of ion channels. In this technique, the current flowing through the phospholipid bilayer is monitored under voltage-clamp conditions. **Figure 3.15** shows a diagram of a voltage clamp experiment. Planar bilayer membrane is formed in a microscopic orifice on a central partition between two chambers. Two electrodes are immersed in the buffer solutions loaded inside the chambers. As a sealed bilayer membrane has good resistance, when there is no ion channel present in the membrane, few ions can move across the bilayer and the observed current is zero. When channels are formed within a planar bilayer membrane, in response to the applied potential, ions from the electrolyte solution can move across the membrane to produce an observed electric current. This measurement allows direct observation of ion transport through a channel embedded in a phospholipid membrane.

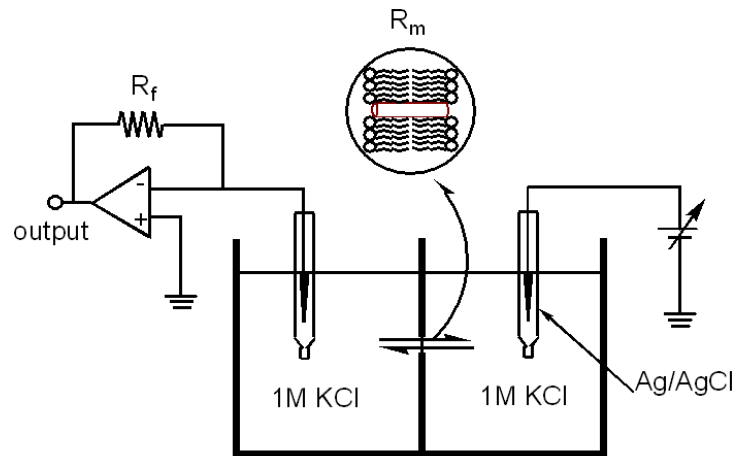


**Figure 3.15** The setup of voltage clamp experiment. The bilayer membrane was prepared with soybean phospholipid supplemented with 0.5% asolectin, 0.5% DPPC and 0.1% cholesterol. The buffer solution is 1M KCl, 2mM MgCl<sub>2</sub>, and 5mM Pipes. All the measurements were done at 25 °C.

In this study, the ion channel activity of guanosine-sterol conjugate **3-1** was assessed using the planar bilayer experiment. Acting as a cell membrane model, planar phospholipid membranes were prepared by the monolayer method across a 100- $\mu\text{m}$  diameter hole in a Saran partition.<sup>131</sup> The monolayers were made from a solution of 0.5% w/v asolectin, 0.5% w/v dipalmitoylphosphatidylcholine (DPPC), and 0.1% w/v cholesterol in hexane. Because of the poor water solubility of compound **3-1**, we used two different methods to incorporate **3-1** into the bilayer membrane. Method A involved adding 25  $\mu\text{L}$  of a solution of **3-1** in DMSO (31.4  $\mu\text{M}$ , final concentration) to the *cis* side of the chamber after the planar bilayer membrane was formed. Alternatively, Method B involved pre-mixing compound **3-1** (2.6  $\mu\text{M}$ , final concentration) with the lipid mixture (asolectin, DPPC, and cholesterol) to form a bilayer membrane.

In both methods, the conductance changes were observed during the voltage clamp experiment, indicating compound **3-1** was successfully incorporated into the membrane to form single ion channels. **Figure 3.16** shows representative conductance records for ion channels formed by guanosine-sterol **3-1** at an applied voltage of 10 mV under 1M KCl(*trans*)/KCl(*cis*) solution. Some of these ion channels formed by **3-1** had remarkably large conductances in the nanoSiemens (nS) range and long lifetime of seconds (s), as compared with many other synthetic ion channels reported in the literature, with typical conductance values in picosiemens range (pS) and ms life-time.<sup>129</sup> Similar to the natural ion channels, these synthetic ion channels formed from **3-1** showed conductance values of different magnitudes that appeared and disappeared over a 2-3 hour period. This pattern of “open” and “closed” conductance state is consistent with the

dynamic formation and disintegration of self-assembled ion channels from guanosine-sterol conjugate **3-1**.

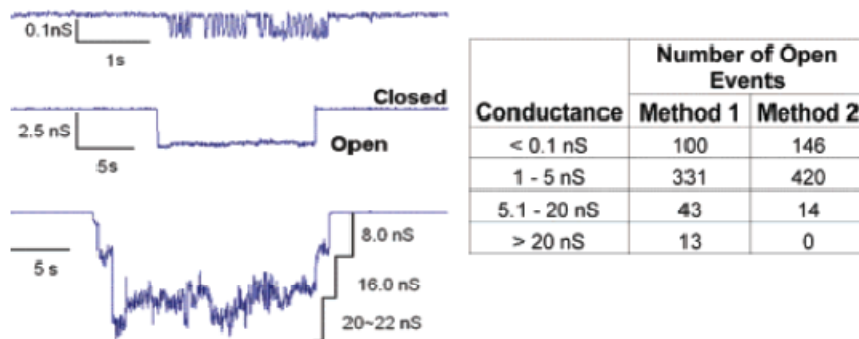


**Figure 3.16** Representative traces from voltage-clamp experiments. The distinct conductance values were recorded in the presence of **3-1** at -10 mV in 1 M KCl. The number of open events was counted from a total of six experiments. Three of the experiment results were from method A, another three were from method B.

The conductance data shown in **Figure 3.16** were obtained from 6 separate experiments, including 3 experiments that employed sample introduction using either method A or method B. We observed that the magnitude and lifetimes of ion conductance produced by **3-1** varied during each single experiment. Channels with conductance values of 0.1-1.0 nS typically had the shortest open lifetimes (10-80 ms), suggesting these smaller channels are much more labile than those larger channels. Larger channels with conductance levels of 1-5 nS had much longer open lifetimes, typically lasting longer than 10 s. Statistical analysis shows that formation and disassembly of pores with 1-5 nS conductance were also the most frequent events observed during any experiment. Occasionally, long periods of multi-step larger conductance (>20 nS) were observed in the three experiments that used the Method A protocol for introduction of compound **3-1**.

We also noticed that the voltage clamp experiments, using Method B where the sample was loaded into the membrane, displayed discrete single ion channels during most of the recording time. While under the same test conditions, ion channels with smaller conductance were observed for the experiments using Method A. This phenomenon might arise from the different amount of compound **3-1** in the solution, where the concentration of **3-1** in Method A (31.4  $\mu\text{M}$ ) was about 12 times greater than that in Method B (2.6  $\mu\text{M}$ ). The macroscopic ion channels might result from either one independent giant channel or several small ion channels that open cooperatively at the same time. This dilemma will be addressed in the next section 3.5.1.

The table in **Figure 3.16** shows the statistical summary of the 6 voltage-clamp experiments. Apparently, sample introduction using Method A resulted in larger ion channel conductance than when using Method B. In addition, the ion channels with conductance level of 1-5 nS occurred most frequently, regardless of how much **3-1** was loaded into the bilayer membrane. This result indicates that the formation of the particular type of ion channel with conductance range of 1-5 nS from guanosine-sterol conjugate **3-1** is a thermodynamically favorable process.

Analysis of data from these 6 separate experiments showed similar numbers of increments and decrements at discrete conductance values, consistent with the opening and closing of channels of the same size (**Figure 3.17**). In addition, the conductance data clearly revealed that the most frequent conductance value was of 1 to 5 nS magnitude, regardless of how compound **3-1** was incorporated into the phospholipid bilayer. These results indicate the formation of certain active pores mediated by compound **3-1** within lipid bilayer. Significantly, addition of the control compound **3-16** to planar bilayer

membranes never resulted in any measurable conductance. This outcome rules out the possibility that the channels are able to self-assemble solely due to the hydrophobic effect of the bis-sterol linker. Apparently, the guanosine end groups in compound **3-1** are absolutely essential for pore formation and transmembrane ion transport.

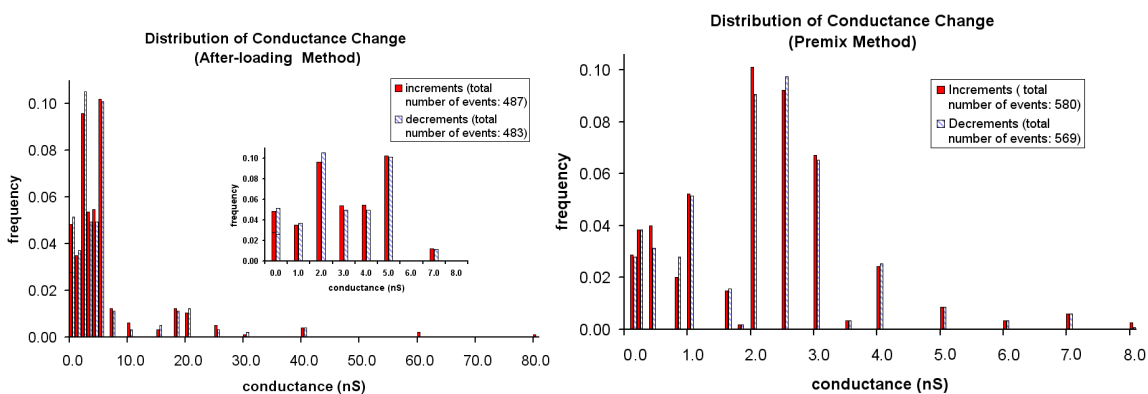


**Figure 3.17** Distribution of conductance change. The frequency was calculated based on the total number of increment (channel open) events or decrement (channel close) events.

### 3.7.1 Ion Selectivity of the Synthetic Ion Channels

In nature, ion channels possess the remarkable ability to discriminate among different ions and transport specific ions across cell membranes. For instance, potassium, sodium, calcium and chloride channels selectively conduct their namesake ions through the membrane.<sup>132</sup> Ion selectivity reflects the fact that there is a free energy difference for ions that compete to flow through the channel. Different combination of phase, cavity size, rigidity and chemical structure controls the different mechanisms for ion selectivity. In this research, the determination of ion selectivity would help us to gain insight into the hydrophilic properties of the ion channels formed from guanosine-sterol conjugate **3-1**. It

would also allow us to estimate the effect of channel size on the ion selectivity, since an increase in channel size usually leads to a decrease in ion selectivity. The final results would help us to understand whether the macroscopic ion channels observed in the conductance measurements (**Figure 3.14**) are originated from single ion channels or from multiple, smaller structures that gate simultaneously.

Typically, electrophysiological measurements are used to quantitatively characterize the ion selectivity of channels. Using the reversal potential (zero net current) under bionic conditions, the permeability ratio  $P_{K^+} / P_{Cl^-}$  can be calculated by using the Goldman-Hodgkin-Katz (GHK) equation:<sup>133</sup>

$$E_{rev} = - \frac{RT}{F} \ln \frac{P_K[K]_o + P_{Cl}[Cl]_i}{P_K[K]_i + P_{Cl}[Cl]_o}$$

where  $[K]_o$ ,  $[K]_i$  and  $[Cl]_o$ ,  $[Cl]_i$  refer to the bulk activities of  $K^+$  ion species and  $Cl^-$  ion species at concentrations of 1 M and 0.1 M respectively, R is the gas constant, T is the absolute temperature, and F is Faraday's constant.

Here, the ion selectivity between opposite charged  $K^+/Cl^-$  ions was first characterized by voltage clamp experiments under an asymmetric condition with 0.1 M KCl on the *cis* side of the membrane and 1 M KCl on the *trans* side. The reversal potential  $E_{rev}$  following a series of conductance changes was recorded at zero net current. The permeability ratios of the ion channels calculated from the GHK equation revealed that compound **3-1** forms cation-selective channels. For example, the large ion channels with conductance values of 2-5 nS displayed a cation-selective permeability with  $P_{K^+} / P_{Cl^-}$  ratio of  $6.4 \pm 0.3$ . The statistical analysis showed that the ion selectivity ( $P_{K^+} / P_{Cl^-}$ ) decreased from 13 to 3 with a corresponding increase in conductance of the ion channel

from 1 nS to 80 nS (Figure 3.16). Here, the reversal potential corresponding to the single ion channel with a conductance of 0.1 nS was neglected, due to its very short lifetime during the recording. This charge selectivity as a function of conductance level suggested that multiple pore structures are present in the membrane. Additionally, we also observed ion channels with microscopic conductance occurred for the experiments using sample loading Method A.

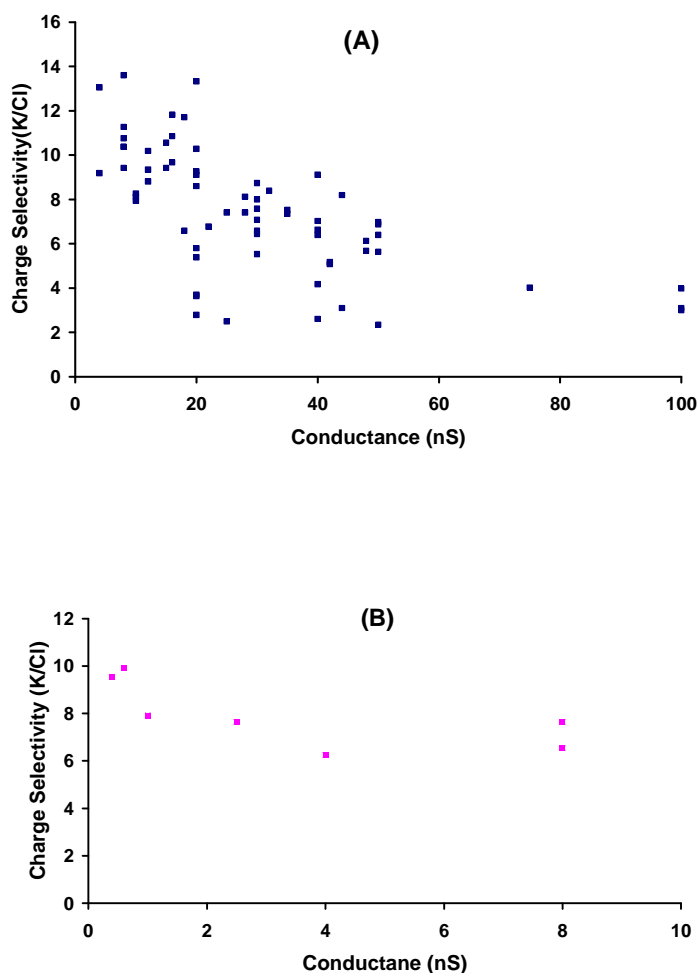


**Figure 3.18** The data analysis showed that ion selectivity ( $P_{K^+} / P_{Cl^-}$ ) decreases with a corresponding increase in conductance of ion channels. These results suggested guanosine-sterol conjugate **1** forms a variety of ion channels with different sizes. Panel A, Panel B showed the ion selectivity data obtained by applying guanosine-sterol conjugate **1** using the sample loading method A and method B, respectively.

These microscopic ion channels gave quite different  $P_{K^+} / P_{Cl^-}$  permeability ratio as shown in **Figure 3.18** (panel A). For example, at conductance level of 20 nS, the permeability ratios varied from 13 to 2. This result suggested the large conductance could be originated from a large discrete single ion channel with lower ion selectivity, or from cooperatively gated multiple small ion channels that show higher ion selectivity. The cation preference between equivalently charged  $K^+$  and  $Na^+$  was determined using 0.1 M KCl on the *cis* side of the membrane and 0.1 M NaCl on the *trans* side. The reversal potentials measurement showed that the ion channels formed from guanosine-sterol conjugate **1** have no cation selectivity for either  $K^+$  or  $Na^+$ .

### 3.7.2 Proposed Active Structure of the Synthetic Ion Channel

Both the conductance measurements and ion selectivity results suggest multiple types of ion channels formed by guanosine-sterol conjugate **3-1** in the membrane. In addition, the control experiment using bis-lithocholamide **3-16** indicates that the guanosine units in compound **3-1** play an essential role in the formation of ion channels in bilayer membrane. However, the structure of active ion channels formed by guanosine-sterol conjugate **3-1** is still unclear.

As mentioned in section 3.1.1, the dendritic folate rosettes ion channels<sup>121</sup> exhibited a maximal single-channel conductance of 21 pS, corresponding to the conductance that would be expected for “folate-quartet” pore with a Hille’s diameter of 3.7 Å.<sup>133</sup> In a similar fashion, small single ion channels conductance in the pS range (< 0.1 nS at 1 M KCl) were observed during the planar bilayer conductance measurements using guanosine-sterol conjugate **3-1**. The pore diameter of 3.7 Å was estimated by the



corrected Hille equation, which is consistent with the G<sub>4</sub>-quartet's central cavity. The self-assembly of **3-1** would be conceived as a barrel-stave type ion channel, where guanosine end groups from four molecules are templated by K<sup>+</sup> to self-associate into G-quartet. The bis-lithocholic acid linker forms hydrophobic wall to span the membrane (Figure 3.19). The conductance for the < 0.1 nS events could derive from ions flowing through the G<sub>4</sub>-quartet's central pore.

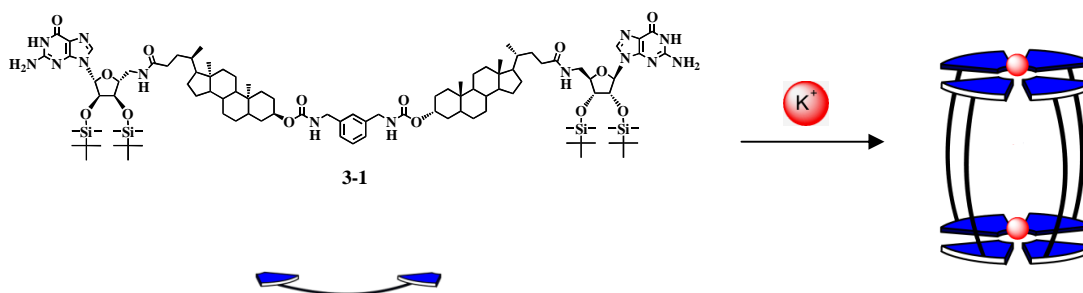


**Figure 3.19** Barrel-stave ion channel formed from guanosine-sterol conjugate **3-1**. The central G-quartet pore is responsible for the <0.1 nS conductance during voltage clamp experiment.

The more frequently observed large conductances in the nS range from the planar bilayer experiment suggested the formation of ion channels with pore sizes much larger than that of the G-quartet's central cavity. Here, Hille's equation was used to estimate the pore size of these ion channels formed from **3-1**.<sup>36</sup> In Hille's model, the ion channel was assumed to be a uniform cylinder bathed in a solution. The conductance  $g$  of a channel can be calculated from the radius and length of the channel, as shown in Hille's equation (Figure 3.20).<sup>133</sup>

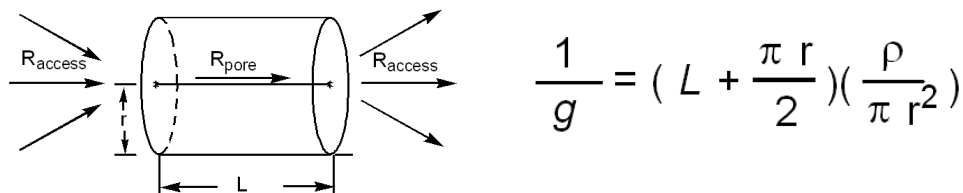


**Figure 3.20** Left: Hille's cylinder model of ion channel; Right: Hille's Equation, where  $L$  is the length of the channel,  $r$  is the radius of the channel and  $\rho$  is the resistivity of the solution. Under our planar voltage experiment condition, the resistivity of 1.0 M KCl solution is  $89 \Omega \cdot \text{m}$ . The length of the channel is estimated as the thickness of the phospholipid bilayer membrane, which is approximately  $50 \text{ \AA}$ .

Corresponding to the conductance level of the ion channels, the calculated Hille's diameters of ion channels formed from compound **3-1** were calculated. As shown in **Table 3.1**, the most frequently observed ion channels with conductance level of 2-5 nS have pore sizes about 14-20  $\text{\AA}$ . For the channel with very large conductance of 20 nS, the active pore diameter is as large as 42  $\text{\AA}$ . These data supported the formation of giant conducting channels within the bilayer membrane. Obviously, many of the active ion channels formed by **3-1** are much larger than a G-quartet "barrel-stave" ion channel.

**Table 3.1** Hille's Diameter of Ion Channels Formed from **3-1**

<u>Conductance</u>	<u>Events</u>	<u>Diameter of Pore(<math>\text{\AA}</math>)</u>
0.1 - 1.0 nS	32%	3
<b>2.0 - 5.0 nS</b>	<b>62%</b>	<b>14-20</b>
6.0 - 20 nS	5%	22-42
> 20 nS	1%	>42

Since the guanosine is the key functional group for the self-assembly of **3-1** into ion channels, it is rationalized that the formation of columnar G-quadruplex structures may be the driving force for self-association of a given pore. With this hypothesis in mind, we proposed a bicyclical ion channel structure from a dimer of guanosine-sterol conjugate **3-1**. The molecular modeling shown in **Figure 3.21** demonstrated that four guanosine end-groups could self-assemble into a G-quartet, which has a central ionophore pore of about 3-3.5 Å. The bis-lithocholic acid linkers are flexible enough to bend into two peripheral large pores with diameters of 15 Å. Such a pore size is in the range of the calculated diameters for channels with large conductance levels of 1.0-5.0 nS. This modeling study supported our proposal for the active ion channel formed from compound **3-1**.

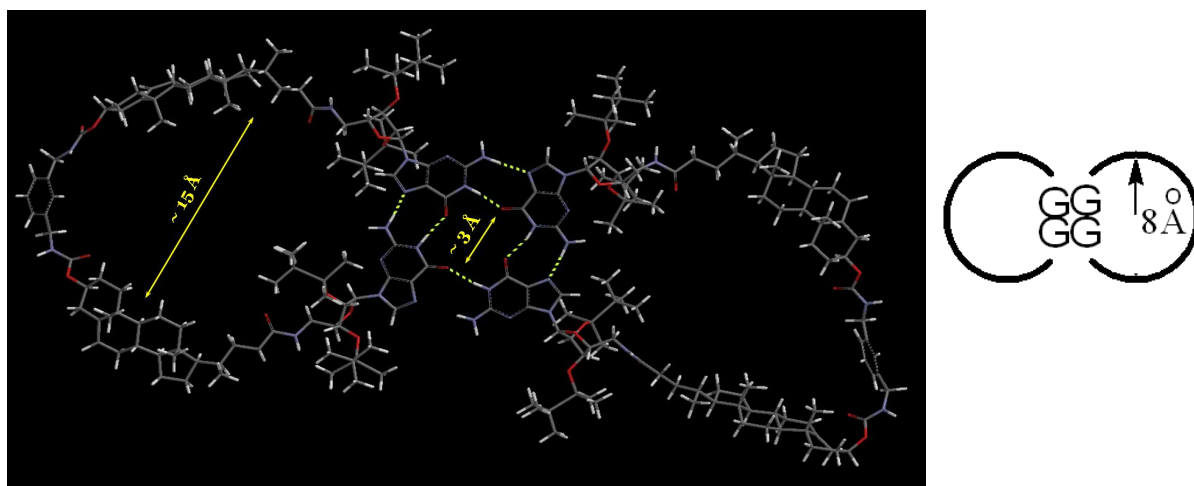


**Figure 3.21** Molecular modelling of one possible self-assembly of two molecules of guanosine-lithocholate **3-1**(Modelling was made by Dr. Monica Melegari)

So far, all the experimental data suggest that the ion channels formed from guanosine-sterol conjugate **3-1** with large conductance could be considered to be the

consequence of the formation of giant supramolecular macrocycles. Molecular modeling also supported the proposal that, in the active channel structure, the lithocholate linker interconnects the G-quartet cores. Similar to the polymeric G-quartet sheet proposed by Lehn and Barboiu et al. (see **Figure 3.6**),<sup>78,122</sup> self-assembly of stacked G<sub>4</sub>-quartets from ditopic compound **3-1** would result in a bis-sterol linker network within the membrane. The structures of the ion channels could be envisioned to be due to the stacking of such bicyclic dimers, where the G-quadruplex functions as the central pillar, and the hydrophobic lithocholic acid linker acts as the giant pore for ion conduction. Based on this hypothesis, several other possible models of a “barrel-stave” ion channel are proposed (**Figure 3.22**). There are probably other structures that might be considered as well.

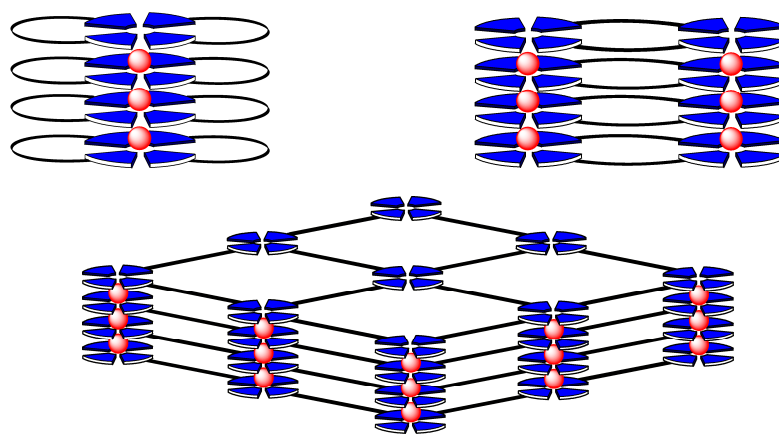


**Figure 3.22** Possible G<sub>4</sub>-quartet stacks formed by bis-G-lithocholate **3-1** within bilayer membrane.

### 3.8 Conclusion

In conclusion, ditopic guanosine-sterol conjugate **3-1** is able to incorporate into a planar phospholipid membrane to self-assemble into single ion channels. Planar bilayer

experiments revealed the formation of discrete stable and large ion channels. The conductance of distinct magnitudes was “open” and “close” during recording, demonstrating their dynamic formation and disintegration properties. The control experiment and CD study showed that stacked G-quartets play a key role in the self-assembly of this ion channel. The Hille diameter of the most prevalent single channels (conductance 2-5 nS) is in the nanometer range, a diameter that is much larger than the diameter of a G-quartet. This result indicated that ion transport proceeded through larger pore(s) that form upon self-assembly of guanosine-lithocholate **3-1**. These transmembrane pore(s) of nanometer diameter size could be envisioned as a “barrel-rosette” supramolecular structure with hydrophobic walls provided by the bis-lithocholate linker and a central pillar of a cation-filled G-quadruplex.

The ability of guanosine-sterol conjugate **3-1** to form transmembrane pores with nanometer diameters provides the potential for a multitude of applications, such as a chemical sensor, and drug delivery. Future efforts are needed to develop more stable and functional systems that are capable of recognizing and transporting molecules from one side of membrane to another.

## Chapter 4. Synthetic Ion Channel from Ditopic Sterol-Guanosine with Bis-urea Linker

*The majority of this chapter has been published in reference 134:*

- **Ma, L.;** Harrell, W. H.; Davis, J. T. “Stabilizing Guanosine-Sterol Channels With a Carbamate to Urea Modification In the Linker”, *Org. Lett.* **2009**, *11*, 1539-1542.

### 4.1 Introduction

The goal of the research in this chapter was to develop more stable transmembrane ion channels using the modified guanosine-sterol conjugate compound **4-1** containing a bisurea linkage (**Figure 4.1**).<sup>134</sup> The previous research described in Chapter 3 demonstrated that the guanosine-bile acid conjugate **3-1**, with a bis-carbamate linker, was able to self-assemble into large ion channels with nano-Siemens (nS) conductance within the phospholipid membrane. The study of structure related ion channel activity revealed that the guanosine units in compound **3-1** played an essential role in the formation of the transmembrane ion channel. Thus, the bis-carbamate lithocholic derivatives, lacking the guanosine end groups, did not form ion channels in the bilayer membrane.

To rationalize the large conductances from guanosine-sterol **3-1**, we proposed the supramolecular structures shown in **Figure 3.22**. These possible structures, of which there may be many, consist of a hydrophobic wall of bis-carbamate lithocholate linkers and a central pillar of self-assembled G-quadruplexes.<sup>117</sup> To test this hypothesis, we

modified the backbone of the linker region in order to introduce additional noncovalent interactions. We hypothesized that this strategy could further promote the self-association and improve the stability of supramolecular structures controlled by the guanosine motif. The cooperative stabilization of a self-assembly of G-quadruplex has been reported by Hamilton and coworkers.<sup>135</sup> By linking a porphyrin macrocycle at the 5'-termini of the oligonucleotide d(TG<sub>n</sub>T<sub>4</sub>) (where n=3-6), a dramatically enhanced stabilization of a parallel G-quadruplex structure was achieved. Hamilton found that allosteric porphyrin-porphyrin self-association was essential for the formation and subsequent stabilization of the DNA G-quadruplex.

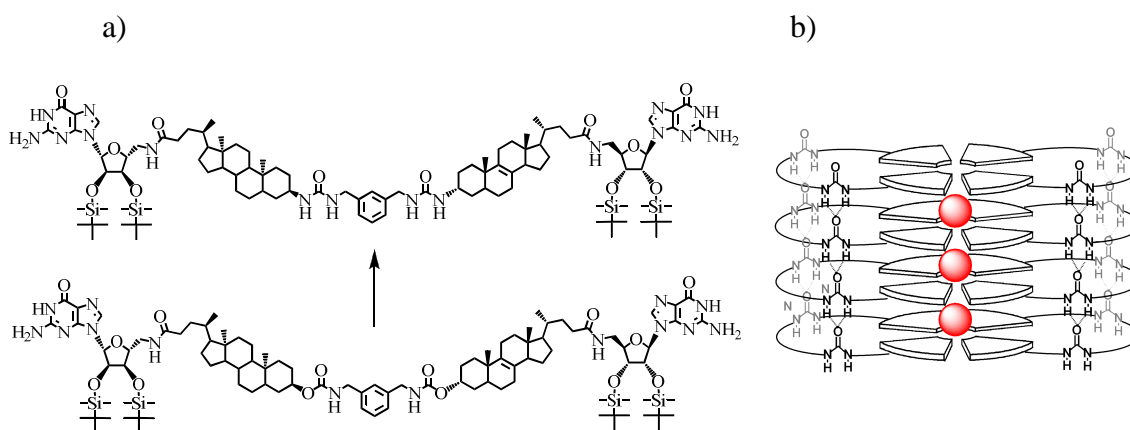


**Figure 4.1** a): Structure represents the modification of sterol linker. b): Scheme depicting the one possible self-assembled structure from bis-urea **4-1**. The bis-urea modified sterol linker might introduce additional hydrogen bonding through urea stacking to stabilize this synthetic ion channel.

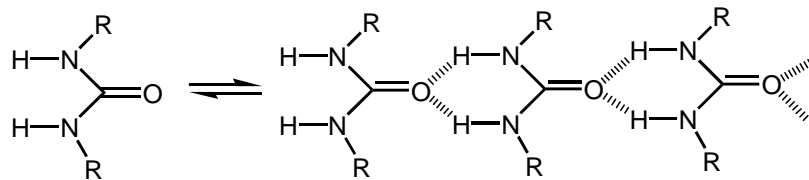
In this work, we reasoned that the self-assembly of guanosine-sterol conjugate **4-1** could be stabilized by replacing the bis-carbamate linker unit in **3-1** with a bis-urea group. **Figure 4.1b** shows one possible self-assembled structure formed by the modified guanosine-sterol **3-1** with the bis-urea linker. The three-centered intermolecular bis-urea

hydrogen bonding on the hydrophobic wall might help cooperatively stabilize the self-assembly of the guanosine-sterol conjugate. This structural modification on the channel precursor (from bis-carbamate **3-1** to bis-urea **4-1**) was expected to result in supramolecular structures with enhanced stability and improved ion channel activity.

#### **4.2 Bis-urea Macrocycles are Known to Form Self-Assembled Cylinders.**

There has been great interest in the development of functional materials and biological devices, by means of self-association.<sup>5,136</sup> Hydrogen bonding has proven to be one effective non-covalent interaction in the self-assembly system, as a result of its highly tailored recognition elements in the manner of hydrogen-bond donor-acceptor arrays. In particular, N,N'-disubstituted ureas as building blocks for the hydrogen-bond-mediated self-assembly has attracted much attention.<sup>137,138</sup> The urea group is able to self-associate into supramolecular structures in a diversity of environment, such as solutions, gels, fibers and crystals.<sup>139-141</sup> The X-ray crystallography of disubstituted ureas revealed that ureas form hydrogen-bonded network through a three-center intermolecular hydrogen-bonding motif (**Scheme 4.1**).<sup>142</sup> Two N-H protons in one urea molecule function as hydrogen-bond donors and carbonyl oxygen atom in the adjacent molecule function as a hydrogen-bond acceptor. This head-to-tail multiple hydrogen-bonding array tends to form a spacing of about between 4.5 Å -4.7 Å. The specific space depends on the rigidity, size and shape of the substitution in the urea groups.





**Scheme 4.1** Three center hydrogen bonding net-work formed by urea derivative.

The directional property of urea hydrogen bonding has been utilized by many research groups to develop self-assembled organic nanotubes.<sup>139,143,144</sup> The design strategy involved in using the macrocyclic urea derivatives include Karle's peptide nanotubes formed by cystine-based cyclic bis-urea **4-2**,<sup>140</sup> and Guichard's chiral nanotubes assembled by a cyclo-tetraurea substituted with alanine residues **4-3**.<sup>144</sup> The structural studies of these different nanotubes exhibited that the contiguous urea-urea hydrogen bonding directed the extended stacking of macrocycles to form tube-like structures. Another inspiring example of this strategy is Shimizu's columnar nanotube, using the self-assembly of rigid bis-urea macrocycles **4-4**.<sup>145,146</sup> In their approach, two meta-xylene spacers are incorporated in a bis-urea macrocycle to introduce the intramolecular hydrogen bond and inhibit the collapse of the central cavity. The X-ray crystallographic analysis revealed a columnar structure (**Figure 4.2**). The macrocycles stacked on top of each other through intermolecular urea-urea hydrogen bonding and  $\pi$ - $\pi$  interaction of phenyl rings. The hydrogen-bonded urea groups were aligned parallel with a general space of 4.614 Å. The macrocyclic ring tilted 26° off the urea center to optimize the aryl  $\pi$ - $\pi$  stacking within the distance of 3.568 Å. Shimizu's topology of bis-urea assembly in the macrocyclic structure provided a detail structural evidence of bis-urea compound stacking in a columnar fashion.

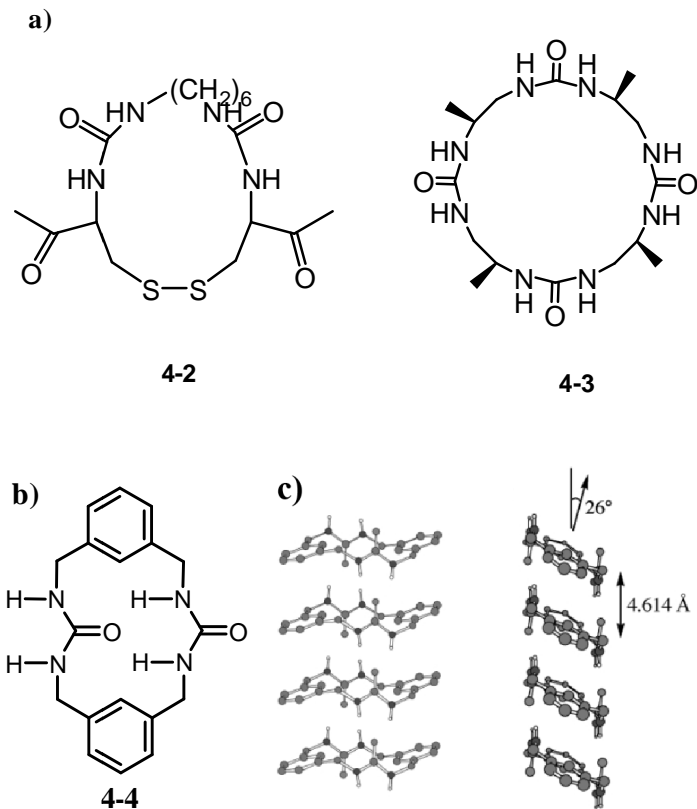


**Figure 4.2** a): Examples of macrocyclic urea derivatives in the development of nanotubes. b) Bis-urea macrocycle **4-4** designed by Shimizu. c) X-ray crystal structure of the self-assembled bis-urea **4-4**, including the 3-centered hydrogen bonding patterns and the skewed orientation of monomers.

In particular, the formation of transmembrane ion channels driven by the head-to-tail hydrogen bonding between urea functional groups has been utilized by Fyles and Barboiu.<sup>147</sup> Ureido crown-ether derivatives **4-5** were designed to self-assemble into crown-ether centered columnar supramolecular structures. The solution <sup>1</sup>H NMR studies showed **4-5** formed intermolecular hydrogen bonds, as indicated by the downfield shift of NH proton with increasing concentration. Solid-state structures also demonstrated the formation of a columnar arrangement of crown ether by means of urea hydrogen bonding. These ureido crown-ether derivatives **4-5** showed the desired ion channel activity with

conductance in the pS (pico-Siemens) range. Fyles proposed that the urea hydrogen bonding directed the stacking of the ureido crowns to form an ion channel (**Figure 4.3**). The crown ether arrays function as the central pore for cation transport. Fyle's ureido-crown ether channel gave a nice example that urea-urea hydrogen bonding could be used to direct the self-assembly of ion channels.

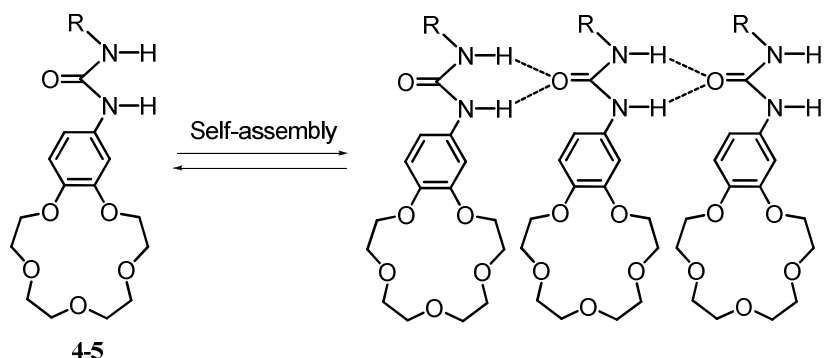


**Figure 4.3** Dynamic self-organization of heteroditopic receptors **4-5**.

In this study, we rationalized that the self-assembly of bis-urea **4-1** would be enhanced by the positive cooperative hydrogen-bonding of the urea groups in the sterol linker (**Figure 4.1**). As mentioned in Chapter 3, the bis-carbamate **3-1** ion channel can be envisioned as a central pillar of self-assembled G-quadruplex. The bis-lithocholate linker may well provide the walls for the transmembrane pore. From the reported crystal structure of lipophilic G-quadruplex (**Figure 4.4a**),<sup>83</sup> we know that the space between two stacking individual G-quartet layers is 3.3 Å. In the case of self-association of **2-1**, the stacking central G-quartet with 3.3 Å apart would be in proper distance range to allow the bis-urea group in the sterol linker to form a hydrogen-bonding array<sup>146</sup> (**Figure 4.4b**).

With the bis-urea modified linker, guanosine–sterol conjugate **4-1** should be able to self-associate into the structures that are even more stable than those formed by **3-1**.

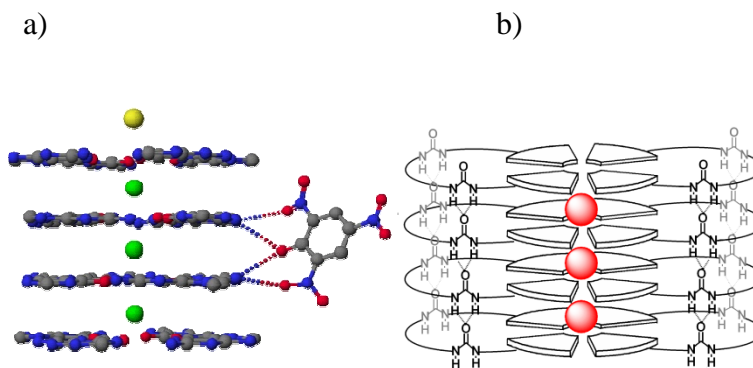
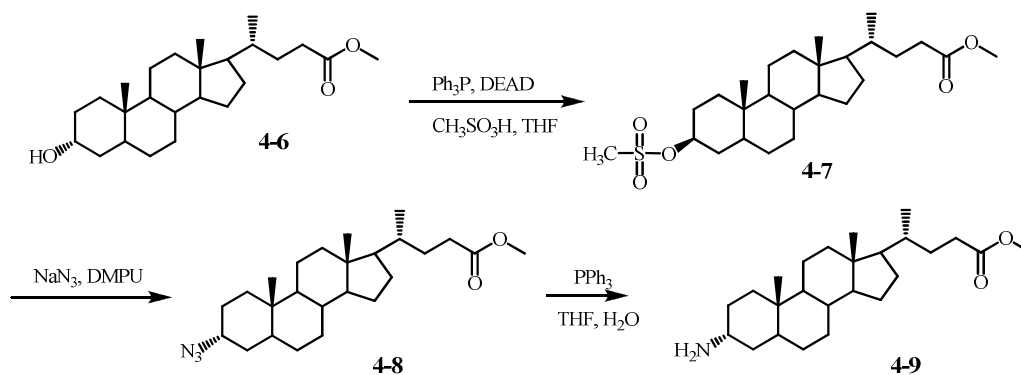


**Figure 4.4** a) Crystal structures of lipophilic G-quadruplex templated by the sodium cation. b) One of the proposed ion channels from self-assembled bis-urea modified guanosine-sterol conjugate. The urea-urea hydrogen bond between the linkers was envisioned to improve the stability of the pore.

### 4.3 Synthesis of Bis-urea Guanosine-Sterol Conjugate **4-1**

To achieve the synthesis of bis-urea **4-1**, the  $3\alpha$ -hydroxy group of lithocholic acid has to be substituted by an amino group. We decided that the displacement with stereo-retention was necessary to rule out the possible conformational changes due to the configurational conversion at the C3-carbon on the sterol backbone. The  $3\alpha$ -amino lithocholate **4-9** was synthesized using the published double inversion transformation.<sup>148</sup> As shown in **Scheme 4.2**, mesylation of  $3\alpha$ -hydroxy lithocholate **4-6** with strict inversion of configuration was achieved by Mitsunobu reaction in the presence of methanesulfonic acid. The subsequent  $S_N2$  reaction of 3-mesylate **4-7** with  $\text{NaN}_3$  gave the equatorial azide derivative **4-8**. The reduction of the azide group under Staudinger reaction conditions gave the desired  $3\alpha$ -amino lithocholate **4-9**. The stereochemistry of the  $3\alpha$ -amino

lithocholate **4-9** was confirmed by  $^1\text{H}$  NMR spectroscopy. The axial  $3\alpha$ -proton exhibited a triplet of triplet splitting pattern, with two anti and two gauche coupling constants of 11.2 Hz and 4.0 Hz, respectively (**Figure 4.5**).



**Scheme 4.2** Synthesis of 3 $\alpha$ -amino lithocholate **4-9**.

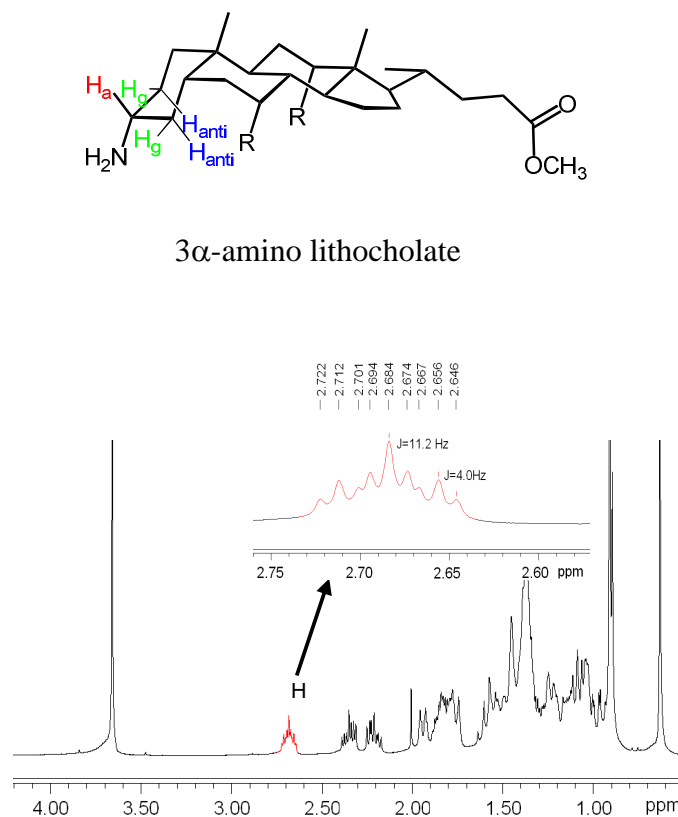
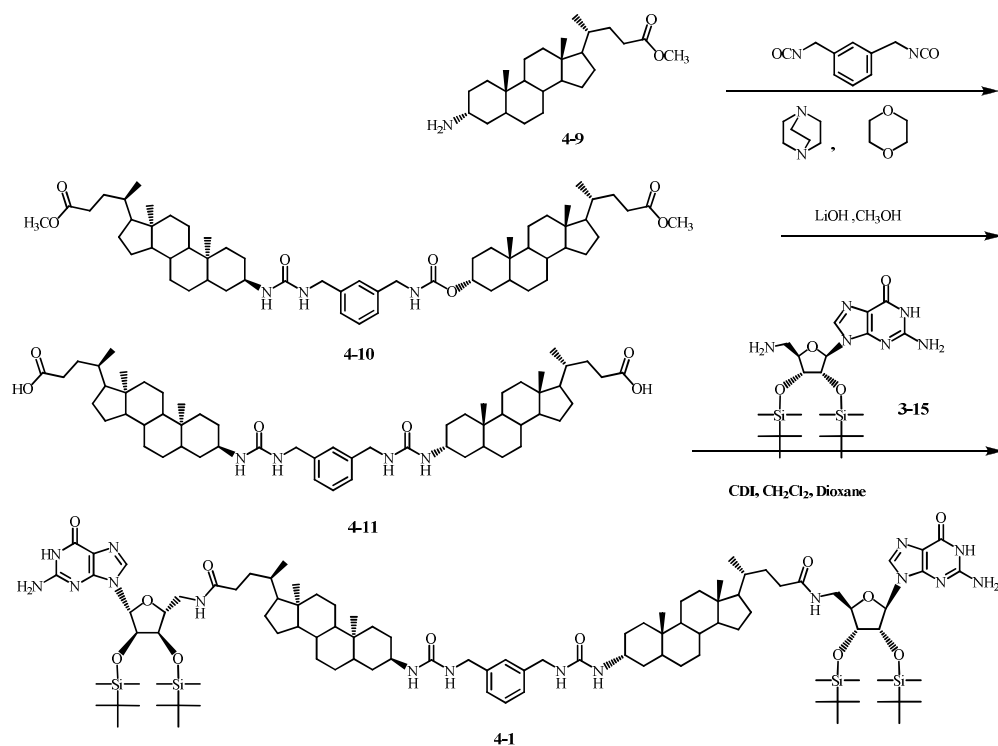


**Figure 4.5**  $^1\text{H}$  NMR spectrum of 3 $\alpha$ -amino lithocholate **4-9** in  $\text{CDCl}_3$ .

The bis-urea lithocholate ester **4-10** was prepared by reacting 3 $\alpha$ -amino lithocholate **4-9** with m-xylene diisocyanate in THF. Hydrolysis of the resulting diester **4-10** gave the corresponding diacid **4-11**. Coupling of **9** with the known 2', 3'-bis-tBDMSi-5'-amino guanosine<sup>83</sup> gave the target bis-urea guanosine-sterol **4-1** (**Scheme 4.3**). The desired final product **4-1** was confirmed by <sup>1</sup>HNMR and ESI-MS characterization (**Figure 3.6**). The ESI-MS characterization of **4-1** shows the (M-H)<sup>+</sup> peak at m/z 1926.2, which is consistent with the theoretical calculation (M.W.= 1926.2) (**Figure 3.6**).



**Scheme 4.3** Synthesis of bis-urea modified guanosine-sterol conjugate **4-1**.

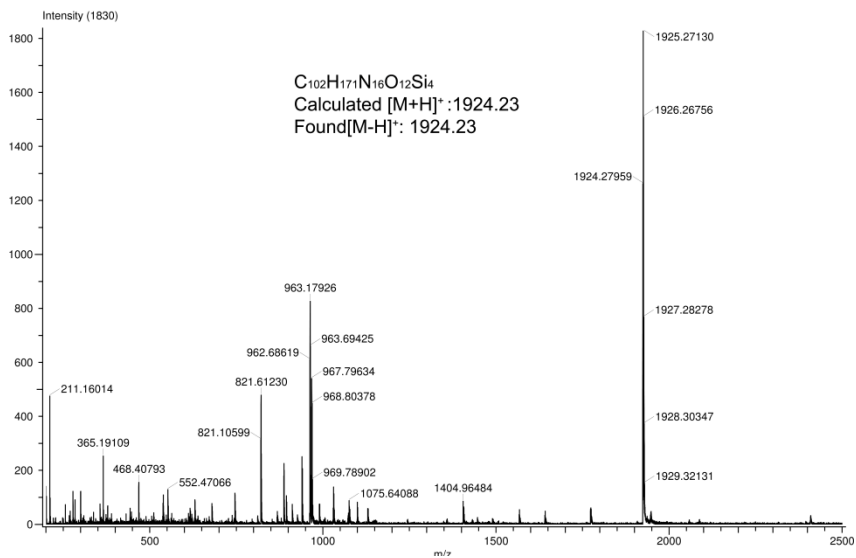
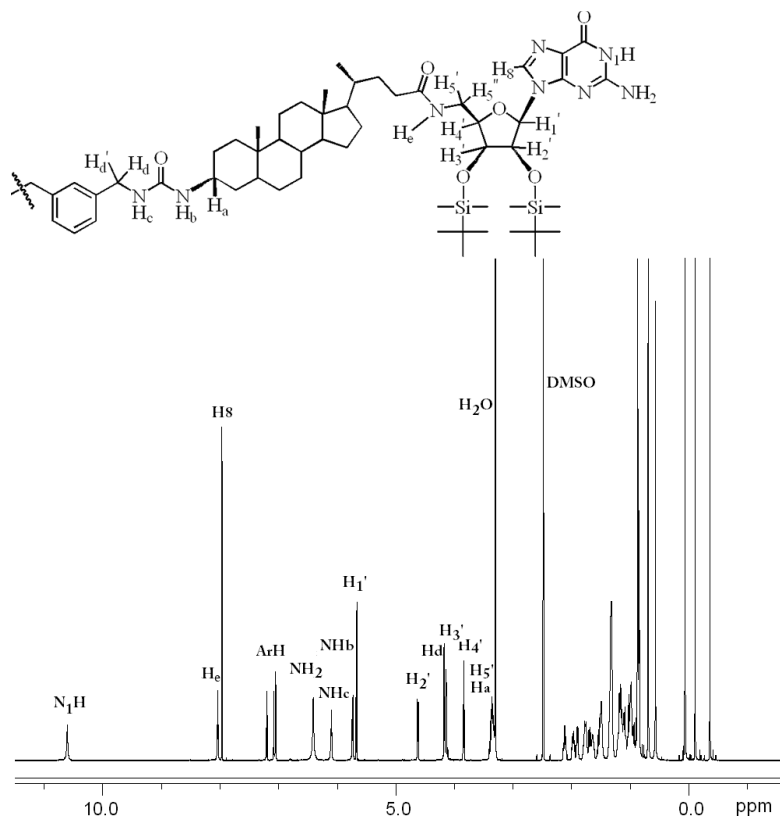


**Figure 4.6**  $^1\text{H}$  NMR and ESI-MS spectra of bis-urea **4-1** in  $\text{DMSO-}d_6$ .

## 4.4 Solution Study of Self-Assembly: Bis-Urea Modified Lithocholate vs. Bis-Carbamate Analogue

### 4.4.1 $^1\text{H}$ NMR Spectroscopy Provides Evidence of Intermolecular Hydrogen Bonding Between Bis-Urea Linker Units.

Various NMR techniques have been successfully applied to the study of hydrogen bonding in either solution or in the solid-state.<sup>137,149</sup> For example,  $^1\text{H}$  NMR spectroscopy can provide the information of intermolecular hydrogen bond by monitoring the chemical shift of protons involved in the hydrogen bond. The formation of a hydrogen bond, in the structure of  $\text{X}-\text{H}\cdots\text{Y}$ , results in the decrease of electron density around the H atoms. Therefore, the H nucleus becomes less shielded from the applied magnetic field, and the chemical shift of the hydrogen-bonded proton moves downfield. On the contrary, the increase in temperature or dilution are expected to disfavor the hydrogen-bond network, and thus the chemical shift of the proton involved in a hydrogen bond interaction moves upfield toward the spectral position of the non-hydrogen bonded species.

The impact of the carbamate to urea modification on the self-association of these modified sterols was first evaluated by solution  $^1\text{H}$  NMR spectroscopy. We chose to compare bis-lithocholate ester **3-13** and **4-10**, rather than guanosine-sterol conjugate **3-1** and **4-1**, so as to eliminate the complications in the spectra that arise from the amide protons of guanosine.  $^1\text{H}$  NMR experiments were conducted on the  $\text{CDCl}_3$  solution of diester **3-13** and **4-10**, and the chemical shift of NH protons was monitored as a function of concentration and temperature. As shown in **Figure 4.7a**, at room temperature, an increase in concentration of bis-urea lithocholate **4-10** in  $\text{CDCl}_3$  resulted in downfield shift of both urea NH protons ( $\Delta\delta \sim 0.8$  ppm from 0.5 to 10 mM). This data suggested the



electron density of the proton decreases, as a result of the formation of intermolecular hydrogen bonding. Both urea protons showed very similar downfield chemical shifts, which would be consistent with urea's characteristic three-center hydrogen bonding pattern. In contrast, the chemical shift of the carbamate NH in compound **3-13** was insensitive to the change in concentration. This result suggested that bis-urea **4-10** has the greater propensity to self-assemble than does the analogous carbamate **3-13**.

Using a 10 mM solution of compound **3-13** and **4-10** in CDCl<sub>3</sub>, the temperature dependence of the NH chemical shifts for these two compounds was also investigated. The NH chemical shifts in **4-10** were also sensitive to temperature, another signature of intermolecular hydrogen bonding. As shown in **Figure 4.6b**, increasing the temperature of the solution of **4-10** caused a significant upfield shift for both urea N-H protons, consistent with increased dissociation of hydrogen bonds with increasing temperature. On the contrary, the carbamate NH proton from bis-carbamate analogue **3-13** displayed little dependence on temperature, corresponding to a monomeric structure in CDCl<sub>3</sub>.

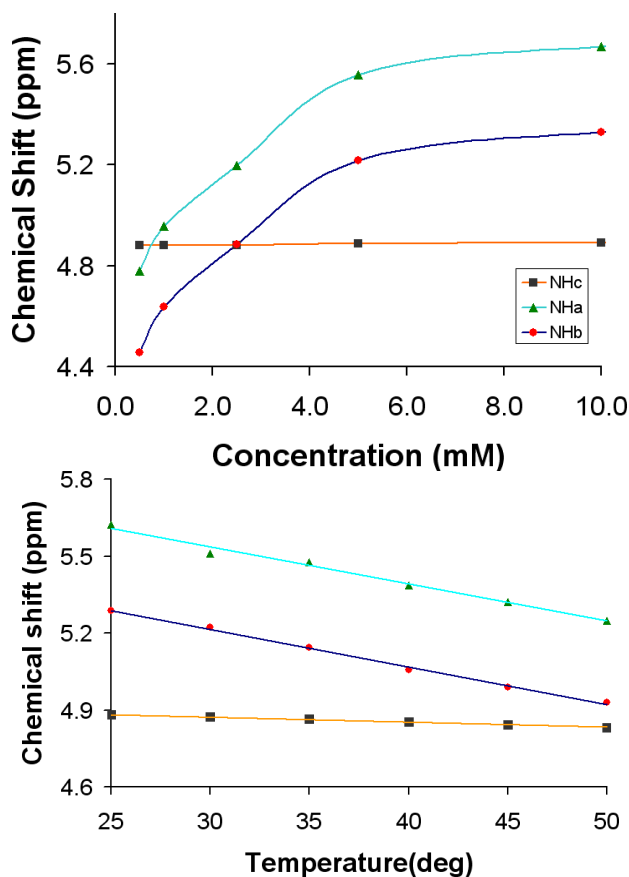


**Figure 4.7**  $^1\text{H}$  NMR spectra of N-H proton of bis-urea lithocholate **4-10** (blue line) and bis-carbamate lithocholate **3-13** (red line) in  $\text{CDCl}_3$ . a) at room temperature, the chemical shift of NH proton is plotted against concentration; b) at 10 mM concentration, the chemical shift of NH proton is plotted against temperature.

#### 4.4.2 Intermolecular Hydrogen Bonding Study by FT-IR Spectroscopy

Using FT-IR spectroscopy, we also confirmed the formation of intermolecular hydrogen bond for bis-urea lithocholate **4-10** in chloroform. For urea derivatives, the urea N-H stretch, amide I (C=O) and amide II (C-N) stretch exhibit characteristic shifting signals upon the formation of intermolecular hydrogen bonds.<sup>150-152</sup> In general, urea N-H stretch and C=O stretch shift toward lower frequency, due to the weakening of these bonds upon the formation of hydrogen bonds. On the contrary, the C-N stretch moves toward higher wave-number due to hydrogen bonding.

**Figure 4.8** shows the N-H stretching region in the FT-IR spectra for the bis-urea lithocholate **4-10** and bis-carbamate lithocholate **3-13**. As the concentration of bis-urea ester **4-10** increased, a broad N-H broad stretch band ( $\sim 3360\text{ cm}^{-1}$ ) grew in on the lower frequency side of the free N-H absorption band ( $\sim 3430\text{ cm}^{-1}$ ), characteristic of the intermolecular hydrogen bonding of urea group. Clearly, increased concentration leads to self-association of **4-10** in a non-polar solvent. In contrast, bis-carbamate ester **3-13** displayed no shift in its N-H absorption band upon a change in concentration, suggesting no intermolecular hydrogen bonding in  $\text{CHCl}_3$ . Compound **3-13** remained monomeric, even at 15 mM.

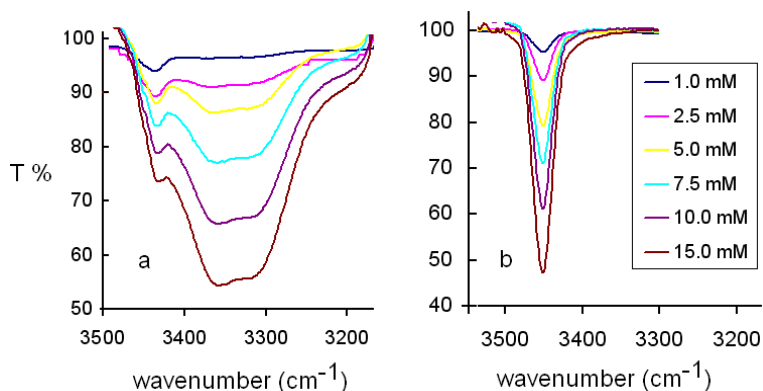


**Figure 4.8** N-H stretching region of the IR spectra as a function of concentration for a) bis-urea lithocholate **4-10**; b) bis-carbamate lithocholate **3-13** in  $\text{CDCl}_3$  at  $25^\circ\text{C}$ .

Furthermore, the concentration-dependent frequency change of the amide I ( $\text{C}=\text{O}$ ) and amide II ( $\text{C}-\text{N}$ ) stretches also supported intermolecular hydrogen bonding for bis-urea ester **4-10**. As shown in **Table 4.1**, as the concentration of **4-10** in  $\text{CDCl}_3$  increased from 1.0 mM to 15 mM, the amide I band shifted from  $1662\text{ cm}^{-1}$  to  $1632\text{ cm}^{-1}$ ; whereas

the amide band II shifted from 1527  $\text{cm}^{-1}$  to 1684  $\text{cm}^{-1}$ . These concentration-dependent band shifts are consistent with the characteristic bis-urea hydrogen-bonding association pattern.<sup>24</sup> Increasing the concentration of **4-10** shifted the equilibrium toward self-assembly *via* the intermolecular H-bonding between the urea moieties. As for bis-carbamate ester **3-13**, little shift of amide I and amide II absorption band was observed as the concentration changed, suggesting no intermolecular hydrogen bonding for compound **3-13**.

**Table 4.1** FT-IR frequencies for bis-urea **4-10** and bis-carbamate lithocholate **3-13**

Compound	Conc [mM]	$\nu_{\text{max}}$ [ $\text{cm}^{-1}$ ]			
		$\nu_f$ N-H	$\nu_b$ N-H	$\nu$ Amide I	$\nu$ Amide II
<b>4-10</b>	1.0 mM	3437	3407	1662	1527
	2.5 mM	3436	3381	1660	1529
	5.0 mM	3435	3371	1659	1529
	7.5 mM	3435	3365	1632	1564
	10.0 mM	3433	3363	1632	1564
	15.0 mM	3431	3361	1632	1564
<b>3-13</b>	1.0 mM	3452	NA	1716	1508
	2.5 mM	3452	NA	1716	1508
	5.0 mM	3452	NA	1716	1508
	7.5 mM	3452	NA	1716	1512
	10.0 mM	3452	NA	1716	1510
	15.0 mM	3452	NA	1716	1510

## 4.5 Large and Stable Ion Channel From Guanosine-Sterol Conjugate With Bis-Urea Modified Linker

Guanosine-sterol conjugate **4-1**, containing the bis-urea modified linker, was designed so that it might further stabilize self-assembled ion channels within the phospholipid bilayer. The ion channel formation from **4-1** in a bilayer membrane was characterized by voltage clamp techniques previously described in Chapter 3. Thus, 50 nM of compound **4-1** (final concentration in isopropanol) was loaded into the *cis* side of the planar membrane under 1.0 M KCl symmetric condition. A voltage-ramp potential of -10mV was applied. Active ion channels with multiple levels of conductance were observed. **Figure 4.9** shows representative conductance changes generated after addition of **4-1**. These multiple open states clearly demonstrate the formation of discrete ion channels with large conductance in the nS range and long lifetimes in the second to minutes range. The transits from “open” to “closed” state indicated the dynamic nature of self-assembled ion channels.

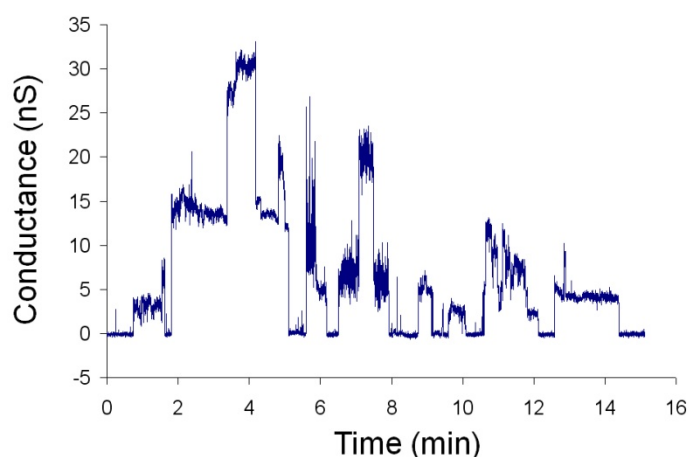


**Figure 4.9** Representative conductance records from voltage clamp experiment. Ion channels formed by **4-1** in a planar bilayer at an applied voltage of -10 mV in 1M KCl (*trans*) / KCl (*cis*) solution (pH 7.0).

During the voltage clamp experiment, we first noticed that the bis-urea **4-1** is membrane active at a much lower concentration than is bis-carbamate **3-1**. Bis-urea **4-1** was active at a concentration of 50 nM but compound **3-1** had to be added to the solution bathing the planar membrane at a much higher concentration (31.4 mM) in order to observe channel formation within a reasonable time. Addition of **4-1** at such mM concentrations typically caused breakage of the planar bilayer membrane during the voltage clamp experiment. This dramatic difference in effective concentrations may be attributed to the fact that bis-urea **4-1** is better able to self-associate into some active structure than is bis-carbamate **3-1**. Despite such difference, both guanosine-sterol conjugate **4-1** and **3-1**, gave multiple channels with similar type of conductance states. In particular, the most frequent conductance increments and decrements were observed on the order of 1-5 nS for both guanosine-sterol **4-1** and **3-1** (**Table 4.2**). This result indicated **4-1** and **3-1** forms very similar pore structures within the phospholipid bilayer, regardless of the differences in their sterol backbone. This result supports our previous conclusion that the guanosine moiety plays an essential role in the self-assembly of the ion channels.

To compare the ion channel activity of guanosine-sterol conjugates **4-1** and **3-1**, we characterized the “open state” of the active ion channels formed from these two different analogues. Histograms of the frequencies of conductance recorded are shown in **Figure 4.10**. While compound **3-1** and **4-1** both formed multiple ion channels with very similar conductance levels, the frequency and life-time of these channel openings are quite different. Bis-urea **4-1** formed, on average, larger channels than did bis-carbamate **3-1**. The statistical data is summarized in Table 1. “Giant” channels with conductance

levels greater than 5 nS were formed more frequently by bis-urea **4-1** (43 % of all events) than by bis-carbamate **3-1** (12 % of all events).

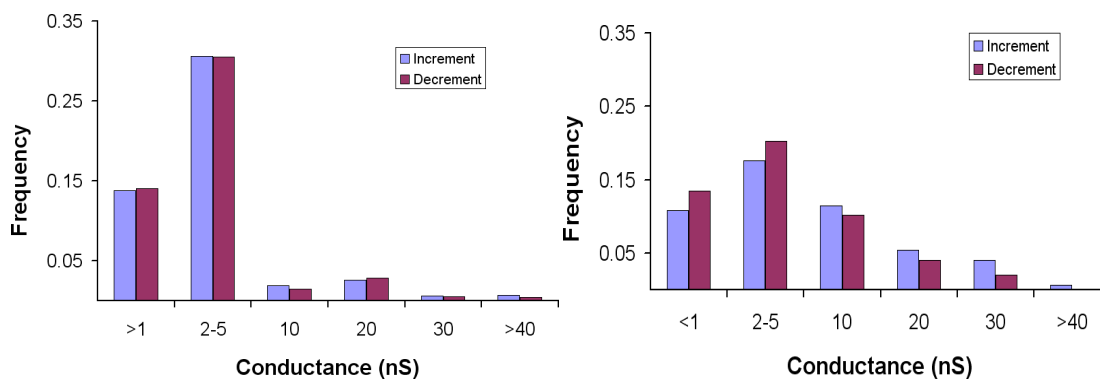


**Figure 4.10** Distribution of conductance change for the ion channels from guanosine-sterol conjugate **4-1** and **3-1**. The frequency was calculated based on the total number of increment (channel open) events or decrement (channel close) events. a) data from compound **4-1**; b) data from compound **3-1**.

**Table 4.2** Frequency of Events for Channels formed from 4-1 and 3-1.

Conductance	Bis-Carbamate <b>3-1</b>		Bis-Urea <b>4-1</b>	
	# Events	% Events	# Events	% Events
0.1 - 1.0 nS	100	20	16	22
1.1 - 5.0 nS	331	68	26	35
5.1 - 20 nS	43	9	17	23
> 20 nS	13	3	13	20

Note: The number and frequency of ion channel open events for **4-1** were taken from the 3 experiments that used Method 1 reported in Chapter 3. For compound **3-1**, the data were taken from a total of 4 experiments. These experiments were conducted by adding either compound **3-1** (31.4  $\mu$ M) or **4-1** (50 nM) to the cis side of the chamber after the planar bilayer membrane was formed (1.0 M KCl and -10 mV applied potential).

The lifetimes of the “open” state have been used to assess the stability of self-assembled ion channels.<sup>153,154</sup> Overall, more stable ion channels give longer lifetimes for active ion transport. To compare the relative stability of channels formed by guanosine-sterol **4-1** and **3-1**, we analyzed the “open” lifetimes for channels formed these compounds. We chose conductance values between 1 and 5 nS, since these conductances were the most frequent events observed for both guanosine-sterols (see **Table 4.2**). As shown in the histogram in **Figure 4.11**, about 70% of the 1-5 nS channels formed from bis-carbamate **3-1** had open lifetimes that were less than 10 seconds. In contrast, over 80% of the 1-5 nS channels formed by bis-urea **4-1** had open lifetimes that were greater than 10 seconds. Remarkably, about 50% of these channels formed by **4-1** were open for 30 seconds or longer. The average lifetime of 1-5 nS channels formed from bis-urea **4-1** was 66 seconds/event, as compared to 16 seconds/event for the 1-5 nS channels formed from bis-carbamate **1**. Our data indicates that the bis-urea units in the linker region of **4-1** help to stabilize transmembrane ion channels formed by this guanosine-lithocholate derivative, relative to those channels formed by compound **3-1**.



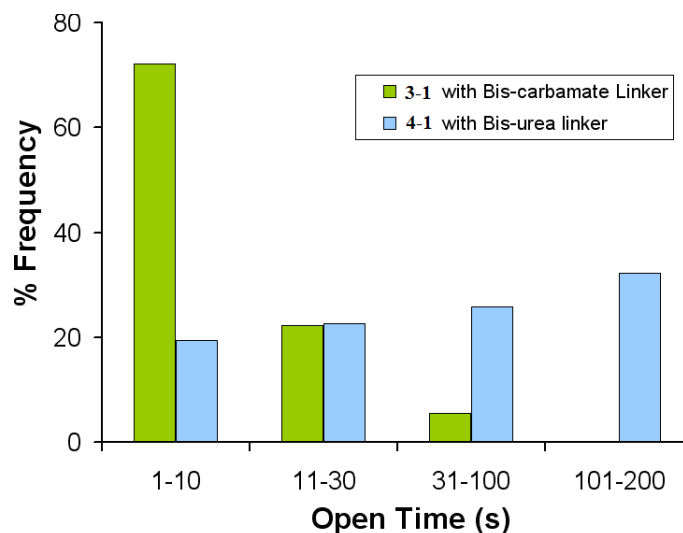
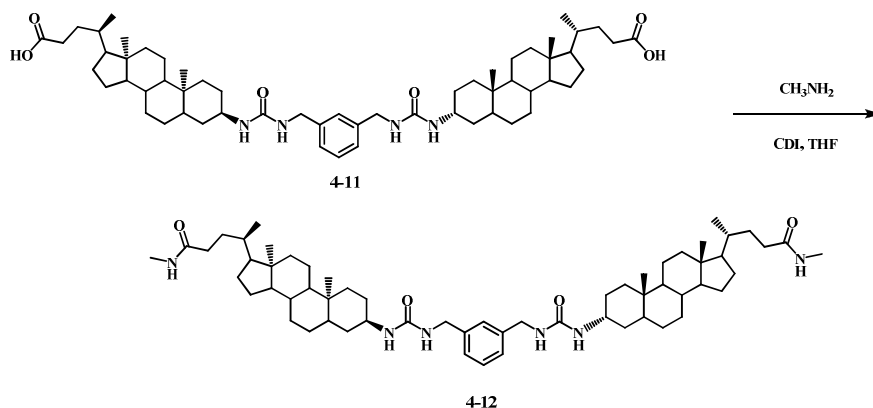


**Figure 4.11** Histogram showing the various open lifetimes for 1-5 nS channels formed from **3-1** and **4-1**. Distribution of conductance change, the frequency was calculated based on the total number of increment (channel open) events.

#### 4.6 Structural Study of Guanosine-Sterol Conjugate With the Bis-Urea Linker

We wanted to gain more insight about the structure-function relationship between ion channels and the molecular precursor, guanosine-sterol conjugate **4-1**. Thus, bis-urea lithocholamide **4-12**, lacking the guanosine end group, was designed as a control compound to evaluate the functionality of the guanosine end-group or the sterol linker in the formation of ion channels. The synthesis of **4-12** was accomplished by coupling bis-lithocholic diacid **4-11** with  $\text{CH}_3\text{NH}_2$ , in the presence of the coupling reagent CDI (**Scheme 4.4**).



**Scheme 4.4** Synthesis of bis-urea lithocholamide **4-12** for the control experiment.

Using the experimental method described in section 4.6 for compound **4-1**, the channel activity of **4-12** in a bilayer membrane was characterized by voltage clamp experiment. After 250 nM of compound **4-12** (final concentration in isopropanol) was loaded into the *cis* side of the preformed membrane under a 1.0 M KCl symmetric condition, it was observed that compound **4-12** was able to form ion channels within phospholipid bilayer. Compared with its channel inactive bis-carbamate analogue **3-16** examined in chapter 3, the bis-urea lithocholate **4-12** demonstrated quite different ion channel properties. This result indicates that the bis-urea moiety in the sterol linker **4-12** plays an essential role in the self-assembly of ion channel. Intermolecular hydrogen bonding between urea groups likely allow for the self-association that occurs within the bilayer membrane. This result is consistent with the previous NMR and IR study that the urea modified sterol backbone can form intermolecular hydrogen bonding in a non-polar environment, while the carbamate backbone could not form intermolecular hydrogen bonds.

The characterization of active ion channels showed that control compound **4-12** forms discrete ion channels with conductance in the range of pS range, occasionally in the nS range. The lifetime of these channels are in the millisecond to second range. Compared with the ion channels from guanosine-sterol conjugate **4-1** (**Figure 4.10**), these ion channels are much smaller and their lifetimes are much shorter. This data indicates that compound **4-12** forms random and unstable ion channels induced by the hydrogen bonding of the bis-urea functionality. On the other hand, this data also confirms our previous structural study that the guanosine motifs in the guanosine-sterol conjugate **4-1** are crucial in the formation of large and stable ion channels.

#### **4.7 Guanosine-Sterol Conjugate Causes Release of Carboxyfluorescein from Liposomes.**

The carboxyfluorescein (CF) release assay has been developed to assess pore formation and membrane stability in a variety of biological applications.<sup>155,156</sup> This fluorescent method relies on the self-quenching of CF entrapped in liposome. A liposome is a spherical vesicle composed of phospholipid bilayers. It has been used as a cell model to study the transmembrane transport of ions and small molecules. When the pore forms in a liposome, the release of internal CF leads to dilution and an increase in fluorescence. In practice, the fluorescence quenching of encapsulated CF can be obtained by either self-quenching of CF at high concentration or mixing CF and a quencher inside a liposome. Carboxyfluorescein is about 10 Å long and 6.5 Å wide. **Figure 4.12** shows the chemical structure of CF and the scheme of the carboxyfluorescein assay that was used in this study.

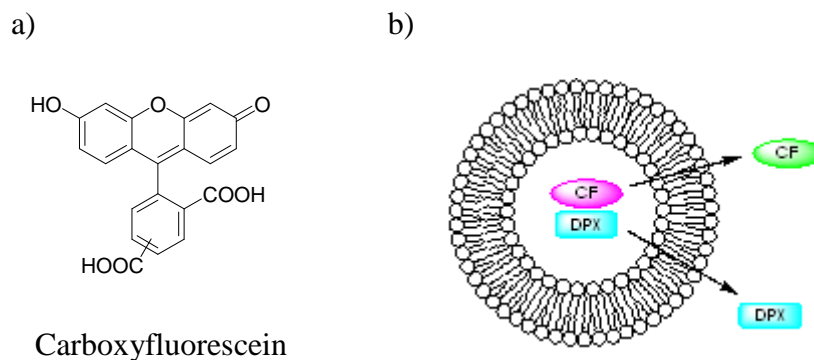


**Figure 4.12** a) Chemical structure of carboxyfluorescein. b) Scheme of a fluorescent assay of carboxyfluorescein release from liposome.

The study of CF release, as mediated by guanosine-sterol conjugate **3-1** and **4-1**, was monitored by the change in CF fluorescence. Here, liposomes (100 nm) were prepared from EYPC (egg yolk phosphatidylcholine) phospholipids. Both CF and the p-xylylene-bis-pyridinium bromide quencher were pre-loaded inside the liposome. The final concentration of liposome was maintained at 330  $\mu\text{M}$  in a HEPES buffer solution (10 mM HEPES, 50 mM NaCl, 1 mM EDTA, pH = 7). Upon addition of a 100  $\mu\text{M}$  DMSO solution of either **3-1** or **4-1** into the liposome solution, a significant fluorescence increase occurred, indicating CF efflux across the phospholipid bilayer. **Figure 4.13** demonstrates the CF release data as a function of time. It is clear that both guanosine-sterol conjugates **3-1** and **4-1** promote CF transport from liposome into the extravesicular solution. The data provides direct evidence for the formation of large pore mediated by these compounds within liposome.

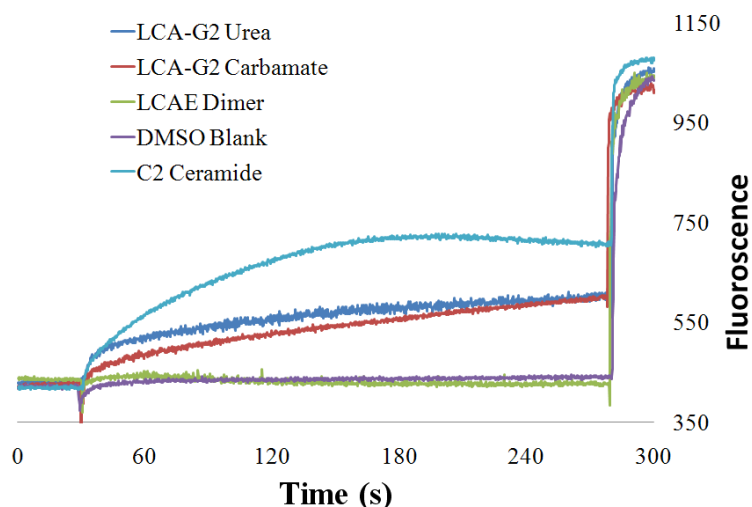


**Figure 4.13** Carboxyfluorescein release assay confirmed the pore formation mediated by guanosine-sterol conjugate **3-1** and **4-1**.

Compound **4-1** with a urea linker was slightly more active than **3-1** with a biscarbamate linker. There was no transport of CF for the control bis-urea lithocholate **4-1** that lacked guanosine end groups, consistent with our previous structural study that the guanosine moiety play a key role in the self-assembly of the ion channels. C2-ceramide was chosen as a positive control in these experiments. Ceramides are sphingosine-based lipid molecules that are believed to be key regulators in apoptosis by inducing cytochrome c release from mitochondria.<sup>157</sup> Siskind and Colombini reported that C(2)-ceramide forms large channels in phospholipid membrane.<sup>131,158</sup> The formation of ceramide channels is thought to be the origin for the increasing the permeability of the mitochondrial outer membrane to small proteins. The CF release study shown in **Figure 4.15** supported the formation of pores by guanosine-sterol conjugates **3-1** and **4-1** within phospholipid bilayers.

## 4.8 Conclusion

Guanosine-sterol conjugate **4-1**, containing a bis-urea group in its linker region, was designed so that it might further stabilize self-assembled ion channels within the phospholipid bilayer. Our hypothesis is that strengthening the intermolecular interactions between the bis-lithocholate linker regions might work cooperatively with the guanosine-based self-association to provide highly stable conducting structures. Bis-urea **4-1** forms large ion channels whose lifetimes are longer than those channels formed by bis-carbamate **3-1**, and is consistent with our structural hypothesis. Our future work will focus on investigating whether this new guanosine-lithocholic acid derivative **4-1**, which can form channels that must have nm diameters, can be used to transport larger compounds in and out of phospholipid vesicles.

## Chapter 5. Final Conclusion and Future Directions

The study of cation exchange between solvated cations ( $K^+$ ,  $NH_4^+$ ) and bound cations in the G-quadruplex  $[G\ 1]_{16} \cdot 4Na^+ \cdot 4DNP^-$  revealed that cations of these lipophilic G-quadruplex do not move through the ends of the central channel (**Chapter 2**). In reality, the cation exchange occurs first in the middle of the assembly. This result suggested that the lipophilic G-quadruplex is too kinetically labile to function as an intact structure for ion transport. To overcome this problem, covalent linkers are needed to connect lipophilic G units so as to generate an appropriate building block for a synthetic ion channel. Such covalent linkages should stabilize the G-quadruplex structures.

A ditopic design strategy involving a bis-sterol linker capped with two guanosine end-groups was described in **Chapter 3**. This guanosine-lithocholate conjugate **3-1** is able to self-assemble into discrete synthetic ion channels in phospholipid membranes. The pores are large (nS conductance) and stable, with “open” times of seconds, distinguishing them from most synthetic channels, which typically conduct in the pS range with millisecond lifetimes. The structure-property studies suggested that the guanosine subunits play an important role in the self-assembly of an active ion channel. The importance of the hydrophobic effect of the bis-sterol linker on the channel formation was ruled out.

The replacement of the carbamate group with the urea group in the sterol linker of **3-1** was designed to achieve a more stable and efficient system (**Chapter 4**). As a result, guanosine-sterol **4-1** with bis-urea modifications also resulted in formation of large and

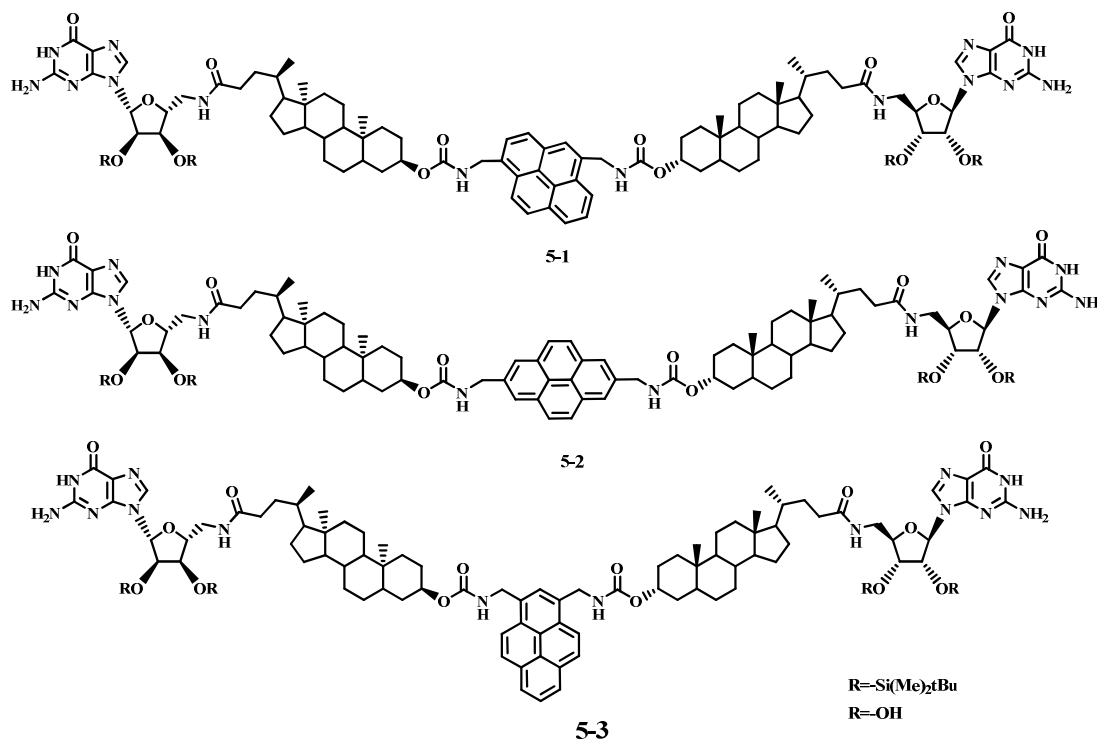
stable ion channels. The channels were longer-lived than those formed by the corresponding bis-carbamate analogue. In addition, both guanosine-sterol **3-1** and **4-1** can transport organic molecule (carboxyfluorescein) across phospholipid bilayer membrane.

The research discussed in this thesis has demonstrated our approach toward synthetic ion channels based on ditopic lipophilic guanosine building molecules. The insight into the structure, properties, and functionality of this lipophilic nucleobase may lead to more potential applications in biomembranes or as functional biomaterials. So far, there are only limited numbers of examples of membrane active lipophilic guanosine derivatives that have been reported. Since nanometer-size pores formed by both ditopic guanosine-sterol **3-1** and **4-1** were proposed by the planar bilayer membrane study, stabilization and functionalization of these large pores may create new systems for biosensor or drug delivery.

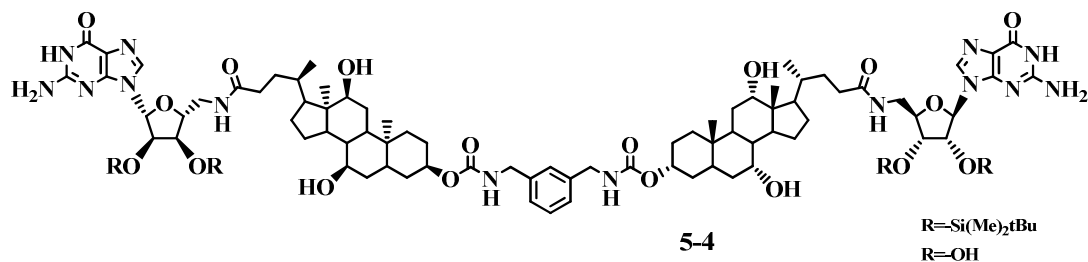
The first strategy involves incorporating additional noncovalent interactions into the linker region of ditopic guanosine-sterol conjugate, similar to that of compound **4-1**. A possible target molecule includes pyrene-modified guanosine-sterol conjugate **5-1**, **5-2**, **5-3**, with varying substitution positions on the pyrene ring. This strategy is expected to generate more stable ion channels, since strong  $\pi$ - $\pi$  interaction between pyrene subunit in the sterol linker might work cooperatively with the self-association of guanosine group. In addition, compounds **5-1**, **5-2**, **5-3** can be further modified by replacing bis-carbamate with bis-urea moiety in the sterol linker. Planar bilayer measurements are a must to evaluate the activity and stability of the self-assembled ion channel formed by these



guanosine-sterol analogues. Liposome studies are needed to characterize whether these channels are capable of transporting larger molecules across the phospholipid membranes.



The second strategy involves the development of functional ion channel using guanosine-cholic acid conjugate **5-4**. The hydroxyl groups on the concave  $\alpha$ -face of cholic acid are ideal places to introduce variable functionality. These approaches are based on our structural hypothesis of the ion channels formed from the guanosine-lithocholic acid conjugate **5-4**, where the G-quadruplex serves as a central pillar and the sterol linker provides the hydrophobic wall of the ion channel.



The incorporation of certain functionality into cholic acid linker of compound **5-4** may provide molecular recognition property for the self-assembled pores. This research may direct our approach to synthetic channels or pores that can be used to recognize and eventually selectively transport larger biomolecules in and out of liposomes and/or cells.

## Chapter 6. Experimental and References

### 6.1 General Experimental

All  $^1\text{H}$  NMR spectra were recorded on a Bruker DRX-400, a Bruker Avance 400 instrument operating at 400.13 MHz, or on a Bruker DRX-500 operating at 500.13 MHz. The  $^{13}\text{C}$  NMR spectra were recorded on a Bruker DRX-400 and Bruker Avance 400 instrument operating at 100.61 MHz. Chemical shifts are reported in ppm relative to the residual protonated solvent peak. Variable temperature  $^1\text{H}$  NMR experiments were controlled to  $\pm 0.1$  °C and calibrated with methanol at low temperatures and ethylene glycol at high temperature. All NMR spectra were recorded at 20-25 °C (room temperature) unless otherwise specified. Two dimensional  $^1\text{H}$ - $^1\text{H}$  COSY ( $^1\text{H}$ - $^1\text{H}$  three-bond coupling),  $^1\text{H}$ - $^1\text{H}$  NOESY ( $^1\text{H}$ - $^1\text{H}$  through space magnetization transfer),  $^1\text{H}$ - $^{13}\text{C}$  HSQC ( $^1\text{H}$ - $^{13}\text{C}$  one-bond coupling) and  $^1\text{H}$ - $^{13}\text{C}$  HMQC ( $^1\text{H}$ - $^{13}\text{C}$  multibond coupling) experiments were run using previously published standard protocols.<sup>159-161</sup> ESI-MS experiments were recorded on a JOEL AccuTOF CS. All fluorimetric experiments were carried out on a Hitachi F4500 fluorescence spectrophotometer. The pH of solutions was monitored with a Fisher Scientific AR25 dual channel pH/ion meter. Circular dichroism (CD) spectra were recorded on a JASCO-810 spectropolarimeter with a 1.0 cm and 1.0 mm path length quartz cuvette. Variable temperature CD experiments were controlled by an attached PFD425S Peltier system with a 1.0 cm and 1.0 mm path length quartz cuvette. Deuterated solvents were purchased from Cambridge Isotope Laboratories. Chromatography was performed using 60-200 mesh silica purchased from Baker and 40-120  $\mu$  Sephadex G-10 purchased from Pharmacia Fine Chemicals. Thin layer

chromatography was performed on Kieselgel 60 F254 and Uniplate<sup>TM</sup> Silica Gel GF silica-coated glass plates and visualized by UV or by staining with I<sub>2</sub> or an aqueous solution of ceric ammonium molybdate (CAM). All chemicals and solvents were purchased from Sigma, Fluka, or Acros. Phospholipids used in the voltage clamp and liposome experiments were purchased from Avanti Polar Lipids. Guanosine (G **1**), (G **1**)<sub>16</sub>·4K<sup>+</sup>·4DNP<sup>-</sup> G-quadruplex, and the potassium, sodium phenolates and ammonium (<sup>15</sup>N) tetraphenyl-borate were prepared following the published methods. All solvents were dried and distilled following standard procedures.

## 6.2 Synthesis

**5'-t-butyl-dimethylsilyl-2',3'-O-isopropylidene-Guanosine (G **1**).** To a suspension of guanosine (10.0 g, 35.0 mmol) in acetone (500 mL) was added p-TsOH-H<sub>2</sub>O (13.5 g, 71.0 mmol) and 2,2-dimethoxypropane (53 mL, 430 mmol). The resulting solution was stirred at room temperature until it turned clear. Triethylamine (10 mL, 71.0 mmol) was added to neutralize the solution. A precipitate formed, and the solvent was removed *in vacuo*. To a suspension of the residue and imidazole (1.94 g, 29.0 mmol) in methylene chloride (150 mL) was added *t*-butyl dimethylsilyl chloride (4.32 g, 29.0 mmol). The reaction mixture was stirred overnight, and TLC analysis indicated the reaction was complete. The reaction mixture was washed with 0.1 N HCl, saturated NaHCO<sub>3</sub> and saturated brine and concentrated *in vacuo*. Recrystallization of the crude product from isopropanol gave a white solid G **1** (3.85 g, 59 %). <sup>1</sup>H NMR (400 MHz, 1:1 CD<sub>2</sub>Cl<sub>2</sub>:CD<sub>3</sub>CN): δ 9.59 (s, 1H, NH1), 7.66 (s, 1H, H8), 5.93 (d, 1H, H1', J = 2.0 Hz),

5.50 (s, 2H, N2), 5.15 (dd, 1H, H2', J = 2.2, 6.0 Hz), 4.94 (dd, 1H, H3', J = 2.7, 6.0 Hz), 4.23 (m, 1H, H4', J = 2.7 Hz, 10.0 Hz), 3.76 (m, 2H, H5', H5'', J = 6.0, 10.0 Hz, 6.0 Hz), 1.55 (s, 3H, CH<sub>3</sub>), 1.34 (s, 3H, CH<sub>3</sub>), 0.85 (s, 9H, *t*-Bu), 0.01 (s, 3H, Si (CH<sub>3</sub>)), 0.00 (s, 3H, Si (CH<sub>3</sub>)).

**Hexadecamer of (G 1)<sub>16</sub>•4Na<sup>+</sup>•4DNP<sup>+</sup>.** A suspension of G 1 (100 mg, 228 μmol) in 6 mL of CH<sub>2</sub>Cl<sub>2</sub> was stirred with a NaDNP solution in water (4 mL, 228 mM) at room temperature for 5 h. The organic layer was separated and dried under vacuum. The residue was dissolved in 4 mL of CH<sub>2</sub>Cl<sub>2</sub> and 4 mL of CH<sub>3</sub>CN. The resulting clear solution was allowed to evaporate slowly at room temperature. Yellow crystals of G<sub>16</sub>•4Na<sup>+</sup>•4DNP<sup>-</sup> formed after 3 days. <sup>1</sup>H NMR (400 MHz, 1:1 CD<sub>2</sub>Cl<sub>2</sub>:CD<sub>3</sub>CN): δ 11.71 (s, 1H, NH1<sub>a</sub>), 11.46 (s, 1H, NH1<sub>b</sub>), 9.95 (s, 1H, N2 H<sub>Aa</sub>), 8.09 (d, 2H, DNP anion *m*-H, J = 8.1 Hz), 7.58 (s, 1H, H8<sub>a</sub>), 6.89 (s, 1H, H8<sub>b</sub>), 6.33 (s, 1H, H1'<sub>a</sub>), 6.20 (t, 1H, anion *p*-H, J = 8.1 Hz), 6.01 (d, 1H, H2'<sub>a</sub>, J = 6.0 Hz), 5.68 (s, 1H, N2 H<sub>Ba</sub>), 5.56 (t, 1H, H2'<sub>b</sub>, J = 4.0 Hz), 4.78 (d, 1H, H1'<sub>b</sub>, J = 3.7 Hz), 4.38 (d, 1H, H3'<sub>a</sub>, J = 6.0 Hz), 4.28-4.10 (m, 4H, H4', H5'), 3.72 (d, 1H, H3'<sub>b</sub>, J = 6.4 Hz), 3.68 (d, 1H, H5'<sub>b</sub>, J = 9.3 Hz), 3.19-3.16 (m, 2H, H5'), 1.57 (s, 3H, CH<sub>3a</sub>), 1.54 (s, 3H, CH<sub>3b</sub>), 1.47 (s, 3H, CH<sub>3b</sub>), 1.37 (s, 3H, CH<sub>3a</sub>), 0.85 (s, 9H, Si-*t*Bu<sub>a</sub>), 0.47 (s, 9H, Si-*t*Bu<sub>b</sub>), 0.15 (s, 6H, Si-CH<sub>3a</sub>), 0.14 (s, 6H, Si-CH<sub>3b</sub>), -0.41 (s, 3H, Si-CH<sub>3b</sub>), -0.46 (s, 3H, Si-CH<sub>3a</sub>). The designators a) and b) reflect the upper and lower G-quartets respectively.

**Hexadecamer of the G<sub>16</sub>•4NH<sub>4</sub><sup>+</sup>•4DNP<sup>-</sup>.** To a solution of 3.3N NH<sub>4</sub>OH (138 μl, 457 μmol) in H<sub>2</sub>O (4 mL) was added 2,6-dinitrophenol (84 mg, 457 μmol). The mixture solution was stirred at room temperature for 40min. A suspension of G 1 (100 mg, 228

$\mu\text{mol}$ ) in 6 mL of  $\text{CH}_2\text{Cl}_2$  was stirred with  $\text{NH}_4\text{DNP}$  aqueous solution at room temperature for 4h. The organic layer was separated and dried under vacuum. The organic layer was separated and dried under vacuum. The residue was dissolved in 4 mL of  $\text{CH}_2\text{Cl}_2$  and 4 mL of  $\text{CH}_3\text{CN}$ . The resulting clear solution was allowed to evaporate slowly at room temperature. Orange rod crystals of  $\text{G}_{16}\cdot 4\text{NH}_4^+ \cdot 4\text{DNP}^-$  formed after 2 days.  $^1\text{H}$  NMR (400 MHz, 1:1  $\text{CD}_2\text{Cl}_2:\text{CD}_3\text{CN}$ ):  $^1\text{H}$  NMR (400 MHz, 1:1  $\text{CD}_2\text{Cl}_2:\text{CD}_3\text{CN}$ ):  $\delta$  11.50 (s, 1H,  $\text{NH}_{1a}$ ), 11.36 (s, 1H,  $\text{NH}_{1b}$ ), 9.25 (s, 1H, N2  $\text{H}_{Aa}$ ), 8.11 (d, 2H, DNP anion *m*-H,  $J = 8.1$  Hz), 7.62 (s, 1H,  $\text{H}_{8a}$ ), 7.07 (s, 1H,  $\text{H}_{8b}$ ), 6.28 (s, 1H,  $\text{H}_{1'a}$ ), 6.21 (t, 1H, anion *p*-H,  $J = 8.1$  Hz), 5.72 (d, 1H,  $\text{H}_{2'a}$ ,  $J = 6.0$  Hz), 5.58 (s, 1H, N2  $\text{H}_{Ba}$ ), 4.74 (t, 1H,  $\text{H}_{2'b}$ ,  $J = 4.0$  Hz), 4.34 (d, 1H,  $\text{H}_{1'b}$ ,  $J = 3.7$  Hz), 4.21-4.09 (m, 4H,  $\text{H}_{4'}$ ,  $\text{H}_{5'}$ ), 3.68 (d, 1H,  $\text{H}_{3'a}$ ,  $J = 6.0$  Hz), 3.13 (d, 1H,  $\text{H}_{3'b}$ ,  $J = 6.4$  Hz), 3.01 (d, 1H,  $\text{H}_{5'b}$ ,  $J = 9.3$  Hz), 3.19-3.16 (m, 2H,  $\text{H}_{5'}$ ), 1.57 (s, 3H,  $\text{CH}_{3a}$ ), 1.54 (s, 3H,  $\text{CH}_{3b}$ ), 1.47 (s, 3H,  $\text{CH}_{3b}$ ), 1.37 (s, 3H,  $\text{CH}_{3a}$ ), 0.85 (s, 9H, Si-*t*Bu<sub>a</sub>), 0.47 (s, 9H, Si-*t*Bu<sub>b</sub>), 0.15 (s, 6H, Si- $\text{CH}_{3a}$ ), 0.14 (s, 6H, Si- $\text{CH}_{3b}$ ), -0.41 (s, 3H, Si- $\text{CH}_{3b}$ ), -0.46 (s, 3H, Si- $\text{CH}_{3a}$ ). The designators a) and b) reflect the upper and lower G-quartets respectively.

**Methyl lithocholate (3-12).** Methyl lithocholate **3-12** was prepared following the procedure of Thchtrop and Covey <sup>1</sup> and purified by crystallization from acetonitrile to give a white solid in 96% yield. mp 122-123 °C.  $^1\text{H}$  NMR (400 MHz,  $\text{CDCl}_3$ )  $\delta$  3.64 (s, 3 H,  $-\text{CO}_2\text{CH}_3$ ), 3.60 (m, 1 H,  $-\text{CH}-\text{OH}$ ), 2.35-0.89 (m, 34 H), 0.62 (s, 3 H,  $-\text{CH}_3$ );  $^{13}\text{C}$  NMR (100 MHz,  $\text{CDCl}_3$ ):  $\delta$  174.8, 71.9, 56.5, 55.9, 51.5, 42.7, 42.1, 40.4, 40.2, 36.4, 35.8, 35.4, 35.3, 34.6, 31.1, 31.0, 30.5, 28.2, 27.2, 26.4, 24.2, 23.4, 20.8, 18.3, 12.0. ESI-MS  $[\text{M}+\text{H}]^+$  calcd for  $\text{C}_{25}\text{H}_{43}\text{O}_3$  391.3, found 391.1.

**Bis[(24-methoxycarbonyl)-3-lithocholanyl]-N',N-xylylene Dicarbamate (3-13).** To a solution of **3-12** (1.06 g, 2.70 mmol) in dioxane (23 mL), m-xylylene diisocyanate (0.21 mL, 1.36 mmol) and DABCO (0.06g, 0.53 mmol). The mixture solution was stirred under N<sub>2</sub> at 70°C for two days. The organic solvent was evaporated under reduce pressure and the remaining solid was purified by column chromatography (SiO<sub>2</sub>, 6:1 Benzene: EtOAc) to give **3-13** as a white solid (1.27 g, 73%). <sup>1</sup>H NMR (400 MHz, CDCl<sub>3</sub>) δ 7.28 (m, 1 H, Ar-H), 7.18-7.16 (m, 3 H, Ar-H), 4.87 (m, 2 H, 2-NH-CH<sub>2</sub>Ar), 4.63 (m, 2 H, 2-CH-O-CONH), 4.33 (d, 4 H, J = 6.0 Hz, 2-NH-CH<sub>2</sub>Ar), 3.64 (s, 6 H, 2-CO<sub>2</sub>CH<sub>3</sub>), 2.34-0.89 (m, 68 H), 0.62 (s, 6 H, 2-CH<sub>3</sub>). <sup>13</sup>C NMR (100 MHz, CDCl<sub>3</sub>): δ 174.7, 156.2, 139.1, 128.9, 126.5, 75.0, 56.9, 51.4, 44.8, 42.7, 41.8, 40.4, 40.1, 35.7, 35.3, 34.5, 32.6, 31.0, 30.9, 28.1, 27.0, 26.3, 24.1, 23.2, 20.8, 18.2, 12.0. ESI-MS [M+NH<sub>4</sub>]<sup>+</sup> calcd for C<sub>60</sub>H<sub>96</sub>N<sub>3</sub>O<sub>8</sub> 986.7, found 986.6.

**Bis(24-carboxyl-3-lithocholanyl)-N',N-xylylene Dicarbamate (3-14).** A mixture of **3-13** (0.35 g, 0.36 mmol) in MeOH(100 mL) was stirred at 70°C until complete dissolution. Then 18 mL of 1N NaOH solution was added. The reaction mixture was allowed to stir under N<sub>2</sub> for 4 h at 70°C. Then the solution was acidified by 1N HCl to pH 4-5. The solvent was removed under reduced pressure. The solid mixture was dissolved in CH<sub>2</sub>Cl<sub>2</sub> and washed with water. The organic solvent was evaporated under reduced pressure to give **6a** as white solid (0.17 g, 50%). <sup>1</sup>H NMR (100 MHz, DMSO- d<sub>6</sub>) δ 7.50 (m, 2 H, 2-NH-CH<sub>2</sub>Ar), 7.23 (m, 1 H, Ar-H), 7.10 (m, 3 H, Ar-H), 4.46 (m, 2 H, 2-CH-O-CONH), 4.12 (d, 4 H, J = 3.2 Hz, 2-NH-CH<sub>2</sub>Ar), 2.20-0.89 (m, 68 H), 0.60 (s, 6 H, 2-CH<sub>3</sub>). <sup>13</sup>C NMR (100 MHz, DMSO-d<sub>6</sub>): 175.0, 156.0, 140.0, 128.0, 125.4, 73.4, 56.0, 55.5, 43.6,

42.3, 41.3, 40.3, 39.5, 35.3, 34.8, 34.7, 34.2, 32.4, 30.9, 30.8, 27.7, 26.6, 26.0, 23.8, 23.1, 20.4, 18.2, 11.9. ESI-MS  $[M+NH_4]^+$  calcd for  $C_{58}H_{92}N_3O_8$  958.8, found 958.7.

**Bis[24-(2',3'-bis-TBDMS,5'-amino guanosine)-3-lithocholanyl]-N',N'-xylylene dicarbamate (3-1).** A solution of **3-14** (0.10 g, 0.11 mmol) and CDI (0.04 g, 0.27 mmol) in THF (20 mL) was stirred at reflux under  $N_2$  for 4 h. Then 2',3'-bis-TBDMS,5'-amino guanosine (0.14 g, 0.28 mmol) was added and the reaction mixture was allowed to stir at reflux for another 24 h. Solvent was removed under reduced pressure and the crude product was purified by column chromatography ( $SiO_2$ , 1:0.05  $CH_2Cl_2$ :MeOH) to give **1** as a white solid (0.12 g, 59%).  $^1H$  NMR (500 MHz,  $DMSO-d_6$ )  $\delta$  10.71 (bs, 2 H, 2-NH), 8.07 (t, 2 H,  $J = 5.75$  Hz, 2-NH-COCH<sub>2</sub>), 7.97 (s, 2 H, 2- $H_8$ ), 7.50 (t, 2 H,  $J = 5.25$  Hz, 2- $CH_2NH-CO_2$ ), 7.23 (m, 1 H, Ar- $H$ ), 7.08 (m, 3 H, Ar- $H$ ), 6.48 (s, 4 H, 2- $C_2-NH_2$ ), 5.69 (d, 2 H,  $J = 8.0$  Hz, 2- $H_1'$ ), 4.66 (dd, 2 H,  $J_1 = 7.25$  Hz,  $J_2 = 4.25$  Hz, 2- $H_2'$ ), 4.45 (m, 2 H, 2- $CH-O-CONH$ ), 4.19 (d, 2 H,  $J = 4.0$  Hz, 2- $H_3'$ ), 4.13 (bd, 4 H, 2-NH- $CH_2$ Ar), 3.84 (t, 2 H,  $J = 6.5$  Hz, 2- $H_4'$ ), 3.41-3.33 (m, 4 H, 2- $H_5'$ , 2- $H_5''$ ), 2.21-0.88 (m, 86 H), 0.66 (s, 18 H, 2-3 $CH_3$ ), 0.57 (s, 6 H, 2- $CH_3$ ), 0.07 (d, 12 H, -Si $CH_3$ ), -0.06 (s, 6 H, 2-Si $CH_3$ ), -0.31 (s, 6 H, 2-Si $CH_3$ );  $^{13}C$  NMR (100 MHz,  $DMSO-d_6$ ): 173.7, 157.2, 156.6, 153.9, 151.9, 140.3, 136.7, 128.4, 125.9, 117.1, 85.9, 85.2, 74.2, 73.9, 73.6, 56.3, 55.9, 43.9, 42.6, 41.6, 41.2, 40.5, 35.6, 35.2, 35.0, 34.5, 32.7, 31.7, 30.8, 28.0, 27.0, 26.3, 26.0, 25.8, 24.1, 23.4, 20.8, 18.6, 18.1, 17.8, 12.1, -4.4, -4.5, -5.4. ESI-MS  $[M+H]^+$  calcd. for  $C_{102}H_{169}N_{14}O_{14}Si_4$  1926.2, found 1926.3.



**Bis[(24-N-methylamide)-3-lithocholanyl]-N',N'-xylylene Dicarbamate (3-16).** To a mixture of **3-14** (0.15 g, 0.27 mmol) in CH<sub>2</sub>Cl<sub>2</sub> (6.0 mL), 2.0M CH<sub>3</sub>NH<sub>2</sub> in THF (0.10 mL, 0.20 mmol), EDC (0.02g, 0.13 mmol) and DMAP (0.01g, 0.10 mmol) were added. The reaction mixture was stirred under N<sub>2</sub> at 40°C for 48 h. The crude mixture was concentrated and the remaining solid was purified by column chromatography (SiO<sub>2</sub>, 20:1 CH<sub>2</sub>Cl<sub>2</sub>:MeOH) to give **3-16** as a white solid (20 mg, 40%). <sup>1</sup>H NMR (400 MHz, CDCl<sub>3</sub>) δ 7.28 (m, 1 H, Ar-H), 7.18-7.16 (m, 3 H, Ar-H), 5.38 (bs, 2H, 2-NHCH<sub>3</sub>), 4.87 (m, 2H, 2-NH-CH<sub>2</sub>Ar), 4.63 (m, 2 H, 2-CH-O-CONH), 4.33 (d, 4 H, *J* = 5.6 Hz, 2-NH-CH<sub>2</sub>Ar), 2.79 (d, 6 H, *J* = 3.2 Hz, 2-NHCH<sub>3</sub>), 2.34-0.89 (m, 68 H), 0.62 (s, 6H, 2-CH<sub>3</sub>). ESI-MS [M+H]<sup>+</sup> calcd for C<sub>60</sub>H<sub>95</sub>N<sub>4</sub>O<sub>6</sub> 967.7, found 967.7.

**Methyl 3β-mesyl lithocholate (4-7).** To a solution of **4-6** (5.00 g, 12.80 mmol) and triphenylphosphine (10.07 g, 38.40 mmol) in dry THF (40 mL) was added methanesulfonic acid (1.66 mL, 25.60 mmol). The reaction was heated to 40 °C and DIAD (7.56 mL, 38.40 mmol) was added dropwise over 15 min. The mixture solution became viscous white suspension. The reaction was stirred vigorously under N<sub>2</sub> at 40 °C for 24 hours. The suspension was filtered and washed by THF; the filtrate was dried by remove the solvent under reduced pressure. The crude product was purified by flash chromatography (SiO<sub>2</sub>, 9:1 hexane:EtOAc) to give mesylate **4-7** as a white crystalline (3.44 g, 57%). mp. 103.5-105 °C. <sup>1</sup>H NMR (400 MHz, CDCl<sub>3</sub>) δ 5.02 (m, 1H, -CH-O-SO<sub>2</sub>CH<sub>3</sub>), 3.64 (s, 3 H, -CO<sub>2</sub>CH<sub>3</sub>), 2.97 (s, 3 H, -SO<sub>3</sub>CH<sub>3</sub>), 2.34-0.89 (m, 34 H), 0.63 (s, 3 H, -CH<sub>3</sub>). <sup>13</sup>C NMR (100 MHz, CDCl<sub>3</sub>): δ 174.7, 80.6, 56.5, 56.0, 51.5, 42.7, 40.1, 40.0,

38.6, 36.8, 35.5, 35.3, 34.7, 31.7, 31.0, 30.9, 30.0, 28.1, 26.2, 26.1, 26.0, 24.1, 23.6, 21.0, 18.2, 12.0. ESI-MS  $[M-H]^+$  calcd. for  $C_{26}H_{45}O_5S$  469.3, found 469.3.

**Methyl 3 $\alpha$ -azido lithocholate (4-8).** **4-7** (3.11 g, 6.65 mmol) and sodium azide (2.59 g, 39.91 mmol) were dissolved in DMPU. The reaction was stirred at 60 °C for 48 hours. Water (60 mL) was added to the solution and a white precipitate formed. The white solid was filtered and washed with water to yield **4-8** (2.55 g, 93%). mp. 92-94 °C.  $^1H$  NMR (400 MHz,  $CDCl_3$ )  $\delta$  3.64 (s, 3 H,  $-CO_2CH_3$ ), 3.27 (m, 1H,  $-CH-N_3$ ), 2.34-0.89 (m, 34 H), 0.63 (s, 3 H,  $-CH_3$ ).  $^{13}C$  NMR (100 MHz,  $CDCl_3$ ):  $\delta$  174.7, 61.2, 56.3, 55.9, 51.5, 42.7, 42.3, 40.4, 40.0, 35.7, 35.5, 35.3, 34.6, 32.4, 31.0, 30.9, 28.1, 27.0, 26.7, 26.3, 24.1, 23.4, 20.8, 18.2, 12.0. ESI-MS  $[M+H]^+$  calcd. for  $C_{25}H_{42}N_3O_2$  416.3, found 416.4.

**Methyl 3 $\alpha$ -amino lithocholate (4-9).** To a solution of **4-8** (1.51 g, 3.63 mmol) in THF (56 mL) was added triphenylphosphine (1.34 g, 5.09 mmol). The mixture was stirred at RT for 1 hour, water (3.0 mL) was then added into the solution. The reaction was stirred at RT overnight. The solvent was removed by the deduced pressure, the solid residue was crystallized with  $CH_3CN$  to give **4-9** as a white crystalline (0.82 g, 58%). mp. 98-99 °C.  $^1H$  NMR (400 MHz,  $CDCl_3$ )  $\delta$  3.64 (s, 3 H,  $-CO_2CH_3$ ), 2.68 (m, 1 H,  $-CH-NH_2$ ), 2.34-0.89 (m, 34 H), 0.63 (s, 3 H,  $-CH_3$ ).  $^{13}C$  NMR (100 MHz,  $CDCl_3$ ):  $\delta$  174.8, 56.5, 55.9, 51.5, 42.7, 42.5, 40.4, 40.1, 37.5, 36.1, 35.8, 35.4, 34.6, 31.4, 31.0, 30.9, 28.2, 27.3, 26.4, 24.2, 23.6, 20.8, 18.2, 12.0 (missing 1 C). ESI-MS  $[M+H]^+$  calcd. for  $C_{25}H_{45}NO_2$  390.3, found 390.3.

**Bis[(24-methoxycarbonyl)-3-lithocholanyl]-N',N-xylylene Diurea (4-10).** A m-xylylene diisocyanate (0.13mL, 0.84 mmol) THF (2 mL) solution was added dropwise to a solution of **4-9** (0.82 g, 2.10 mmol) in THF (6 mL). A white precipitate formed after 5 min. The reaction was stirred at RT overnight. The solid was filtered and washed with THF to yield **4-10** (0.53 g, 65%). mp. 184-186 °C. <sup>1</sup>H NMR (400 MHz, CDCl<sub>3</sub>) δ 7.11 (m, 1 H, Ar-H), 7.05-7.00 (m, 3 H, Ar-H), 5.63 (m, 2 H, 2-NH-CH<sub>2</sub>Ar), 5.31 (m, 2 H, 2-CONH-CH), 4.08 (m, 4H, 2 NH-CH<sub>2</sub>Ar), 3.64 (s, 6 H, 2-CO<sub>2</sub>CH<sub>3</sub>), 3.32 (m, 2H, 2NH-CH-CH), 2.34-0.89 (m, 68 H), 0.62 (s, 6 H, 2-CH<sub>3</sub>). <sup>13</sup>C NMR (100 MHz, CDCl<sub>3</sub>): δ 174.7, 158.5, 139.9, 128.5, 126.2, 126.0, 56.4, 56.0, 51.5, 50.4, 43.8, 42.6, 42.5, 40.4, 40.1, 36.1, 35.7, 35.4, 34.6, 34.3, 31.1, 31.0, 28.5, 28.2, 27.1, 26.4, 24.1, 23.6, 20.8, 18.2, 12.0. ESI-MS [M+H]<sup>+</sup> calcd for C<sub>60</sub>H<sub>95</sub>N<sub>4</sub>O<sub>6</sub> 967.7, found 967.7.

**Bis[(24-carboxyl)-3-lithocholanyl]-N',N-xylylene Diurea (4-11).** To a solution of **4-10** (0.82 g, 2.10 mmol) in THF (100 mL) was added 1N LiOH solution (25 mL). The mixture was reflux overnight. Then the solution was acidified with 1N HCl (28 mL) and white solid crushed out of solution. Filtered the precipitate and washed it with water provide desired compound **4-11** (0.68g, 97%). mp. 236 °C (dec). <sup>1</sup>H NMR (400 MHz, DMSO) δ 12.0 (s, 2H, COOH), 7.22 (m, 1 H, Ar-H), 7.05-7.00 (m, 3 H, Ar-H), 6.12 (t, 2 H, J = 4Hz, 2-NH-CH<sub>2</sub>Ar), 5.77 (d, 2 H, J = 8 Hz, 2-CONH-CH), 4.15 (m, 4H, 2 NH-CH<sub>2</sub>Ar), 3.32 (m, 2H, 2NH-CH-CH), 2.34-0.89 (m, 68 H), 0.62 (s, 6 H, 2-CH<sub>3</sub>). <sup>13</sup>C NMR (100 MHz, DMSO): δ 175.7, 158.2, 141.8, 128.9, 126.5, 126.2, 56.9, 56.5, 50.1,

43.7, 43.1, 42.9, 36.7, 36.2, 35.7, 35.1, 34.8, 31.6, 31.5, 29.0, 28.6, 27.6, 27.0, 24.7, 24.2, 21.3, 19.0, 12.7.(missing 2 C) ESI-MS  $[M+H]^+$  calcd for  $C_{58}H_{91}N_4O_6$  939.7, found 939.7.

**Bis[24-(2',3'-bis-TBDMS,5'-amino guanosine)-3-lithocholanyl]-N',N'-xylylene diurea (4-1).** CDI (0.11g, 0.66 mmol) was added into the a solution of **4-11**(0.25 g, 0.26 mmol) in THF(20 mL). The mixture was stirred at reflux under  $N_2$  for 4 h. Then 2',3'-bis-TBDMS,5'-amino guanosine (0.35 g, 0.68 mmol) was added and the reaction mixture was allowed to stir at reflux for another 24h. Solvent was removed under reduced pressure and the crude product was purified by column chromatography ( $SiO_2$ , 1:0.05  $CH_2Cl_2$ :MeOH) to give **4-1** as a pale-white solid (0.09 g, 34%). mp. 250 °C (dec).  $^1H$  NMR (600 MHz,  $DMSO-d_6$ )  $\delta$  10.62 (bs, 2 H, 2-NH), 8.06 (m, 2 H, 2-NH-COCH<sub>2</sub>), 7.99 (s, 2 H, 2- $H_8$ ), 7.22 (m, 1 H, Ar-H), 7.08 (m, 3 H, Ar-H), 6.43 (s, 4 H, 2-C<sub>2</sub>-NH<sub>2</sub>), 6.12 (t, 2 H,  $J = 7.2$  Hz, Ar-CH<sub>2</sub>-NH-CO), 5.76 (d, 2 H,  $J = 7.8$  Hz, 3 $\alpha$ -CH-NH-CO), 5.69 (d, 2 H,  $J = 7.8$  Hz, 2- $H_1'$ ), 4.66 (dd, 2 H,  $J_1 = 9.6$  Hz,  $J_2 = 3.0$  Hz, 2- $H_2'$ ), 4.18 (d, 4 H,  $J = 4.2$  Hz, 2-NH-CH<sub>2</sub>Ar), 4.14 (m, 2 H, 2- $H_3'$ ), 3.84 (t, 2 H,  $J = 6.6$  Hz, 2- $H_4'$ ), 3.42-3.33 (m, 4 H, 2- $H_5'$ , 2- $H_5''$ ), 2.13-0.89 (m, 86 H), 0.71 (s, 18 H, 2-3CH<sub>3</sub>), 0.59 (s, 6 H, 2-CH<sub>3</sub>), 0.08(d, 12 H,  $J = 2.4$  Hz, -SiCH<sub>3</sub>), -0.09 (s, 6 H, 2-SiCH<sub>3</sub>), -0.34 (s, 6H, 2-SiCH<sub>3</sub>);  $^{13}C$  NMR (100 MHz,  $DMSO-d_6$ ): 172.8, 157.3, 156.7, 153.6, 151.5, 140.9, 136.0, 128.0, 125.6, 125.3,116.8, 85.3, 84.8, 74.2, 73.4, 56.0, 55.6, 49.3, 42.8, 42.2, 42.0, 40.9, 35.8, 35.3, 34.9, 34.2, 33.9, 32.2, 31.4, 28.1, 27.7, 26.8, 26.1, 25.7, 25.4, 23.8, 23.3, 20.8, 18.3, 17.8, 17.5, 11.8, -4.70, -4.77, -4.83, -5.68. ESI-MS  $[M+H]^+$  calcd.  $C_{102}H_{171}N_{16}O_{12}Si_4$  1924.23, found 1924.29.

### **Bis[(24-amino)-3-lithocholanyl]-N',N'-xylylene diurea (4-12)**

Carbonyl di-imidazole (0.04 g, 0.27 mmol) was added to a solution of **4-11** (0.10 g, 0.11 mmol) in THF (10 mL). The reaction mixture was stirred at reflux under N<sub>2</sub> for 4 h. Then 2M CH<sub>3</sub>NH<sub>2</sub> in CH<sub>3</sub>CN solution (0.14 mL, 0.28 mmol) was added and the reaction mixture was allowed to stir at reflux for another 24 h. White crude product was precipitated out when the solvent was reduced under vacuum. Filtered the crude product and washed it with 1:1 CH<sub>3</sub>CN and THF, giving **4-12** as a white solid (0.05 g, 49%). mp. 226 °C (dec). <sup>1</sup>H NMR (400 MHz, DMSO-*d*<sub>6</sub>) δ 11.97 (bs, 2H, -NHCH<sub>3</sub>), 7.67 (m, 1 H, Ar-*H*), 7.66-7.05 (m, 3 H, Ar-*H*), 6.11 (t, 2 H, J = 5.6 Hz, 2-CONH-CH<sub>2</sub>Ar), 5.77 (d, 2 H, J = 7.6 Hz, 2-CONH-CH), 4.14 (m, 4 H, 2 NH-CH<sub>2</sub>Ar), 3.31 (s, 6 H, 2NH-CH<sub>3</sub>), 2.21-0.88 (m, 68 H), 0.60 (s, 6 H, 2-CH<sub>3</sub>). <sup>13</sup>C NMR (100 MHz, DMSO-*d*<sub>6</sub>): δ 172.9, 157.3, 141.0, 128.0, 125.3, 56.1, 55.7, 55.6, 49.3, 42.9, 42.3, 42.1, 35.9, 35.4, 35.0, 34.8, 34.2, 34.0, 28.1, 27.7, 26.8, 26.1, 25.4, 23.9, 23.4, 20.4, 18.3, 18.1, 11.9. ESI-MS [M+H]<sup>+</sup> calcd for C<sub>60</sub>H<sub>97</sub>N<sub>6</sub>O<sub>4</sub> 964.75, found 964.75.

### **6.3 ESI-MS Experiment of G-quadruplex**

Electrospray ionization mass experiments were performed on AccuTOF spectrometry, using the positive ionization mode. The G-quadruplex/salt mixture solutions (~ 71 μM) in 1:1 CD<sub>2</sub>Cl<sub>2</sub>: CD<sub>3</sub>CN were injected into the mass spectrometer at a flow rate of 4 μL/min. The ion intensities increased with the ion spray potential and the orifice 1 voltage, which were set to 4-5 kV and 200-300 V, respectively. Spectra were required over an *m/z* range of 7000 – 8100.

## 6.4 NMR Titration

A stock solution of the  $G16\cdot 4Na^+\cdot 4DNP^-$  (2 mL) was prepared at a concentration of 3.57 mM in  $CD_2Cl_2$ , and 2 mL sample of cation solution ( $KPh_4B$  and  $^{15}NH_4Ph_4B$ ) in a range of 17.8-35.7 mM was prepared in  $CD_3CN$ . Equal amount of  $G16\cdot 4Na^+\cdot 4DNP^-$  (200  $\mu$ l) was loaded into six 5 mm NMR tubes. An increasing amount of cation solution (from 10  $\mu$ l to 24  $\mu$ l) was added into the aliquots of  $G16\cdot 4Na^+\cdot 4DNP^-$  in NMR tubes, giving mixtures the following mole ratios: 1:0, 1:0.5, 1:1, 1:2, 1:3, 1:4. The extra solvents were added into the NMR tube to make a titration sample in 1:1  $CD_2Cl_2:CD_3CN$ . A constant volume of 500  $\mu$ L was used in the NMR tube for each titration, so that the concentration of  $G16\cdot 4Na^+\cdot 4DNP^-$  remained constant. The NMR spectra were recorded after each titration.

*$^1H$  NMR titration:* the chemical shifts of the amide protons of the G-quadruplex were monitored, as the concentration of free cation ( $K^+$  and  $^{15}NH_4^+$ ) increased in the titration.

*$^{15}N$  filtered  $^1H$  NMR titration:* the chemical shift of the  $^{15}N$ -labeled ammonium protons were monitored, as the concentration of  $^{15}NH_4^+$  cation increased in the titration.

## 6.5 $^{15}N$ Filtered $^1H$ NMR Experiment

$^{15}N$  filtered  $^1H$  NMR experiments of  $^{15}NH_4 Ph_4B$  titration a solution of  $G16\cdot 4Na^+\cdot 4DNP^-$  in 1:1  $CD_2Cl_2: CD_3CN$  were recorded at 298 K with the HSQC pulse sequence.<sup>112</sup>The experiments were conducted in the phase sensitive mode using the Echo/Antiecho-TPPT gradient selection method. The relaxation delay was 8.0 s. The

spectra were taken with a sweep of 16.0 ppm. A total of 48 scans were applied for data collection.

## 6.6 NOESY Experiment

The NOESY experiments of equimolar  $^{15}\text{NH}_4 \text{Ph}_4\text{B}$  titration a solution of  $\text{G16}\cdot 4\text{Na}^+ \cdot 4\text{DNP}^-$  in 1:1  $\text{CD}_2\text{Cl}_2$ :  $\text{CD}_3\text{CN}$  were recorded at 298 K with the NOESYGPTP pulse sequence.<sup>160</sup> The experiments were conducted in the phase sensitive mode using the TPPI method. The relaxation delay was 2.5 s, and the mixing time was 500 ms. The spectral width was 8012 Hz in each dimension. A total of 48 scans were collected for each time increment. A total of 512 serial files were collected, resulting in a data matrix of  $512 \times 2048$ .

## 6.7 Selective NOE Experiment

The selective NOE experiments of two equivalent  $^{15}\text{NH}_4 \text{Ph}_4\text{B}$  titration of a solution of  $\text{G16}\cdot 4\text{Na}^+ \cdot 4\text{DNP}^-$  in 1:1  $\text{CD}_2\text{Cl}_2$ :  $\text{CD}_3\text{CN}$  were recorded at 298 K with the 1 D NOE pulse sequence.<sup>161</sup> The experiments were conducted using a selective inversion pulse on the peak of interest. The relaxation delay was 5.0 s and mixing time was 500 ms. The spectra were taken with a sweep of 16.0 ppm. A total of 1600 scans were applied for the data collection.

## 6.8 Planar Bilayer Conductance Experiments

Planar phospholipid membranes were prepared by the monolayer method, across a 100- $\mu\text{m}$ -diameter hole in a Saran partition. Monolayers were produced using a solution of 0.5% w/v asolectin, 0.5% w/v DiPhyPC, 0.1% w/v cholesterol in hexane. This technique produces solvent-free phospholipid membranes whose lipid composition (focusing on the polar head-groups) is similar to that found in the mitochondrial outer membrane. It differs from the natural membrane in lacking proteins. The aqueous solution contained 1.0 M KCl, 1 mM MgCl<sub>2</sub>, and 5 mM PIPES (pH 7.0). The voltage was clamped (*trans* side was ground) and the current recorded.

## 6.9 Reversal Potential Measurements

Planar membranes were formed as above using a 0.5% (w/v) asolectin, 0.5% (w/v) DiPhyPC, 0.1% (w/v) cholesterol in hexane solution. The aqueous solution on the *trans* side contained 100 mM KCl, 1 mM MgCl<sub>2</sub>, and 5 mM PIPES (pH 7.0), and on the *cis* side 1.0 M KCl, 1 mM MgCl<sub>2</sub>, and 5 mM PIPES (pH 7.0). The voltage was clamped at 10 mV and the current recorded. Guanosine-sterol **3-1** was added either by stirring into the water phase on the *cis* side of sealed membrane (after-loading method) or by premixing with phosphate lipid (premix method). As the compound **3-1** started to form channel, the voltage required to achieve a zero net current across the membrane was measured.



## 6.10 Liposome Preparation

Liposomes were prepared by previously published methods.<sup>279</sup> High pressure extrusion was performed on the Avanti™ mini-extruder with a 100 nm polycarbonate membrane. EYPC was purchased from Avanti Polar Lipids. Egg yolk L- $\alpha$ -phosphatidylcholine (EYPC ethanol solution, 70  $\mu$ L, 92  $\mu$ mol) was dissolved in  $\text{CHCl}_3$  (3 mL), the solution was slowly evaporated under reduced pressure overnight. The resulting thin lipid film was hydrated in 39 mM NaCl, 6.0 mM DPX, 1.5 mM carboxyfluorescein and subjected to four freeze-thaw cycles. The large multilamellar liposome suspension (1.0 mL) was submitted to a high-pressure extrusion at room temperature (21 extrusions) through a 100 nm polycarbonate membrane. A sequential gel filtration column that equilibrated and eluted with HEPES buffer solution (10 mM HEPES, 50 mM NaCl, 1 mM EDTA, pH = 7) afforded a suspension of unicellular vesicles (LUVs).

## References

- (1) Lehn, J. M. "Supramolecular chemistry - scope and perspectives. Molecules-supermolecules-molecular devices. Nobel lecture, 8 December 1987." *Chemica Scripta* **1988**, 28, 237-262.
- (2) Lehn, J.-M. "Toward self-organization and complex matter." *Science (Washington, DC, U. S.)* **2002**, 295, 2400-2403.
- (3) Wilson, A. J. "Supramolecular chemistry." *Annu. Rep. Prog. Chem., Sect. B: Org. Chem.* **2007**, 103, 174-192.
- (4) Tamerler, C.; Sarikaya, M. "Molecular biomimetics: building materials nature's way, one molecule at a time." *Nanofabr. Biomed. Appl.* **2005**, 119-134.
- (5) Schalley, C. A.; Luetzen, A.; Albrecht, M. "Approaching supramolecular functionality." *Chem.Eur. J.* **2004**, 10, 1072-1080.
- (6) Stryer, L. *Biochemistry*; 3rd ed.; W. H. Freeman and Co.: New York, **1988**.
- (7) Bloomfield, V. A. C., D. M.; Tinoco, Jr., I. "Nucleic acids: properties, structures, and functions." **2000**.
- (8) Saenger, W. *Principles of Nucleic Acid Structure*; Springer Verlag: New York, **1984**.
- (9) Watson, J. D.; Crick, F. H. C. "Molecular structure of nucleic acids - a structure for deoxyribose nucleic acid." *Nature* **1953**, 171, 737-738.
- (10) Sessler, J. L.; Lawrence, C. M.; Jayawickramarajah, J. "Molecular recognition via base-pairing." *Chem. Soc. Rev.* **2007**, 36, 314-325.
- (11) Hoogsteen, K. "The structure of crystals containing a hydrogen-bonded complex of 1-methylthymine and 9-methyladenine." *Acta Crystallographica* **1959**, 12, 822-823.
- (12) Incles, C. M.; Schultes, C. M.; Kempfski, H.; Koehler, H.; Kelland, L. R.; Neidle, S. "A G-quadruplex telomere targeting agent produces p16-associated senescence and chromosomal fusions in human prostate cancer cells." *Mol.Cancer Ther.* **2004**, 3, 1201-1206.
- (13) Marsh, T. C.; Henderson, E. "G-wires - self-assembly of a telomeric oligonucleotide, d(GGGGTTGGGG), into large superstructures." *Biochemistry* **1994**, 33, 10718-10724.

- (14) Davis, J. T. "G-quartets 40 years later: From 5'-GMP to molecular biology and supramolecular chemistry." *Angew. Chem. Int. Ed.* **2004**, *43*, 668-698.
- (15) Masiero, S.; Gottarelli, G.; Pieraccini, S. "G-quartets as a self-assembled scaffold for circular porphyrin arrays." *Chem. Commun.* **2000**, 1995-1996.
- (16) Gottarelli, G.; Masiero, S.; Mezzina, E.; Pieraccini, S.; Spada, G. P.; Mariani, P. "A new lyotropic liquid crystalline phase formed in hydrocarbon solvents by a deoxyguanosine derivative through extensive hydrogen bonding." *Liq. Cryst.* **1999**, *26*, 965-971.
- (17) Gottarelli, G.; Spada, G. P. "The stepwise supramolecular organisation of guanosine derivatives." *Chem. Rec.* **2004**, *4*, 39-49.
- (18) Garidel, P.; Johann, C.; Blume, A. "Thermodynamics of lipid organization and domain formation in phospholipid bilayers." *J. Liposome Res.* **2000**, *10*, 131-158.
- (19) Kumar, V. V. "Lipid Molecular Shapes And Membrane Architecture." *Indian J. Biochem. Biophys.* **1993**, *30*, 135-138.
- (20) Lee, A. G. "Lipid-protein interactions in biological membranes: a structural perspective." *Biochim. Biophys. Acta-Biomembr.* **2003**, *1612*, 1-40.
- (21) Pomorski, T.; Menon, A. K. "Lipid flippases and their biological functions." *Cell. Mol. Life Sci.* **2006**, *63*, 2908-2921.
- (22) Rosemeyer, H. "Nucleolipids: Natural occurrence, synthesis, molecular recognition, and supramolecular assemblies as potential precursors of life and bioorganic materials." *Chem. Biodiversity* **2005**, *2*, 977-1062.
- (23) Kimura, K.; Kagami, S.; Ikeda, Y.; Takahashi, H.; Yoshihama, M.; Kusakabe, H.; Osada, H.; Isono, K. "New types of liposidomycins that inhibit bacterial peptidoglycan synthesis and are produced by *Streptomyces* - I. Producing organism and medium components." *J. Antibiot.* **1998**, *51*, 640-646.
- (24) Fu, X.; Schmitz, F. J.; Tanner, R. S.; Kelly-Borges, M. "Agelasines H and I, 9-methyladenine-containing diterpenoids from an *Agelas* sponge." *J. Nat. Prod.* **1998**, *61*, 548-550.
- (25) Stryer, L. *Biochemie*; F. Vieweg & Sohn: Braunschweig, **1979**.
- (26) Carstensen, S.; Pliska-Matyshak, G.; Bhuvaramurthy, N.; Robbins, K. M.; Murthy, P. P. N. "Biosynthesis and localization of phosphatidyl-scylo-inositol in barley aleurone cells." *Lipids* **1999**, *34*, 67-73.

- (27) Houtkooper, R. H.; Vaz, F. M. "Cardiolipin, the heart of mitochondrial metabolism." *Cell. Mol. Life Sci.* **2008**, *65*, 2493-2506.
- (28) Larson, T. J.; Dowhan, W. "Ribosomal-Associated Phosphatidylserine Synthetase From *Escherichia-Coli* - Purification By Substrate-Specific Elution From Phosphocellulose Using Cytidine "5'-Diphospho-1,2-Diacyl-Sn-Glycerol." *Biochemistry* **1976**, *15*, 5212-5218.
- (29) Heifetz, A.; Keenan, R. W.; Elbein, A. D. "Mechanism Of Action Of Tunicamycin On The Udp-Glcnae-Dolichyl-Phosphate Glcnae-1-Phosphate Transferase." *Biochemistry* **1979**, *18*, 2186-2192.
- (30) Brandish, P. E.; Kimura, K.; Inukai, M.; Southgate, R.; Lonsdale, J. T.; Bugg, T. D. H. "Modes of action of tunicamycin, liposidomycin B, and mureidomycin A: Inhibition of phospho-N-acetylmuramyl-pentapeptide translocase from *Escherichia coli*." *Antimicrob. Agents Chemother.* **1996**, *40*, 1640-1644.
- (31) Bonaccio, S.; Capitani, D.; Segre, A. L.; Walde, P.; Luisi, P. L. "Liposomes from phosphatidyl nucleosides: An NMR investigation." *Langmuir* **1997**, *13*, 1952-1956.
- (32) Bonaccio, S.; Walde, P.; Luisi, P. L. "Liposomes Containing Purine And Pyrimidine-Bases - Stable Unilamellar Liposomes From Phosphatidyl Nucleosides." *J. Phys. Chem.* **1994**, *98*, 6661-6663.
- (33) Yun, Y. J.; Park, S. M.; Kim, B. H. "Novel thymidine-based organogelators and their gelation behaviours." *Chem. Commun.* **2003**, 254-255.
- (34) Kitano, H.; Ringsdorf, H. "Surface behaviors of nucleic-acid base-containing lipids in monolayer and bilayer systems." *Bull. Chem. Soc. Jpn.* **1985**, *58*, 2826-2828.
- (35) Ahlers, M.; Ringsdorf, H.; Rosemeyer, H.; Seela, F. "Orientation, recognition, and photoreaction of nucleolipids in model membranes." *Colloid Polym. Sci.* **1990**, *268*, 132-142.
- (36) Paleos, C. M.; Tsiourvas, D. "Molecular recognition of organized assemblies via hydrogen bonding in aqueous media." *Adv. Matter.* **1997**, *9*, 695-710.
- (37) Huang, J. G.; Liang, Y. Q. "Fourier transform infrared spectroscopic investigation on Langmuir-Blodgett films of octadecanoyl ester of 1-(2-carboxyethyl) thymine: Molecular orientation, molecular recognition to complementary base of nucleic acid and order-disorder transition." *Spectrosc. Lett.* **1997**, *30*, 1441-1466.
- (38) Huang, J. G.; Liang, Y. Q. "Molecular recognition of nucleolipid amphiphile octadecanoyl ester of 1-(2-carboxyethyl) adenine to the complementary nucleobases: Part II. a Fourier transform infrared spectroscopic study of Langmuir-Blodgett films." *Thin Solid Films* **1998**, *325*, 210-217.

- (39) Baglioni, P.; Berti, D. "Self assembly in micelles combining stacking and H-bonding." *Curr. Opin. Colloid Interface Sci.* **2003**, *8*, 55-61.
- (40) Berti, D.; Baglioni, P.; Bonaccio, S.; Barsacchi-Bo, G.; Luisi, P. L. "Base complementarity and nucleoside recognition in phosphatidyl nucleoside vesicles." *J. Phys. Chem. B* **1998**, *102*, 303-308.
- (41) Berti, D.; Barbaro, P.; Bucci, I.; Baglioni, P. "Molecular recognition through H-bonding in micelles formed by dioctylphosphatidyl nucleosides." *J. Phys. Chem. B* **1999**, *103*, 4916-4922.
- (42) Itojima, Y.; Ogawa, Y.; Tsuno, K.; Handa, N.; Yanagawa, H. "Spontaneous formation of selical structures from phospholipid-nucleoside conjugates." *Biochemistry* **1992**, *31*, 4757-4765.
- (43) Gottarelli, G.; Masiero, S.; Spada, G. P. "Self-assembly in organic solvents of a deoxyguanosine derivative induced by alkali metal picrates." *Chem. Commun.* **1995**, 2555-2557.
- (44) Gottarelli, G.; Masiero, S.; Mezzina, E.; Spada, G. P.; Mariani, P.; Recanatini, M. "The self-assembly of a lipophilic deoxyguanosine derivative and the formation of a liquid-crystalline phase in hydrocarbon solvents." *Helv. Chim. Acta* **1998**, *81*, 2078-2092.
- (45) Gosse, C.; Boutorine, A.; Aujard, I.; Chami, M.; Kononov, A.; Cogne-Laage, E.; Allemand, J. F.; Li, J.; Jullien, L. "Micelles of lipid-oligonucleotide conjugates: Implications for membrane anchoring and base pairing." *J. Phys. Chem. B* **2004**, *108*, 6485-6497.
- (46) Pincet, F.; Lebeau, L.; Cribier, S. "Short-range specific forces are able to induce hemifusion." *Eur. Biophys. J. Biophys. Lett.* **2001**, *30*, 91-97.
- (47) Cruciani, O.; Mannina, L.; Sobolev, A. P.; Segre, A.; Luisi, P. "Multilamellar Liposomes formed by phosphatidyl nucleosides: An NMR-HR-MAS characterization." *Langmuir* **2004**, *20*, 1144-1151.
- (48) Yoshina-Ishii, C.; Miller, G. P.; Kraft, M. L.; Kool, E. T.; Boxer, S. G. "General method for modification of liposomes for encoded assembly on supported bilayers." *J. Am. Chem. Soc.* **2005**, *127*, 1356-1357.
- (49) Scheidt, H. A.; Flasche, W.; Cismas, C.; Rost, M.; Herrmann, A.; Liebscher, J.; Huster, D. "Design and application of lipophilic nucleosides as building blocks to obtain highly functional biological surfaces." *J. Phys. Chem. B* **2004**, *108*, 16279-16287.

- (50) Mackellar, C.; Graham, D.; Will, D. W.; Burgess, S.; Brown, T. "Synthesis and physical-properties of anti-Hiv antisense oligonucleotides bearing terminal lipophilic groups." *Nucleic Acids Res.* **1992**, *20*, 3411-3417.
- (51) Chillemi, R.; Aleo, D.; Granata, G.; Sciuto, S. "Synthesis of very short chain lysophosphatidyloligodeoxynucleotides." *Bioconjugate Chem.* **2006**, *17*, 1022-1029.
- (52) Lorenz, C.; Hadwiger, P.; John, M.; Vornlocher, H. P.; Unverzagt, C. "Steroid and lipid conjugates of siRNAs to enhance cellular uptake and gene silencing in liver cells." *Bioorg. Med. Chem. Lett.* **2004**, *14*, 4975-4977.
- (53) Barthelemy, P. "Nucleoside-based lipids at work: From supramolecular assemblies to biological applications." *C. R. Chim.* **2009**, *12*, 171-179.
- (54) Gissot, A.; Camplo, M.; Grinstaff, M. W.; Barthelemy, P. "Nucleoside, nucleotide and oligonucleotide based amphiphiles: a successful marriage of nucleic acids with lipids." *Org. Biomol. Chem.* **2008**, *6*, 1324-1333.
- (55) Nowick, J. S.; Chen, J. S. "Molecular recognition in aqueous micellar solution - adenine thymine base-pairing in SDS micelles." *J. Am. Chem. Soc.* **1992**, *114*, 1107-1108.
- (56) Nowick, J. S.; Cao, T.; Noronha, G. "Molecular recognition between uncharged molecules in aqueous micelles." *J. Am. Chem. Soc.* **1994**, *116*, 3285-3289.
- (57) Nowick, J. S.; Chen, J. S.; Noronha, G. "Molecular recognition in micelles - the roles of hydrogen-bonding and hydrophobicity in adenine thymine base-pairing in SDS micelles." *J. Am. Chem. Soc.* **1993**, *115*, 7636-7644.
- (58) Kurz, A.; Bunge, A.; Windeck, A. K.; Rost, M.; Flasche, W.; Arbusova, A.; Strohbach, D.; Mueller, S.; Liebscher, J.; Huster, D.; Herrmann, A. "Lipid-anchored oligonucleotides for stable double-helix formation in distinct membrane domains." *Angew. Chem. Int. Ed.* **2006**, *45*, 4440-4444.
- (59) Bunge, A.; Kurz, A.; Windeck, A. K.; Korte, T.; Flasche, W.; Liebscher, J.; Herrmann, A.; Huster, D. "Lipophilic oligonucleotides spontaneously insert into lipid membranes, bind complementary DNA strands, and sequester into lipid-disordered domains." *Langmuir* **2007**, *23*, 4455-4464.
- (60) Gissot, A.; Di Primo, C.; Bestel, I.; Giannone, G.; Chapuis, H.; Barthelemy, P. "Sensitive liposomes encoded with oligonucleotide amphiphiles: a biocompatible switch." *Chem. Commun.* **2008**, 5550-5552.
- (61) Jung, Y. G.; Yeo, W. S.; Lee, S. B.; Hong, J. I. "Improved transport of nucleotide monophosphates by lipophilic phosphonium-nucleobase conjugates." *Chem. Commun.* **1997**, 1061-1062.

- (62) Yeo, W. S.; Hong, J. I. "Thiouroninm-thymine conjugate as a new carrier for selective transport of 5 '-AMP." *Tetrahedron Lett.* **1998**, *39*, 3769-3772.
- (63) Chabaud, P.; Camplo, M.; Payet, D.; Serin, G.; Moreau, L.; Barthelemy, P.; Grinstaff, M. W. "Cationic nucleoside lipids for gene delivery." *Bioconjugate Chem.* **2006**, *17*, 466-472.
- (64) Moreau, L.; Barthelemy, P.; Li, Y. G.; Luo, D.; Prata, C. A. H.; Grinstaff, M. W. "Nucleoside phosphocholine amphiphile for in vitro DNA transfection." *Mol. BioSyst.* **2005**, *1*, 260-264.
- (65) Sen, D.; Gilbert, W. "Novel DNA superstructures formed by telomere-like oligomers." *Biochemistry* **1992**, *31*, 65-70.
- (66) Kerwin, S. M. "G-quadruplex DNA as a target for drug design." *Curr. Pharm. Des.* **2000**, *6*, 441-471.
- (67) Han, H. Y.; Hurley, L. H. "G-quadruplex DNA: a potential target for anti-cancer drug design." *Trends Pharmacol. Sci.* **2000**, *21*, 136-142.
- (68) Kato, Y.; Ohyama, T.; Mita, H.; Yamamoto, Y. "Dynamics and thermodynamics of dimerization of parallel G-quadruplexed DNA formed from d(TTAG(n)) (n=3-5)." *J. Am. Chem. Soc.* **2005**, *127*, 9980-9981.
- (69) Simonsson, T. "G-quadruplex DNA structures - Variations on a theme." *Biol. Chem.* **2001**, *382*, 621-628.
- (70) Chowdhury, S.; Bansal, M. "G-quadruplex structure can be stable with only some coordination sites being occupied by cations: A six-nanosecond molecular dynamics study." *J. Phys. Chem. B* **2001**, *105*, 7572-7578.
- (71) Basu, S.; Szewczak, A. A.; Cocco, M.; Strobel, S. A. "Direct detection of monovalent metal ion binding to a DNA G-quartet by T1-205 NMR." *J. Am. Chem. Soc.* **2000**, *122*, 3240-3241.
- (72) Wong, A.; Ida, R.; Wu, G. "Direct NMR detection of the "invisible" alkali metal cations tightly bound to G-quadruplex structures." *Biochem. Biophys. Res. Commun.* **2005**, *337*, 363-366.
- (73) Phillips, K.; Dauter, Z.; Murchie, A. I. H.; Lilley, D. M. J.; Luisi, B. "The crystal structure of a parallel-stranded guanine tetraplex at 0.95 angstrom resolution." *J. Mol. Biol.* **1997**, *273*, 171-182.
- (74) Hud, N. V.; Schultze, P.; Feigon, J. "Ammonium ion as an NMR probe for monovalent cation coordination sites of DNA quadruplexes." *J. Am. Chem. Soc.* **1998**, *120*, 6403-6404.

- (75) Hud, N. V.; Schultze, P.; Sklenar, V.; Feigon, J. "Binding sites and dynamics of ammonium ions in a telomere repeat DNA quadruplex." *J. Mol. Biol.* **1999**, *285*, 233-243.
- (76) Marlow, A. L.; Mezzina, E.; Spada, G. P.; Masiero, S.; Davis, J. T.; Gottarelli, G. "Cation-templated self-assembly of a lipophilic deoxyguanosine: Solution structure of a K<sup>+</sup>-dG(8) octamer." *J. Org. Chem.* **1999**, *64*, 5116-5123.
- (77) Spada, G. P.; Gottarelli, G. "The disclosure of the stepwise supramolecular organization of guanosine derivatives: Serendipity or programmed design?" *Synlett* **2004**, 596-602.
- (78) Ghossoub, A.; Lehn, J. M. "Dynamic sol-gel interconversion by reversible cation binding and release in G-quartet-based supramolecular polymers." *Chem. Commun.* **2005**, 5763-5765.
- (79) Araki, K.; Takasawa, R.; Yoshikawa, I. "Design, fabrication, and properties of macroscale supramolecular fibers consisted of fully hydrogen-bonded pseudo-polymer chains." *Chem. Commun.* **2001**, 1826-1827.
- (80) Pieraccini, S.; Gottarelli, G.; Mariani, P.; Masiero, S.; Saturni, L.; Spada, G. P. "Columnar lyomesophases formed in hydrocarbon solvents by chiral lipophilic guanosine-alkali metal complexes." *Chirality* **2001**, *13*, 7-12.
- (81) Cai, M. M.; Shi, X. D.; Sidorov, V.; Fabris, D.; Lam, Y. F.; Davis, J. T. "Cation-directed self-assembly of lipophilic nucleosides: the cation's central role in the structure and dynamics of a hydrogen-bonded assembly." *Tetrahedron* **2002**, *58*, 661-671.
- (82) Shi, X. D.; Mullaugh, K. M.; Fettinger, J. C.; Jiang, Y.; Hofstadler, S. A.; Davis, J. T. "Lipophilic G-quadruplexes are self-assembled ion pair receptors, and the bound anion modulates the kinetic stability of these complexes." *J. Am. Chem. Soc.* **2003**, *125*, 10830-10841.
- (83) Forman, S. L.; Fettinger, J. C.; Pieraccini, S.; Gottarelli, G.; Davis, J. T. "Toward artificial ion channels: A lipophilic G-quadruplex." *J. Am. Chem. Soc.* **2000**, *122*, 4060-4067.
- (84) Wei, A.; Raymond, M. K.; Roberts, J. D. "N-15 nuclear magnetic resonance spectroscopy. Changes in nuclear overhauser effects and T-1 with viscosity." *J. Am. Chem. Soc.* **1997**, *119*, 2915-2920.
- (85) Ma, L.; Iezzi, M.; Kaucher, M. S.; Lam, Y. F.; Davis, J. T. "Cation exchange in lipophilic G-quadruplexes: Not all ion binding sites are equal." *J. Am. Chem. Soc.* **2006**, *128*, 15269-15277.



- (86) Shi, X.; Fettinger, J. C.; Davis, J. T. "Ion-pair recognition by nucleoside self-assembly: guanosine hexadecamers bind cations and anions." *Angew. Chem., Int. Ed.* **2001**, *40*, 2827-2831.
- (87) Kotch, F. W.; Sidorov, V.; Lam, Y. F.; Kayser, K. J.; Li, H.; Kaucher, M. S.; Davis, J. T. "Water-mediated association provides an ion pair receptor." *J. Am. Chem. Soc.* **2003**, *125*, 15140-15150.
- (88) Kaucher, M. S.; Lam, Y. F.; Pieraccini, S.; Gottarelli, G.; Davis, J. T. "Using diffusion NMR to characterize guanosine self-association: Insights into structure and mechanism." *Chem.-Eur. J.* **2005**, *11*, 164-173.
- (89) Gellert, M.; Lipsett, M. N.; Davies, D. R. "Helix formation by guanylic acid." *Proc. Natl. Acad. Sci. U. S. A.* **1962**, *48*, 2013-2018.
- (90) Pinnavaia, T. J.; Miles, H. T.; Becker, E. D. "Self-assembled 5'-guanosine monophosphate - nuclear magnetic-resonance evidence for a regular, ordered structure and slow chemical exchange." *J. Am. Chem. Soc.* **1975**, *97*, 7198-7200.
- (91) Guschlbauer, W.; Chantot, J. F.; Thiele, D. "4-Stranded nucleic-acid structures 25 years later - from guanosine gels to telomer DNA." *J. Biomol. Struct. Dyn.* **1990**, *8*, 491-511.
- (92) Pinnavaia, T. J.; Marshall, C. L.; Mettler, C. M.; Fisk, C. I.; Miles, H. T.; Becker, E. D. "Alkali-metal ion specificity in solution ordering of a nucleotide, 5'-guanosine monophosphate." *J. Am. Chem. Soc.* **1978**, *100*, 3625-3627.
- (93) Mergny, J. L.; Helene, C. "G-quadruplex DNA: A target for drug design." *Nature Medicine* **1998**, *4*, 1366-1367.
- (94) Hud, N. V.; Smith, F. W.; Anet, F. A. L.; Feigon, J. "The selectivity for  $K^+$  versus  $Na^+$  in DNA quadruplexes is dominated by relative free energies of hydration: A thermodynamic analysis by H-1 NMR." *Biochemistry* **1996**, *35*, 15383-15390.
- (95) Kang, C.; Zhang, X. H.; Ratliff, R.; Moyzis, R.; Rich, A. "Crystal-structure of 4-stranded oxytricha telomeric DNA." *Nature* **1992**, *356*, 126-131.
- (96) Wong, A.; Wu, G. "Selective binding of monovalent cations to the stacking G-quartet structure formed by guanosine 5'-monophosphate: A solid-state NMR study." *J. Am. Chem. Soc.* **2003**, *125*, 13895-13905.
- (97) Crnugelj, M.; Hud, N. V.; Plavec, J. "The solution structure of d(G(4)T(4)G(3))<sub>2</sub>: a bimolecular G-quadruplex with a novel fold." *J. Mol. Bio.* **2002**, *320*, 911-924.
- (98) Sket, P.; Crnugelj, M.; Plavec, J. "Identification of mixed di-cation forms of G-quadruplex in solution." *Nucleic Acids Research* **2005**, *33*, 3691-3697.

- (99) Laughlan, G.; Murchie, A. I. H.; Norman, D. G.; Moore, M. H.; Moody, P. C. E.; Lilley, D. M. J.; Luisi, B. "The High-resolution crystal-structure of a parallel-stranded guanine tetraplex." *Science* **1994**, *265*, 520-524.
- (100) Haider, S.; Parkinson, G. N.; Neidle, S. "Crystal structure of the potassium form of an Oxytricha nova G-quadruplex." *J. Mol. Biol.* **2002**, *320*, 189-200.
- (101) Wu, G.; Wong, A.; Gan, Z. H.; Davis, J. T. "Direct detection of potassium cations bound to G-quadruplex structures by solid-state K-39 NMR at 19.6 T." *J. Am. Chem. Soc.* **2003**, *125*, 7182-7183.
- (102) Rovnyak, D.; Baldus, M.; Wu, G.; Hud, N. V.; Feigon, J.; Griffin, R. G. "Localization of Na-23(+) in a DNA quadruplex by high-field solid-state NMR." *J. Am. Chem. Soc.* **2000**, *122*, 11423-11429.
- (103) Wong, A.; Fettinger, J. C.; Forman, S. L.; Davis, J. T.; Wu, G. "The sodium ions inside a lipophilic G-quadruplex channel as probed by solid-state Na-23 NMR." *J. Am. Chem. Soc.* **2002**, *124*, 742-743.
- (104) Jiang, Y. X.; Lee, A.; Chen, J. Y.; Ruta, V.; Cadene, M.; Chait, B. T.; MacKinnon, R. "X-ray structure of a voltage-dependent K<sup>+</sup> channel." *Nature* **2003**, *423*, 33-41.
- (105) Deng, H.; Braunlin, W. H. "Kinetics of sodium ion binding to DNA quadruplexes." *J. Mol. Biol.* **1996**, *255*, 476-483.
- (106) Hud, N. V.; Sklenar, V.; Feigon, J. "Localization of ammonium lone in the minor groove of DNA duplexes in solution and the origin of DNA A-tract bending." *J. Mol. Biol.* **1999**, *286*, 651-660.
- (107) Sket, P.; Crnugelj, M.; Kozminski, W.; Plavec, J. "(NH<sub>4</sub><sup>+</sup>)-N-15 ion movement inside d(G(4)T(4)G(4))(2) G-quadruplex is accelerated in the presence of smaller Na<sup>+</sup> ions." *Org. Biomol. Chem.* **2004**, *2*, 1970-1973.
- (108) Cai, M.; Marlow, A. L.; Fettinger, J. C.; Fabris, D.; Haverlock, T. J.; Moyer, B. A.; Davis, J. T. "Binding cesium ions with nucleosides: Templated self-assembly of isoguanosine pentamers." *Angew. Chem. Int. Ed.* **2000**, *39*, 1283-1285.
- (109) Schalley, C. A. "Supramolecular chemistry goes gas phase: the mass spectrometric examination of noncovalent interactions in host-guest chemistry and molecular recognition." *Int. J. Mass Spectrom.* **2000**, *194*, 11-39.
- (110) Fukushima, K.; Iwahashi, H. "1: 1 Complex of guanine quartet with alkali metal cations detected by electrospray ionization mass spectrometry." *Chem. Commun.* **2000**, 895-896.

- (111) Manet, I.; Francini, L.; Masiero, S.; Pieraccini, S.; Spada, G. P.; Gottarelli, G. "An ESI-MS and NMR study of the self-assembly of guanosine derivatives." *Helv. Chim. Acta* **2001**, *84*, 2096-2107.
- (112) Bodenhausen, G.; Ruben, D. J. "Natural abundance N-15 NMR by enhanced heteronuclear spectroscopy." *Chemical Physics Letters* **1980**, *69*, 185-189.
- (113) Shi, X.; Fettinger, J. C.; Davis, J. T. "Homochiral G-Quadruplexes with Ba<sup>2+</sup> but Not with K<sup>+</sup>: The Cation Programs Enantiomeric Self-Recognition." *J. Am. Chem. Soc.* **2001**, *123*, 6738-6739.
- (114) Cotton, F. A. W., G. *Advanced Inorganic Chemistry*; Wiley and Sons: New York, **1980**.
- (115) Meyer, M.; Hocquet, A.; Suhnel, J. "Interaction of sodium and potassium ions with sandwiched cytosine-, guanine-, thymine-, and uracil-base tetrads." *J. Comput. Chem.* **2005**, *26*, 352-364.
- (116) Wang, Y.; Patel, D. J. "Guanine residues in d(T<sub>2</sub>AG<sub>3</sub>) And d(T<sub>2</sub>G<sub>4</sub>) Form Parallel-stranded potassium cation stabilized G-quadruplexes with antiglycosidic torsion angles in solution." *Biochemistry* **1992**, *31*, 8112-8119.
- (117) Ma, L.; Melegari, M.; Colombini, M.; Davis, J. T. "Large and stable transmembrane pores from guanosine-bile acid conjugates." *J. Am. Chem. Soc.* **2008**, *130*, 2938-2939.
- (118) Davis, J. T.; Kaucher, M. S.; Kotch, F. W.; Iezzi, M. A.; Clover, B. C.; Mullaugh, K. M. "Kinetic control in noncovalent synthesis: Regioselective ligand exchange into a hydrogen bonded assembly." *Org. Lett.* **2004**, *6*, 4265-4268.
- (119) Chen, L.; Sakai, N.; Moshiri, S. T.; Matile, S. "Toward supramolecular ion channels formed by oligonucleotide analogs: Hydrophobic guanine dimers." *Tetrahedron Lett.* **1998**, *39*, 3627-3630.
- (120) Kaucher, M. S.; Harrell, W. A.; Davis, J. T. "A unimolecular G-quadruplex that functions as a synthetic transmembrane Na<sup>+</sup> transporter." *J. Am. Chem. Soc.* **2006**, *128*, 8-39.
- (121) Sakai, N.; Kamikawa, Y.; Nishii, M.; Matsuoka, T.; Kato, T.; Matile, S. Dendritic folate rosettes as ion channels in lipid bilayers." *J. Am. Chem. Soc.* **2006**, *128*, 2218-2219.
- (122) Arnal-Herault, C.; Pasc, A.; Michau, M.; Cot, D.; Petit, E.; Barboiu, M. "Functional G-quartet macroscopic membrane films." *Angew. Chem. Int. Ed.* **2007**, *46*, 8409-8413.

- (123) Hofmann, A. F. "The continuing importance of bile acids in liver and intestinal disease." *Arch. Inter. Med.* **1999**, *159*, 2647-2658.
- (124) Paquet, V.; Zumbuehl, A.; Carreira, E. M. "Biologically active amphotericin B-calix[4] arene conjugates." *Bioconjugate Chem.* **2006**, *17*, 1460-1463.
- (125) Alrefai, W. A.; Gill, R. K. "Bile acid transporters: Structure, function, regulation and pathophysiological implications." *Pharm. Res.* **2007**, *24*, 1803-1823.
- (126) Kobuke, Y.; Nagatani, T. "Transmembrane ion channels constructed of cholic acid derivatives." *J. Org. Chem.* **2001**, *66*, 5094-5101.
- (127) Yoshii, M.; Yamamura, M.; Satake, A.; Kobuke, Y. "Supramolecular ion channels from a transmembrane bischolic acid derivative showing two discrete conductances." *Org. Biomol. Chem.* **2004**, *2*, 2619-2623.
- (128) Gottarelli, G.; Masiero, S.; Spada, G. P. "The use of CD spectroscopy for the study of the self-assembly of guanine derivatives." *Enantiomer* **1998**, *3*, 429-438.
- (129) Fyles, T. M. "Synthetic ion channels in bilayer membranes." *Chem. Soc. Rev.* **2007**, *36*, 335-347.
- (130) Matile, S.; Som, A.; Sorde, N. "Recent synthetic ion channels and pores." *Tetrahedron* **2004**, *60*, 6405-6435.
- (131) Siskind, L. J.; Colombini, M. "The lipids C-2- and C-16-ceramide form large stable channels - Implications for apoptosis." *J. Biol. Chem.* **2000**, *275*, 38640-38644.
- (132) Gokel, G. W.; Murillo, O. "Synthetic organic chemical models for transmembrane channels." *Acc. Chem. Res.* **1996**, *29*, 425-432.
- (133) Hille, B. *Ionic Channels of Excitable Membrane*; Sinauer Associates: Sunderland, MA, **2001**.
- (134) Ma, L.; Harrell, W. A., Jr.; Davis, J. T. "Stabilizing guanosine-sterol ion channels with a carbamate to urea modification in the linker." *Org. Lett.* **2009**, *11*, 1539-1542.
- (135) Jayawickramarajah, J.; Tagore, D. M.; Tsou, L. K.; Hamilton, A. D. "Allosteric control of self-assembly: Modulating the formation of guanine quadruplexes through orthogonal aromatic interactions." *Angew. Chem. Int. Ed.* **2007**, *46*, 7583-7586.
- (136) Etter, M. C. "Encoding and decoding hydrogen-bond patterns of organic-compounds." *Acc. Chem. Res.* **1990**, *23*, 120-126.

- (137) Schoonbeek, F. S.; van Esch, J. H.; Hulst, R.; Kellogg, R. M.; Feringa, B. L. "Geminal bis-ureas as gelators for organic solvents: Gelation properties and structural studies in solution and in the gel state." *Chem.-Eur. J.* **2000**, *6*, 2633-2643.
- (138) Dewal, M. B.; Lufaso, M. W.; Hughes, A. D.; Samuel, S. A.; Pellechia, P.; Shimizu, L. S. "Absorption properties of a porous organic crystalline apohost formed by a self-assembled bis-urea macrocycle." *Chem. Mater.* **2006**, *18*, 4855-4864.
- (139) Ranganathan, D.; Lakshmi, C.; Karle, I. L. "Hydrogen-bonded self-assembled peptide nanotubes from cystine-based macrocyclic bisureas." *J. Am. Chem. Soc.* **1999**, *121*, 6103-6107.
- (140) Ranganathan, D.; Kurur, S.; Madhusudanan, K. P.; Karle, I. L. "Self-assembling urea-based peptidomimetics: A simple one-step synthesis and crystal structure of core beta-alanyl ureylene retro-bispeptides (MeO-A(aa)-[NH-CO-NH]-CH<sub>2</sub>-CH<sub>2</sub>-CO-NH-A(aa)-OMe; A(aa)=amino acid A)." *Tetrahedron Lett.* **1997**, *38*, 4659-4662.
- (141) de Loos, M.; Friggeri, A.; van Esch, J.; Kellogg, R. M.; Feringa, B. L. "Cyclohexane bis-urea compounds for the gelation of water and aqueous solutions." *Org. Biomol. Chem.* **2005**, *3*, 1631-1639.
- (142) Custelcean, R. "Crystal engineering with urea and thiourea hydrogen-bonding groups." *Chem. Commun.* **2008**, 295-307.
- (143) Ranganathan, D.; Haridas, V.; Gilardi, R.; Karle, I. L. "Self-assembling aromatic-bridged serine-based cyclodepsipeptides (serinophanes): A demonstration of tubular structures formed through aromatic pi-pi interactions." *J. Am. Chem. Soc.* **1998**, *120*, 10793-10800.
- (144) Ghadiri, M. R.; Granja, J. R.; Buehler, L. K. "Artificial Transmembrane Ion Channels From Self-Assembling Peptide Nanotubes." *Nature* **1994**, *369*, 301-304.
- (145) Shimizu, L. S.; Hughes, A. D.; Smith, M. D.; Davis, M. J.; Zhang, B. P.; zur Loye, H. C.; Shimizu, K. D. "Self-assembled nanotubes that reversibly bind acetic acid guests." *J. Am. Chem. Soc.* **2003**, *125*, 14972-14973.
- (146) Shimizu, L. S.; Smith, M. D.; Hughes, A. D.; Shimizu, K. D. "Self-assembly of a bis-urea macrocycle into a columnar nanotube." *Chem. Commun.* **2001**, 1592-1593.
- (147) Cazacu, A.; Tong, C.; van der Lee, A.; Fyles, T. M.; Barboiu, M. "Columnar self-assembled ureido crown ethers: An example of ion-channel organization in lipid bilayers." *J. Am. Chem. Soc.* **2006**, *128*, 9541-9548.
- (148) Davis, A. P.; Dresen, S.; Lawless, L. J. "Mitsunobu reactions with methanesulfonic acid; The replacement of equatorial hydroxyl groups by azide with net retention of configuration." *Tetrahedron Lett.* **1997**, *38*, 4305-4308.

- (149) Carr, A. J.; Melendez, R.; Geib, S. J.; Hamilton, A. D. "The design of organic gelators: Solution and solid state properties of a family of bis-ureas." *Tetrahedron Lett.* **1998**, *39*, 7447-7450.
- (150) Dobrowolski, J. C.; Jamroz, M. H.; Mazurek, A. P. "Infrared study on the double hydrogen-bond between the urea molecule and halogenated aliphatic hydrocarbon solvents." *Vib. Spectrosc.* **1994**, *8*, 53-60.
- (151) Mido, Y. "Infrared-spectra and configurations of dialkylureas." *Spectrochim Acta Part A* **1972**, *A 28*, 1503-1518.
- (152) Mido, Y.; Gohda, T. "Steric effects of alkyl-groups on N-H stretching vibrations and rotational-isomerism of alkylureas." *Bull. Chem. Soc. Jpn.* **1975**, *48*, 2704-2707.
- (153) Li, J. H. Y.; Cragoe, E. J.; Lindemann, B. "Structure-activity relationship of amiloride analogs as blockers of epithelial Na channels.2. Side-chain modifications." *J. Membr. Biol.* **1987**, *95*, 171-185.
- (154) Jung, G.; Redemann, T.; Kroll, K.; Meder, S.; Hirsch, A.; Boheim, G. "Template-free self-assembling fullerene and lipopeptide conjugates of alamethicin form voltage-dependent ion channels of remarkable stability and activity." *J. Pept. Sci.* **2003**, *9*, 784-798.
- (155) Ferdani, R.; Li, R. Q.; Pajewski, R.; Pajewska, J.; Winter, R. K.; Gokel, G. W. "Transport of chloride and carboxyfluorescein through phospholipid vesicle membranes by heptapeptide amphiphiles." *Org. Biomol. Chem.* **2007**, *5*, 2423-2432.
- (156) Pajewski, R.; Ferdani, R.; Pajewska, J.; Djedovic, N.; Schlesinger, P. H.; Gokel, G. W. "Evidence for dimer formation by an amphiphilic heptapeptide that mediates chloride and carboxyfluorescein release from liposomes." *Org. Biomol. Chem.* **2005**, *3*, 619-625.
- (157) Colombini, M.; Siskind, L. J.; Stiban, J.; Anishkin, A. "Permeabilization of the outer membrane by ceramide channels: role in apoptosis." *Biophys. J.* **2007**, 1A-1A.
- (158) Siskind, L. J.; Davoody, A.; Lewin, N.; Marshall, S.; Colombini, M. "Enlargement and contracture of C-2-ceramide channels." *Biophys. J.* **2003**, *85*, 1560-1575.
- (159) Nowak, I.; Robins, M. J. "Protection of the amino group of adenosine and guanosine derivatives by elaboration into a 2,5-dimethylpyrrole moiety." *Organic Letters* **2003**, *5*, 3345-3348.

(160) Wagner, R.; Berger, S. "Heteronuclear edited gradient selected 1D and 2D NOE spectra: Determination of the NOE effect between chemically equivalent protons." *Magnetic Resonance In Chemistry* **1997**, *35*, 199-202.

(161) Stott, K.; Stonehouse, J.; Keeler, J.; Hwang, T. L.; Shaka, A. J. "Excitation sculpting in high-resolution nuclear-magnetic-resonances spectroscopy - application to selective NOE experiments." *J. Am. Chem. Soc.* **1995**, *117*, 4199-4200.